Title	Particle Induced X-ray Emission (PIXE) Setup and Quantitative Elemental Analysis
Author(s)	KABIR, MD. HASNAT
Citation	高知工科大学, 博士論文.
Date of issue	2007-09
URL	http://hdl.handle.net/10173/366
Rights	
Text version	author

Particle Induced X-ray Emission (PIXE) Setup and Quantitative Elemental Analysis

Md. Hasnat Kabir

A dissertation submitted to
Kochi University of Technology
in partial fulfillment of the requirements
for the degree of

Doctor of Philosophy

Department of Electronic and Photonic Systems Engineering
Graduate School of Engineering
Kochi University of Technology
Kochi, Japan.

September, 2007

Abstract

Among other analytical techniques, Particle Induced X-ray Emission (PIXE) is a highly sensitive, multi-elemental analytical technique which is already proved in all prospective areas such as thin films, water, air, archaeological and biological samples etc. From several decades PIXE is widely used in the above mentioned areas successfully. We have given some efforts to setup general PIXE, analysis of seabed sludge, analysis of shellfish and micro-PIXE setup including its application.

The ion beam facility at Kochi University of Technology (KUT) has been extended to allow elemental concentrations analysis by PIXE. RONTEC XFlash 2001, a Silicon Drift Detector (SDD) type x-ray detector was used in the setup. XFlash supply unit with high resolution pulse processor was connected to an ORTEC (Model 572) amplifier. This amplifier is a general-purpose spectroscopy amplifier. After that, the output of this amplifier was connected to a computer via an ADC and a multi-channel analyzer.

We have investigated the polluted areas of Uranouchi Bay by heavy and toxic elements. As a result of analyses of samples collected from eleven different places in the bay, seventeen elements including toxic ones were detected. It is found that the center region of the bay is mostly polluted in contrast to the other regions. The major elements show characteristic features especially in center (Sam7) than that of inlet (Sam11), where sulfur concentration is considerably higher by five times. The concentration ratios of toxic elements indicate that the concentrations of Cr, Ni, Cu and Zn pronouncedly increase in center regions in comparison with those in the other samples. The highest values of copper and zinc concentration are found to be 2.72 and 2.6 times larger, respectively, in comparison with those for Sam11 collected from the inlet of the bay.

Another attempt has been taken to analyze heavy metals in shellfish (*Ruditapes philippinarum*) those were collected from Uranouchi Bay also. Nine elements were

detected after analyzing shellfish collected from this bay. Calcium is the high concentrated major element among others. The heavy elements concentration are compared with market shellfish and found that almost all heavy elements in Uranouchi shellfish show higher concentration in contrast to market one except Cu in zone 2. Cu has lower concentration in zone 2 in contrast to Market but more than two and four times higher in zone 1 and zone 3, respectively. Nevertheless, Zn and Br in zone 1 are approximately four and eight times higher, respectively, while that of Sr and Zr in zone 2 and zone 1 are four times higher, respectively than that of Market. According to this result, biological species of this bay are certainly affected by heavy metals in various ways.

We have developed a novel microbeam using a glass capillary optics. This is an external as well as microbeam technique. The system introduces high energy ion beams to atmospheric environment. Slightly tapered glass capillary optics with a few micrometers of outlet size is placed between vacuum and atmospheric environment. The capillary works as a differential pumping orifice as well as a focusing lens. This is a very simple technique to produce different size of microbeam than conventional ones by changing the capillary only within a few minutes. This technique was applied for in-air PIXE analysis. The dried and wet samples of seabed sludge were analyzed. We observed that the ion beam is successfully introduced to the atmospheric environment and in-air PIXE measurements can be carried out without any difficulties. This result indicates that the technique is suitable to obtain in-air PIXE spectra and virtually any type of samples such as solids, liquids and gases can be measured as they are.

Table of Contents

Chapter Four: Elemental Analysis of Uranouchi Bay Seabed Sludge

Chapter Five: PIXE Analysis of Biological Bodies

Chapter Six: Micro-PIXE Setup and Its Application

Acknowledgement

The results, presenting in this dissertation have many influence from different professors, institutions, family members and friends. Now it is the time to give thanks to all of them. I would like to give thanks to the authority of Kochi University of Technology (KUT), Japan for giving a chance to pursue PhD at this University.

My deepest gratitude goes to my respective supervisor Professor Tadashi Narusawa at first for providing me the opportunity to join his research group. I believe that without his proper guidance, advices, kind assistances and encouragement, this research would not be possible. He gave me strong support during the whole period of my research works as a local guardian.

Prof. Keiichi Enomoto, Prof. Tetsuya Yamamoto, Prof. Akimitsu Hatta and Associate Prof. Katsuhiro Sumi were the potential panel members of the reviewer committee for my dissertation. I would like to express my profound thanks to all of the above members for evaluating me and for delivering their valuable suggestions.

I feel glad as a doctoral student of KUT and it has been possible for Special Scholarship Program SSP) of KUT. So I would like to appreciate it and express my thanks to the authority. I want to give special thanks to all of the members of International Relation Center (IRC) of KUT for their careful assistances for academic as well as for life in Kochi. I always found them as real friends when I asked any assistance.

My sincere gratefulness goes to Professor Katsuhiro Sumi, department of Environmental Systems and Engineering of KUT for providing me seabed sludge samples and valuable information regarding sampling points of the samples. I would also like to express my thanks to assistant professor Fumitaka Nishiyama, department of Power Engineering and Applied Physics, Hiroshima University, Japan for his wholehearted supports and assistances during the experimental works.

Takuya Nebiki, research assistant of Professor Tadashi Narusawa is a person whom I should give a lot of thanks for his manner assistance during the experimental works. I would like to give thanks other members of our group for making pleasant working environment.

Finally, my pretty thanks go to my wife who encourage me and gives mental support. I also want to express my warm thanks to my mother, family members and friends for their encouragement.

Md. Hasnat Kabir
September, 2007

List of Figures:

List of Tables:

List of Abbreviation

AAS	Atomic Absorption Spectrometry
ADC	Analog to Digital Converter
AXIL	Computer Software
BEA	Impulse Approximation often called BEA
FWHM	Full Width at Half Maximum
GUPIX	Computer Software
IDL	Instrumental Detection Limit
KUT	Kochi University of Technology
LEMO	One kind of circular connector
LLD	Lower Level Discri
LOD	Limit of Detection
MCA	Multi Channel Analyzer
MDL	Minimum detection limit
MeV	Mega Electron Volt
MV	Mega Volt
PVAc	Polyvinyl Acetate
PIXAN	Computer Software
PIXE	Particle Induced X-ray Emission
Ppm	Part Per Million
PUR	Pile-up Rejector
PWBA	Plane Wave Born Approximation
RBS	Rutherford Back Scattering
ROI	Region of Interest
SCA	Semi-Classical Approximation
SDD	Silicon Drift Detector
SEB	Secondary Electron Bremsstrahlung
SRM	Standard Reference Materials
TMP	Turbo Molecular Pump
TTL	Transistor Transistor Logic
TTPIXE	Thick Target Proton Induced X-ray Emission
ULD	Upper Level Discri
XRD	X-ray Diffraction
XRF	X-ray Fluorescence

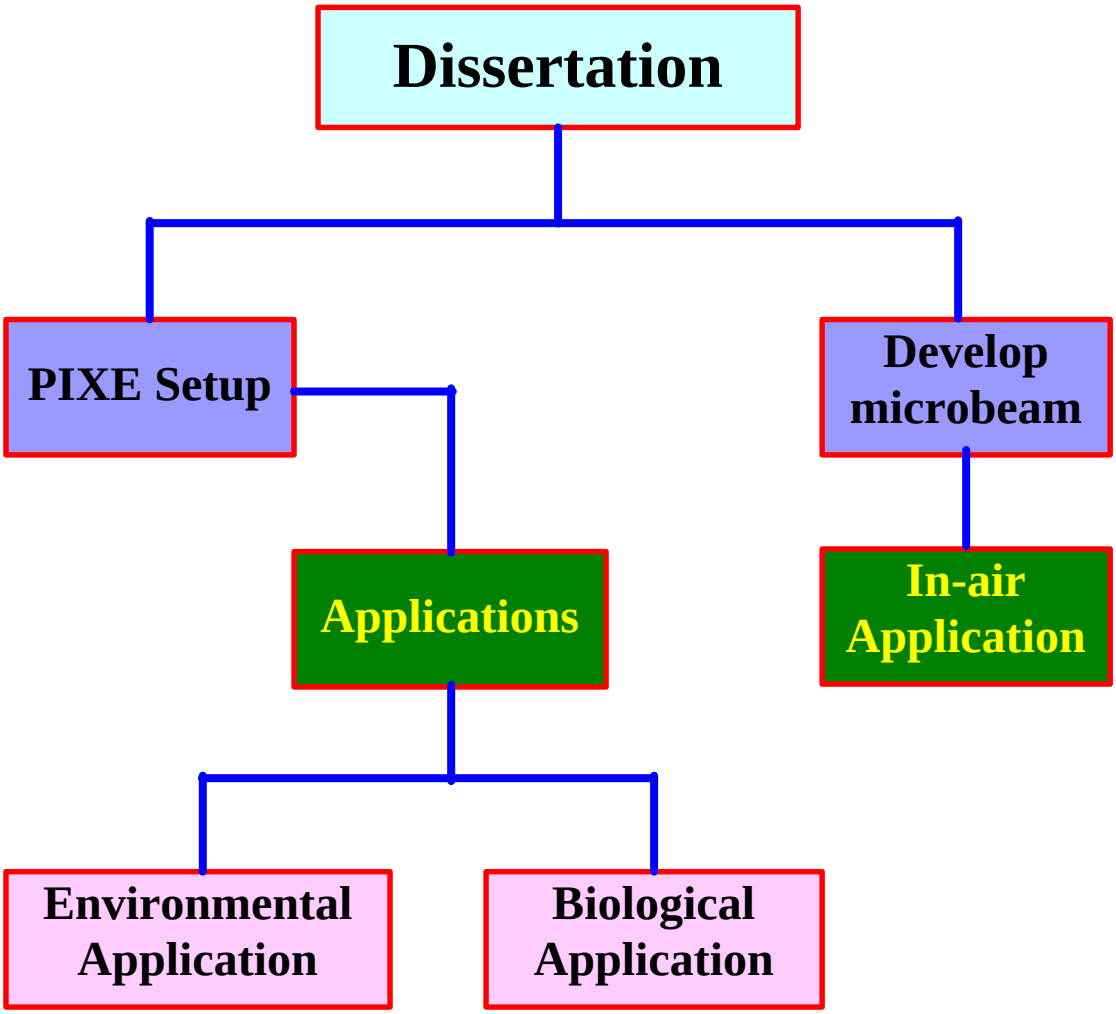
Dissertation
PIXE Setup
Develop microbeam
Applications
In-air Application
Environmental Application
Biological Application

Chapter One

Introduction of Particle Induced X-ray Emission (PIXE)

The enormous applications of Particle Induced X-ray Emission (PIXE) have an excellent attention to the research. Chapter one describes the brief history of PIXE so that reader can easily understand the generation of PIXE. The Basic principle of PIXE also explains here with some easy understandable figures. The purpose of this research and the brief outline of dissertation are presented here.

1.1 Brief History

Roentgen [1] has first invented x-rays since 1895 during his measurement with cathode rays. He has achieved the first Nobel Prize in 1901 for his outstanding discovery. X-rays are one kind of electromagnetic radiation with a very short wavelength. The wide application of x-rays was in medical in the early stage. Now it becomes more and more wide. The characteristic of x-ray generation has an interest in the fundamental atomic physics. X-rays emission from the radioactive sources was first observed by Chadwick [2] in 1912 using heavy ions (alpha-particles). Chadwick found x-ray emission with a low intensity which was not suitable for analytical purposes. This process was not too much useful until the development of accelerators for nuclear physics research.

In the early stage of x-ray spectrometry, it was recognized that this method offers the possibility of systematic and multielemental analysis even though complex matrices. The Swedish geologist Hadding has reported qualitative analysis of various minerals since 1922 [3]. He made a comparison with results between the x-ray spectrometry and the conventional chemical methods and found a good agreement. Unfortunately he could not show the quantitative results due to the lack of knowledge about the analytical parameters. X-ray emission spectrometry was developed by Castaing at the University of Paris [4] since 1950, and it was a mile stone of nuclear physics techniques. He showed that it could be possible to use the x-rays emitted by the specimen in an electron microscope for multielemental analysis.

Electron beam of several keV energies were basically used to produce x-rays before developing accelerators. Though the excitation cross-sections of x-rays for proton and helium ions of MeV energies are similar to those of several keV energies for electron beams but the background contribution from bremsstrahlung of proton is much smaller for heavy ions than for electrons. The above concept was theoretically predicted during the 1960s therefore physicists were interested about the possibility to use heavy charged particles for analytical purposes with the knowledge of x-ray production cross-section as a function of particle energy and atomic number. Some efforts were made during the 1960s to use proton induced x-ray emission to elemental

analysis. An attempt was made by Khan et al. [5] to measure the thickness of thin films with low-energy protons. After that, great progress in nuclear physics was made by developing solid-state surface barrier detectors for charged particles.

Particle Induced X-ray Emission (PIXE) was first introduced by Johansson et al. [6] at the Lund Institute of Technology in 1970 using MeV proton beams and high resolution Si(Li) detector, showed that PIXE is relatively high sensitive, multi-elemental and non-destructive analysis technique. They have shown that their system is capable to analyses the trace elements with a good resolution. Several analytical techniques have been used for trace element analysis, their sample preparation is generally complicated and takes a long time. The ion-beam techniques, especially PIXE is one of the most powerful techniques for material analysis, since its sample-preparation techniques are generally simple and it requires a short measuring time. This powerful technique can easily analyze various elements with atomic number as low as 12 in the ppm range. Two stages procedure are followed in PIXE analysis. Firstly, elements in the target are identified from the energies of the characteristic peaks in the x-ray emission spectrum. Secondly, the quantity of a particular element in the target is determined from the intensity of its characteristic x-ray emission spectrum. The qualitative advantage of x-ray spectrometry was well established before PIXE (Particle Induced X-rays Emission). However, PIXE introduces both qualitative and quantitative advantages simultaneously in a single measurement. The heavy ions produce rather complicated x-ray spectra which contain the information of different elements of target matrices. The historical development can be found in some review papers [6-7]. The technical improvements and the applications of PIXE in several scientific fields were presented in different International PIXE conferences [8-13].

1.2 The Basic Principle of PIXE

X-rays can be produced by exciting the target atoms with an energetic incident ion beam of protons or alpha particles as shown in figure 1.1. The high-energy protons or alpha particles strike the target atoms and eject electrons from the innermost shell in atoms. As a result, a vacancy is created in the innermost shell. It is a common nature

of an excited atom that it seeks to regain a stable energy state. Therefore, the created vacancy is filled by an electron coming from an outer shell, at that time an electromagnetic radiation in the form of characteristic x-rays is emitted. The de-excitation may also be possible by the emission of an electron, so-called Auger electron (figure 1.2 (c)). Figure 1.2 shows the k-shell ionization, x-ray emission, and emission of Auger electron. The probability of the emission of an x-ray quantum (the fluorescence yield) is close to 1 for the heavy elements but only a few percent for the light ones.

The x-ray spectrum is simply determined by the energy levels of the electrons in the atom. The energy level diagram of a medium-heavy element with the x-ray transitions is shown in figure 1.3. The transitions going to the K shell are indicated as K x-rays. When the vacancy is filled by an electron, comes from the L shell, the transition is denoted as K_α , and when it comes from the M shell, K_β. Similarly, the transitions to the L shell are indicated as L x-rays, and these have some components, especially for heavy elements. Generally, the light and medium-heavy elements are identified by their K x-rays and the heavy elements by L x-rays due to the effective detection of the K x-rays which can be obtained in the range $20<Z<50$ and of the L x-rays for $Z>50$.

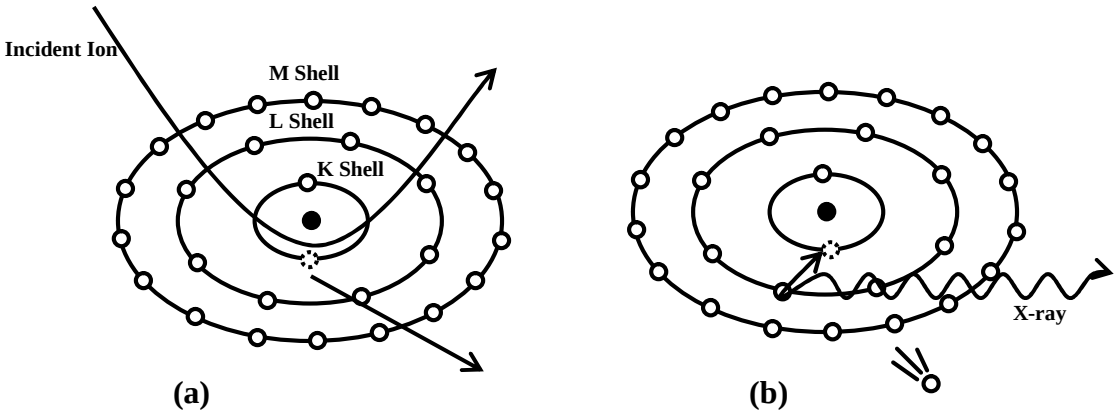

Figure1.1: Basic principle of PIXE. (a) Indicates ion interaction with inner shell electron. (b) Indicates emission of electron, fall of upper shell electron and radiation of x-ray.

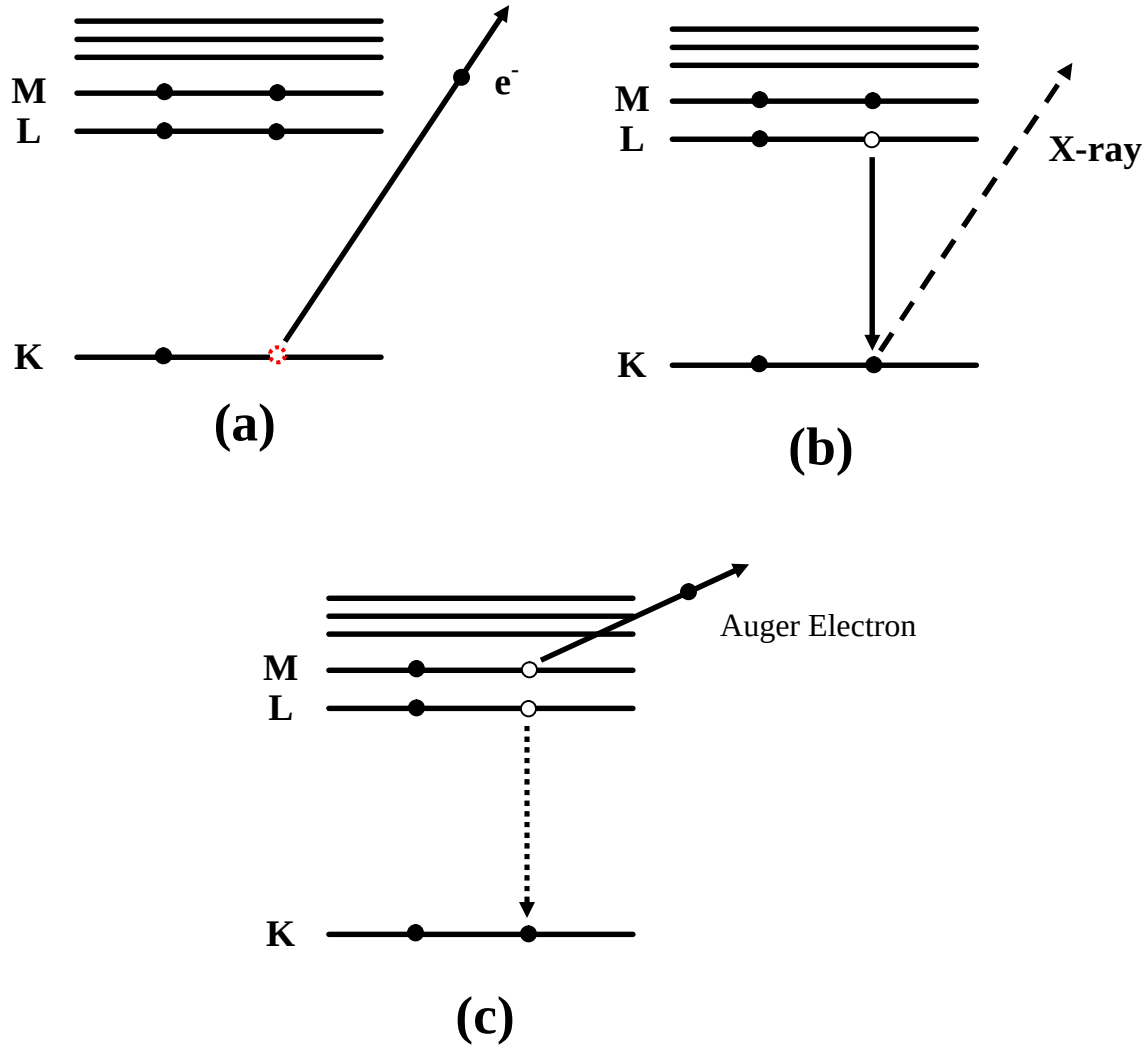

Figure 1.2: Ionization process; (a) k-shell ionization, (b) x-ray emission, and (c) Auger electron.

The energy of characteristic x-ray is equal to the difference between two shell electron binding energies those take part in the transitions express as

$$E_{x\text{-}ray} = E_1 - E_2 \qquad (1.1)$$

where $E_{x\text{-}ray}$ is the characteristic x-ray energy, E_1 is the vacant shell electron binding energy and E_2 is the donor shell electron binding energy.

For instance, Mn K_α x-ray energy

K-shell electron binding energy = 6539.0 eV

L (III) –shell electron binding energy = 638.7 eV

Difference = 5900.3 eV

Therefore, Mn K_α x-ray energy is 5900 eV, i.e. 5.9 keV

Using x-ray spectrum, energy level diagram and knowing x-ray energies, it can be possible to determine the elements those are in the specimen.

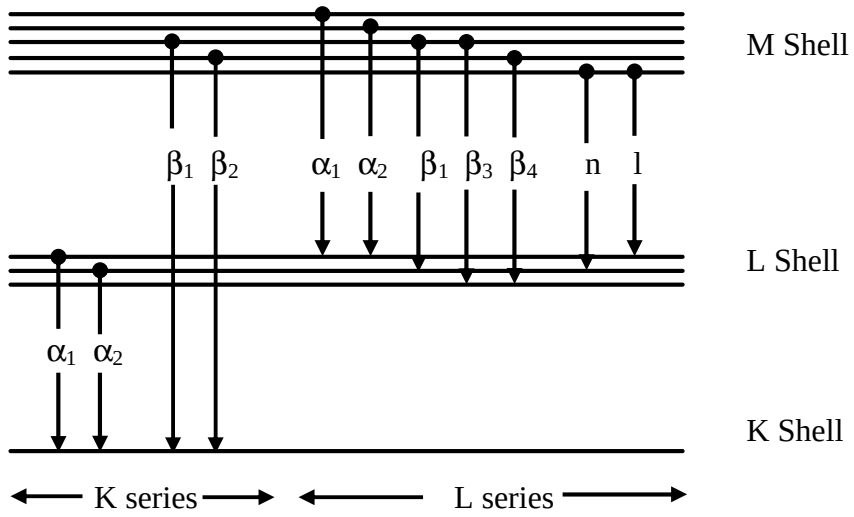

Figure 1.3: Energy levels and X-ray transitions in medium-heavy element.

1.3 Comparison with Electron Beam

In PIXE, generally used ion beam as a projectile has some better advantages in contrast to electron beam. An electron beam case, the mass of projectile and target electrons are same, however, in PIXE the mass of proton is 1836 times higher than that of target electron. Therefore, the overall loses of kinetic energy is very lesser in

the proton beam case and its direction to travel is almost not altered. The depth of penetration per encounter is larger and the scatter angle is smaller in proton beam. The momentum is smaller in the electron beam case than that of proton beam. As a result, a larger fraction of energy losses per encounter in the electron beam case. All of these advantages make proton beam a better projectile. On the other hand, the bremsstrahlung is much higher in electron beam than that of proton beam case because of huge mass fraction difference.

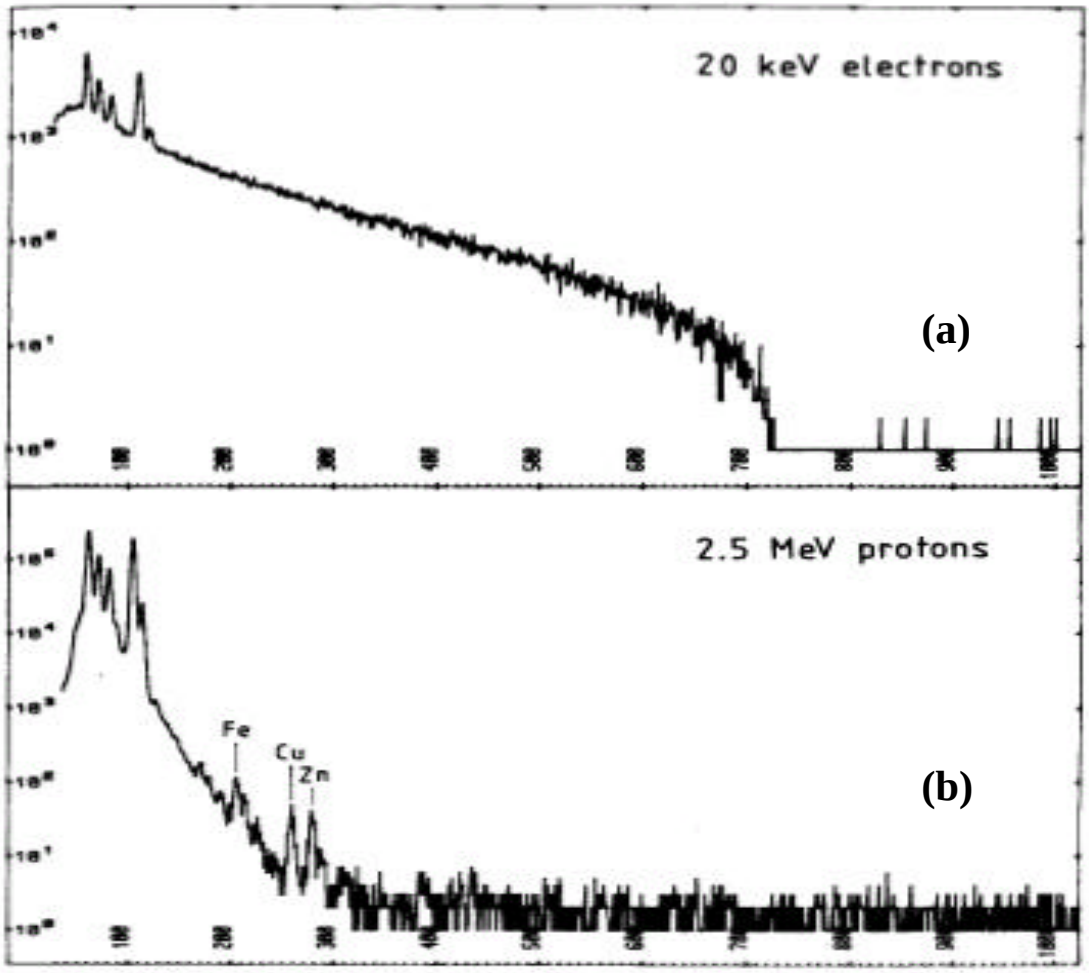

Figure 1.4: X-ray spectra of a brain specimen using (a) an electron microprobe and (b) a proton microprobe [14].

Figure 1.4 shows two spectra of same specimen. One was obtained with an electron microprobe, the other by PIXE. In contrast to PIXE spectrum, electron beam

spectrum shows fewer peaks from the light elements due to the large background while that of PIXE spectrum shows some trace element peaks also.

1.4 An Outline of the PIXE Technique

The accelerators used for PIXE analysis are relatively small machines those provide a beam of protons or heliums or even heavier ions. A typical arrangement of PIXE technique is shown in figure 1.5. The Van de Graaff accelerator was widely used during the PIXE development period. This accelerator uses a continuous moving belt in a high pressure tank to maintain a terminal at a voltage of typically 2-3 MV. Therefore, accelerator can produce energies of 2-3 MeV to protons and twice that to doubly charged helium ions. Several tens of microamperes current are generated by this machine. Such amounts of currents are relatively very high for PIXE analysis, which generally uses a few tens of nanoamperes.

More recently the new generation of small tandem accelerator has been using in PIXE analysis. The tandem machine becomes a popular choice for PIXE analyst because it allows the use of only half the voltage needed in a conventional machine. In this accelerator, the negatively charged ion gains energy due to very high positive voltage at the geometric centre of the pressure vessel. When it arrives at the centre region known as the high voltage terminal, some electrons are stripped from the ion. The ion then becomes positive and accelerated away by the high positive voltage. The accelerator has two stages of acceleration, first pulling and then pushing the charged particles. The tandem machine with a terminal voltage of 1.5 MV is a general choice. It provides protons with energy of 3 MeV which is enough to PIXE analysis.

The beam coming from the accelerator passes first through a bending magnet. The beam is stabilized by passing it through a slit. The deflection in the magnet can be altered due to any small energy changes within the accelerator. Therefore, an imbalance in the currents is intercepted by the left and the right edges of the slit. A differential signal is derived from these currents which is amplified and uses in a feedback loop to control the primary operating voltage of the accelerator. This

energy-analyzed beam is then directed axially down the beam-line using electrostatic and magnetic steering elements. After that the beam enters into the target chamber.

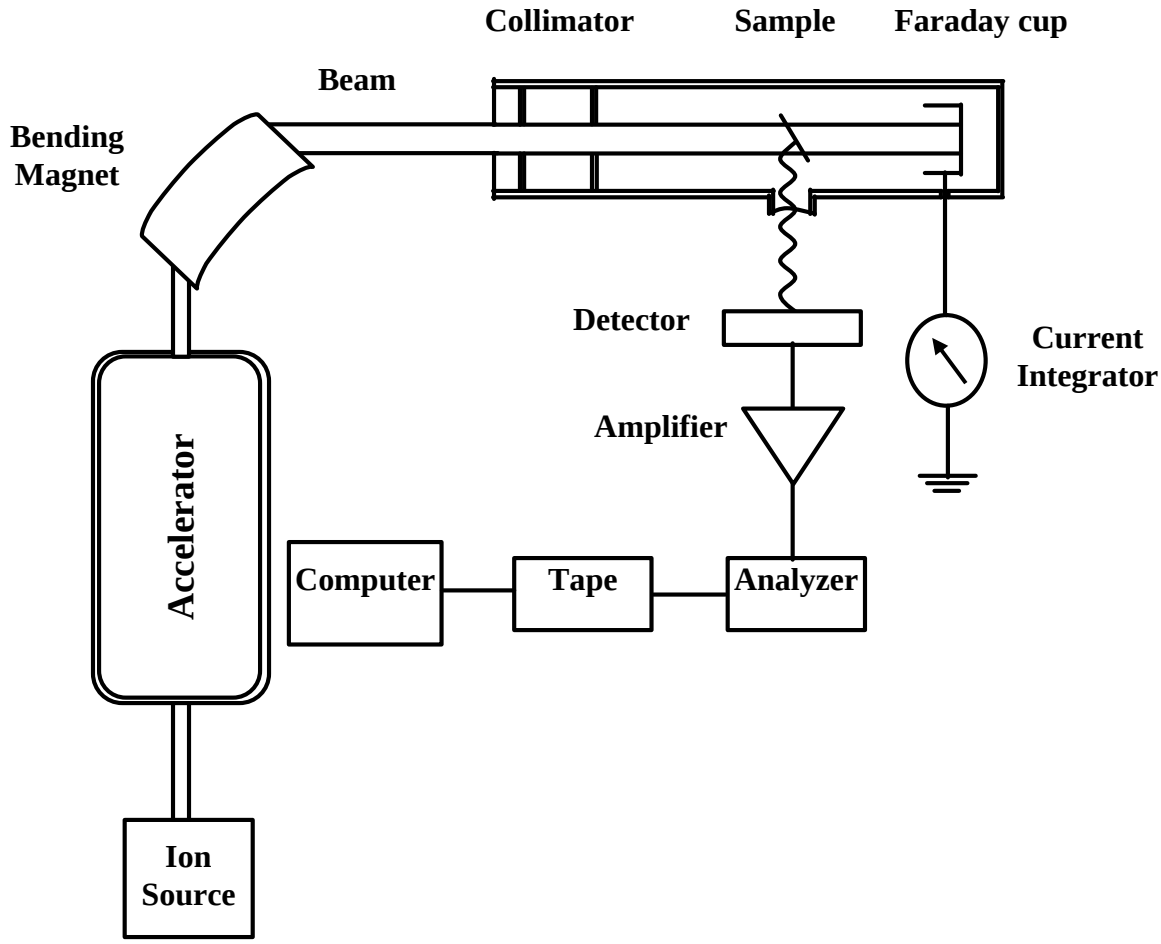

Figure 1.5: Typical arrangement for PIXE technique.

The typical pressure in the chamber is 10^{-6} torr. Usually a larger number of samples are placed in the target chamber in order to avoid the need for frequent opening and re-evacuation. Several subsidiary devices require in the chamber. The x-ray detector and a Faraday cup are the major devices among them. The x-ray detector collects the x-rays those are emitted from the target and Faraday cup monitors the incident beam current on the target. Backing foil is used as a substrate for specimen. The thin target permits the beam to pass through it with a fraction of energy loss which is monitored

by a Faraday cup. On the other hand, thick target stops the beam entirely and it requires a different arrangement.

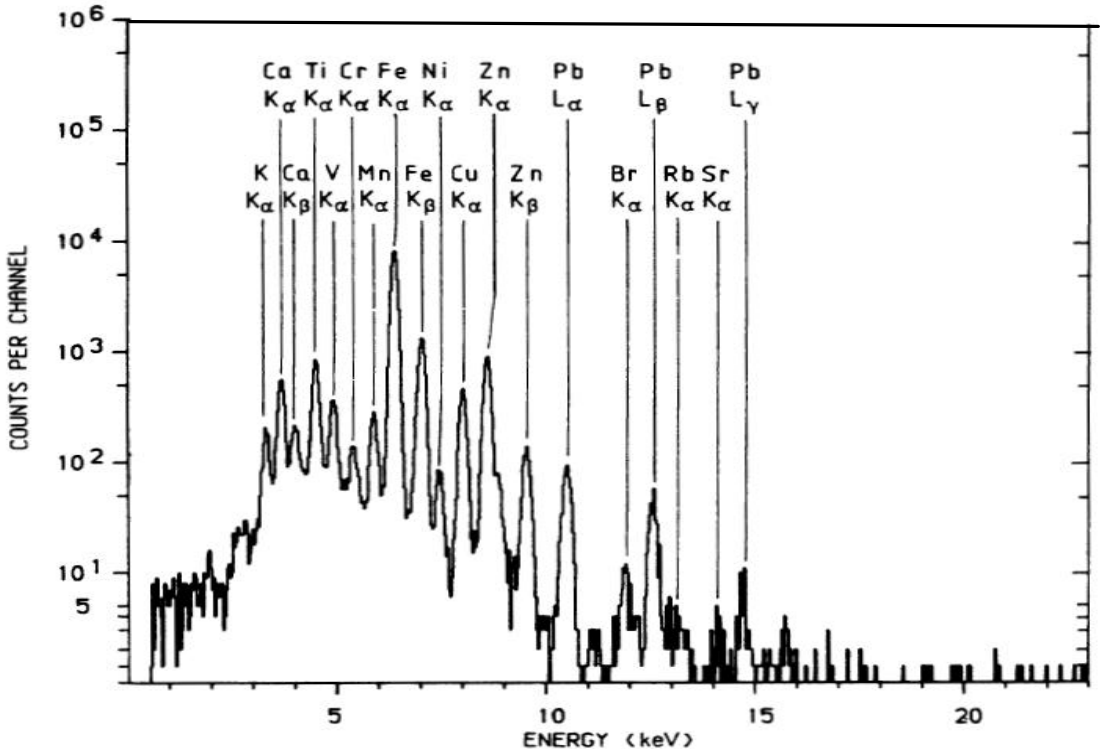

Figure 1.6: Typical PIXE spectra of a rain water sample [6].

In the target chamber, beam strikes the target directly consequently characteristic x-rays are emitted. The x-ray detector detects the incoming x-rays from the target. The x-ray detector data come into computer via processing unit, amplifier, ADC and MCA. Then the data are represented by a spectrum using computer software. A typical PIXE spectrum is shown in figure 1.6. It contains several characteristic x-ray peaks. The spectrum is superimposed on a background due to a variety of atomic bremsstrahlung processes and also due to gamma rays from nuclear reactions induced by the beam. Generally, the medium heavy elements contribute K x-rays whereas heavy elements are L x-rays. At a glance the PIXE spectrum is complex rather than a typical spectrum. The figure shows a large number of x-ray peaks collecting from water sample which indicates the high sensitivity of PIXE. The concentration of the element in the specimen is directly related to the area of the corresponding each peak.

The manual analysis of spectrum is relatively difficult and it is also not feasible due to the number of overlaps and the strongly energy-dependent background. Several software codes have been developed to deconvolute spectra and to calculate peak areas with a high degree of accuracy. From these results absolute amounts of elements present in the specimen can be determined.

1.5 Purpose of Research

The advantages and basic principle of PIXE have been discussed in the above sections. Due to several advantages, it has been proven that PIXE is a superior analytical technique for elemental analysis and it provides quantitative results since development. However, there was no complete PIXE setup at Kochi University of Technology (KUT), Japan before this dissertation. The main objective of this research is to introduce experimental setup of PIXE at KUT and its application for quantitative elemental analysis. Although, PIXE has vast applications such as environmental, biological, medical, atmospheric, geosciences, art, and archaeology etc. but in this dissertation, environmental and biological samples have been chosen for quantitative elemental analysis. Uranouchi bay, Japan was taken as the sampling area because of its beauty and natural landscape. On the other hand, the sea water and the seabed of this bay are no longer clean now. The goal of the present study was to determine the influence of heavy metals on the environment and biological bodies in the bay. Seabed sludge and shellfish were chosen as the representative of the environment and biological species , respectively. Another aspect of this dissertation was to develop micro-beam for PIXE analysis. The growing demand of developing micro-PIXE for analysis of micron size solid as well as liquid samples are made attention of us to develop it.

1.6 Research Outline

This dissertation is outlined as follows:

Chapter One: Introduction

The general introductions on brief history, basic principle and characteristic x-ray transition line of PIXE are given. Some advantages are also described here. A slight touch is given about the applications. In this chapter, it is also pointed out the purpose of this research work.

Chapter Two: Theoretical Background

The fundamental theoretical knowledge is discussed in this chapter. The K-shell fluorescence yield, mechanism of ion-target interaction and ion stopping power in target are mentioned here. The inner-shell ionization cross-section after collisions and its different models are explained. A short description of bremsstrahlung background is presented. The conventional PIXE experimental setup and target preparation techniques are presented for the help to develop PIXE setup at KUT and its applications.

Chapter Three: Setup PIXE at KUT

In the light of theoretical knowledge and experimental methods, the experimental setup at KUT is discussed in detail in this chapter. A data acquisition system with a block diagram is explained here. The energy calibration, escape peak, pile-up, dead time correction and limit of detection of the system are shortly touched up. The data processing methods and common overlapping peaks are explained as elaborated form.

Chapter Four: Elemental Analysis of Uranouchi Bay Seabed Sludge

Reader can get information about the quantitative elemental analysis of seabed sludge as an environmental sample by PIXE. Sampling points, sample preparation technique, experimental methodology, results and discussion are described in this chapter. The experimental results indicate the pollutant areas in the bay and the highest concentrated elements are present in the area. A comparison of toxic elements found from the analyzed samples is also expressed here.

Chapter Five: PIXE Analysis of Biological Bodies

The influence of heavy metals in the biological species in the bay is explained in this chapter. Shellfish were chosen as the representative among the biological species and analyzed by PIXE. Sampling areas, sample preparation technique, experimental method, results and discussion are described here. The elemental concentrations of heavy metals are discussed in detail and these results are compared with market shellfish.

Chapter Six: Micro-PIXE Setup at KUT and Its Application

A brief history of developing micro-PIXE and theoretical background are discussed here. The setup procedure of this technique at KUT is mentioned in this chapter. Application of this microbeam, in air PIXE measurement is also summarized.

Chapter Seven: Summary and Conclusion

The main results obtained from this research work are segmented into four categories and summarized briefly here.

References

[1] W. C. Roentgen, Sitzungsber. dev Wurgburgev Physik-Medic, Gesellsch, Jahrg. 1895, Ann. Dev. Phys., **64**, 1 (1898).

[2] J. Chadwick, Phil. Mag., **24**, 594 (1912).

[3] A. Hadding, Z. Anorg. Allgem. Chem., **122**, 195 (1922).

[4] R. Castaing, Ph.D. Dissertation, University of Paris, 1951. Application des sondes electroniques a une methode d'analyse ponctuelle chimique et cristallo graphique (These, Universite de Paris, 1951).

[5] J.M. Khan, D.L. Potter and R.D. Worley, Phys. Rev., **37**, 564 (1966).

[6] S. A. E. Johansson, and T. B. Johansson, Nucl. Instr. Meth, **137**, 473 (1976).

[7] F. Folkmann, J. Phys. E, **8**, 429 (1975).

[8] S. A. E. Johansson (ed.), Proceedings of the International Conference on Particle Induced X-ray Emission and Its Analytical Applications, Nucl. Instr. Meth., **143** (1977).

[9] S. A. E. Johansson (ed.), Proceedings of the Second International Conference on Particle Induced X-ray Emission and Its Analytical Applications, Nucl. Instr. Meth., **181** (1981).

[10] B. Martin (ed.), Proceedings of the Third International Conference on Particle Induced X-ray Emission and Its Analytical Applications, Nucl. Instr. Meth., **B38** (1984).

[11] H. van Rinsveld, S. Bauman, J.W. Nelson, and J.W. Winchester (eds.), Proceedings of the Fourth International Conference on Particle Induced X-ray Emission and Its Analytical Applications, Nucl. Instr. Meth., **B22** (1987).

[12] R.D. Vis (ed.), Proceedings of the Fifth International Conference on Particle Induced X-ray Emission and Its Analytical Applications, Nucl. Instr. Meth., **B49** (1990).

[13] M. Uda (ed.), Proceedings of the Sixth International Conference on Particle Induced X-ray Emission and Its Analytical Applications, Nucl. Instr. Meth., **B75** (1993).

[14] S. A. E. Johansson and J. L. Campbell, PIXE: A novel technique for elemental analysis (John Wiley & Sons, Chichester, 1988).

Chapter Two

Theoretical Background

The theoretical background can be found in this chapter as a compressed form. In order to do experimental work, basic theoretical knowledge is very important. The K-shell fluorescence yield, mechanism of ion-target interaction and ion stopping power in target are mentioned here. The inner-shell ionization cross-section after collisions and its different models are explained. A short description of bremsstrahlung background is presented. The conventional PIXE experimental setup and target preparation techniques are presented for the help to develop PIXE setup at KUT and applications.

2.1 X-ray Spectra

The creation of K-shell vacancy in an atom may be de-excited within a very short time, producing an emission of either characteristic x-ray or auger electrons or both. The probability of creation x-rays is known as K-shell fluorescence yield which depends on the atomic number of the elements. The atomic number Z dependent K- and L-shell fluorescence yields are shown in figure 2.1[1]. A semi-empirical formula for calculation fluorescence yield was given by Bambynek et. al [2]. The Bambynek formula is as follows

$$\left(\frac{w_K}{1-w_K}\right)^{1/4} = \sum_{i=0}^{3} B_i Z^i \qquad (2.1)$$

where B_i is the coefficients and values are tabulated in table 2.1. The fluorescence yield (w_K) values derived from this equation are very close with calculation [3] based upon a Dirac-Hartree-Slater treatment of the bound atomic electron wave functions. The K shell fluorescence yield is also changed due to the composition of different elements in an alloy [4]. Figure 2.2 [5] shows the principal K and L x-ray lines in the filling of K and L vacancies as a function of atomic number. A full tabulated value of K and L x-ray was given by Bearden [6].

A great variety of theoretical approximations have been done to estimate the relative intensity ratio (K_a / K_b) of all the K components but a deficiency remains in a particular region from Z=21 to Z=32 where the 3d subshell is filling. The exact K_a / K_b ratios are necessary in order to sort the spectral overlaps that occur in this region between K_a of element Z and K_b of element Z - 1. Scofield's work [7] related to the intensity ratio has a merit over other treatments is that it provides also the intensities of the KLL, KLM and KMM Auger satellites. Therefore, using his results PIXE analyst can compile an x-ray intensity library which contains the relative intensities of the various K x-ray lines for every element.

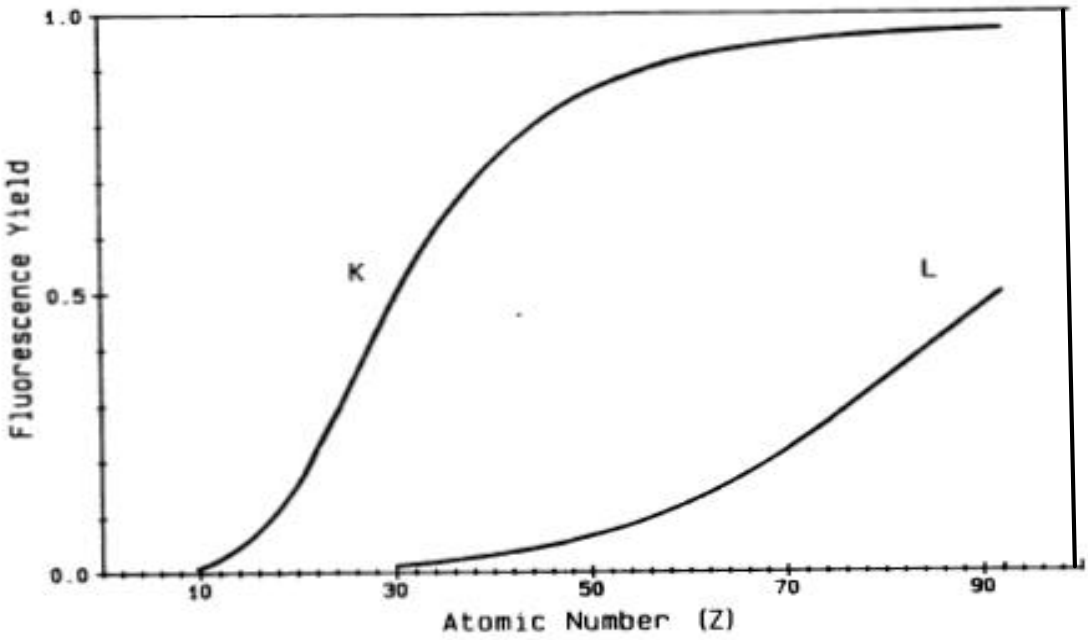

Figure 2.1: The K- and L-shell fluorescence yields as functions of atomic number Z [1].

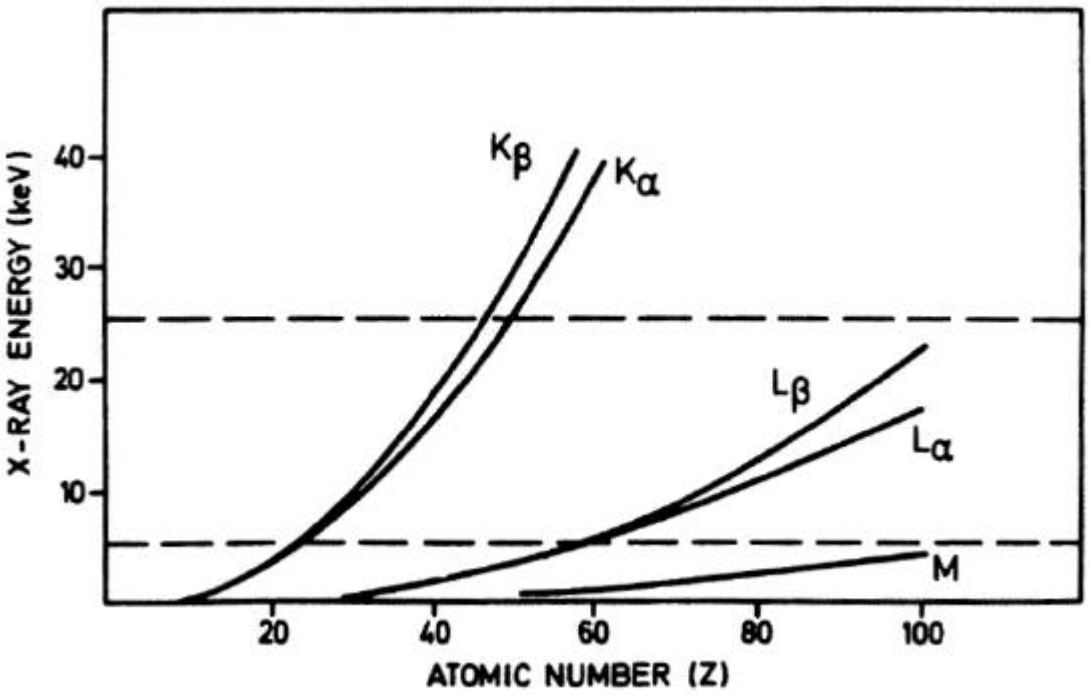

Figure 2.2: Atomic level diagram showing the principal K and L x-ray transitions [5].

Table 2.1: Coefficients for evaluation of K- and L-shell fluorescence yields.

	K	L
B_o	$(3.70 \pm 0.52) \times 10^{-2}$	0.17765
B_1	$(3.112 \pm 0.044) \times 10^{-2}$	2.98937×10^{-3}
B_2	$(5.44 \pm 0.11) \times 10^{-5}$	8.91297×10^{-5}
B_3	$-(1.25 \pm 0.07) \times 10^{-6}$	-2.67184×10^{-7}

2.2 Ion-Target Interaction

If an energetic ion hits upon the surface of a sample or so-called target, a series of elastic and inelastic collisions with the atoms are processed along its path. The electrical forces between nucleus and electrons of the projectile and the target atoms are the reasons for these collisions. The projectile is deflected a few degrees by the collision from its original direction and becomes slow somewhat, releasing some of its kinetic energy to the target atom. The capacity of a target to slow a projectile is called the stopping power, and it is one of the most significant phenomena especially for PIXE because it measures the capacity of a projectile to penetrate within the target. Stopping power is defined as the amount of energy loss by the projectile per unit length of trajectory in the target.

If the energy loss per unit length traveled within the target is dE/dx, then stopping power can be represented as

$$S_o(E) = r^{-1} \frac{dE}{dx} \qquad (2.2)$$

where r is the density of the target. The unit of stopping power is keV/g/cm^2. The atomic stopping cross-section can be expressed as

$$e_o(E) = N^{-1} \frac{dE}{dx} \qquad (2.3)$$

where N is the atom density. The unit of it is keV/atom/cm^2. The equation 2.2 and 2.3 can be correlated as

$$S_o(E) = 6.022 \times 10^{23} e_o(E) A^{-1} \qquad (2.4)$$

where A is the target atomic number and very common unit of it is keV/mg/cm^2. The value of stopping power has been carefully calculated by Andersen and Zeigler [8] and Zeigler et al. [9] based on the both from theory and from surveys of experimental data.

The projectile range can be expressed by numerical integration corresponding to energy E

$$R = \int_0^R dx = \int_E^0 \frac{dE}{dE/dx} \qquad (2.5)$$

The stopping power and range for proton projectiles in various targets are tabulated in table 2.2.

Table 2.2: Range in target R, energy loss dE/dx and stopping power $S_o(E)$ for 2.5 MeV protons in various solids [8-9].

Target	**Z**	**R(㎜)**	**dE/dx (keV/㎜)**	S_o **(keV/mg/cm^2)**
C	6	55	27.8	122.9
Si	14	68	22.8	98.2
Fe	26	27	58.9	74.9
Ag	47	28	58.8	56.1
Pb	82	37	46.0	40.6

From table 2.2, it is clearly seen that the stopping power is a function of elements Z. However, range in target increases with decreasing energy loss per unit length traveled within the target.

2.3 Ionization Cross-Section

The target is stroked by protons or heavier ions definitely emitting electrons from the orbits of the target atom, resulting emission of characteristic x-rays. The cross-section of this process is called as ionization cross-section. It is a probability which measure

how many ionization occurs. The inner-shell ionization is produced by close collisions (Rutherford's scattering) and by distant collisions with the target atoms [10]. At low projectile energies, the principal contribution of ionization is occurred due to close collisions. The cross-section for inner-shell ionization by the impact of protons or helium ions is generally calculated using three basic theoretical methods. According to the Impulse Approximation, the ionization process of two charged particles is a Binary Encounter (BEA) and the cross-section is calculated by summing over momentum exchanges. This approximation is perfectly applicable at low projectile energy cases. On the other hand, Plane Wave Born Approximation (PWBA) is based on perturbation theory to a transition from an initial state to a final state. In PWBA, the initial state is correlated between plane wave projectile and bound atomic electron whereas final state is correlated between plane wave projectile and ejected continuum electron. When, the projectile energies are much greater than the target electron binding energies both BEA and PWBA approximations are appropriate [1]. However, the semi-classical approximation (SCA) is applied when the projectile energies are less compared to binding energies of the target atoms, where, the deflection of the projectile in the Coulomb field of the target nucleus is conducted using impact-parameters.

The cross-section of *i*th shell ionization of a target element increases with projectile energy and achieve a maximum value when the projectile velocity matches that of the ejected *i*-shell electron. Then the projectile energy E_p can be written as

$$E_P = (M/m)K_i \qquad (2.6)$$

where *M* and *m* are respectively the projectile and the electron masses. K_i is the electron binding energy.

If the projectile is proton then equation 2.6 can be written as

$$E_p = 1840\ AK_i \qquad (2.7)$$

where A is the projectile nucleon number. The cross-section decreases slowly for further increasing the projectile energy as can be seen in figure 2.3. Another

important feature can be pointed out from this figure that the cross-section decreases rapidly corresponding to increase of target atomic number.

If we consider that the ionization mechanism is direct Coulombic interaction between projectile charge and bound electron, other atoms does not take part into any interaction virtually unaltered then cross-section can be expressed easily as scaling law. Within this law, the ionization cross-section is simply proportional to the square of projectile charge. The above BEA and PWBA both models follow the scaling law. However, in practical, this law gradually stops working for ions heavier than helium. In this case, direct ionization and projectile pick-up creates multiple vacancies as a result, cross-sections and fluorescence yields both are changed radically. A detail description of the development of the ionization cross-section can be found elsewhere [12].

Johansson and Johansson [13] made a fundamental relationship of the BEA in the parameterized form

$$\ln(s_i U_i^2) = \sum_{n=0}^{5} b_{i,n} \left[\ln\left(\frac{E_p}{l U_i} \right) \right]^n \qquad (2.8)$$

where i represent K or L, σ_i is cross-sections, E_p is proton energy, U_i is K or L shell ionization energy and λ is the ratio of proton and electron masses. They also derived the value of parameters b by fitting the fifth-order polynomial to the experimental data available for protons at that time, as shown in table 2.3. This is a simplest older universal expression of ionization cross-section for proton induced x-ray emission. Akselsson and Johansson [14] derived a different set of values of the parameter b during their measurement in their own laboratory.

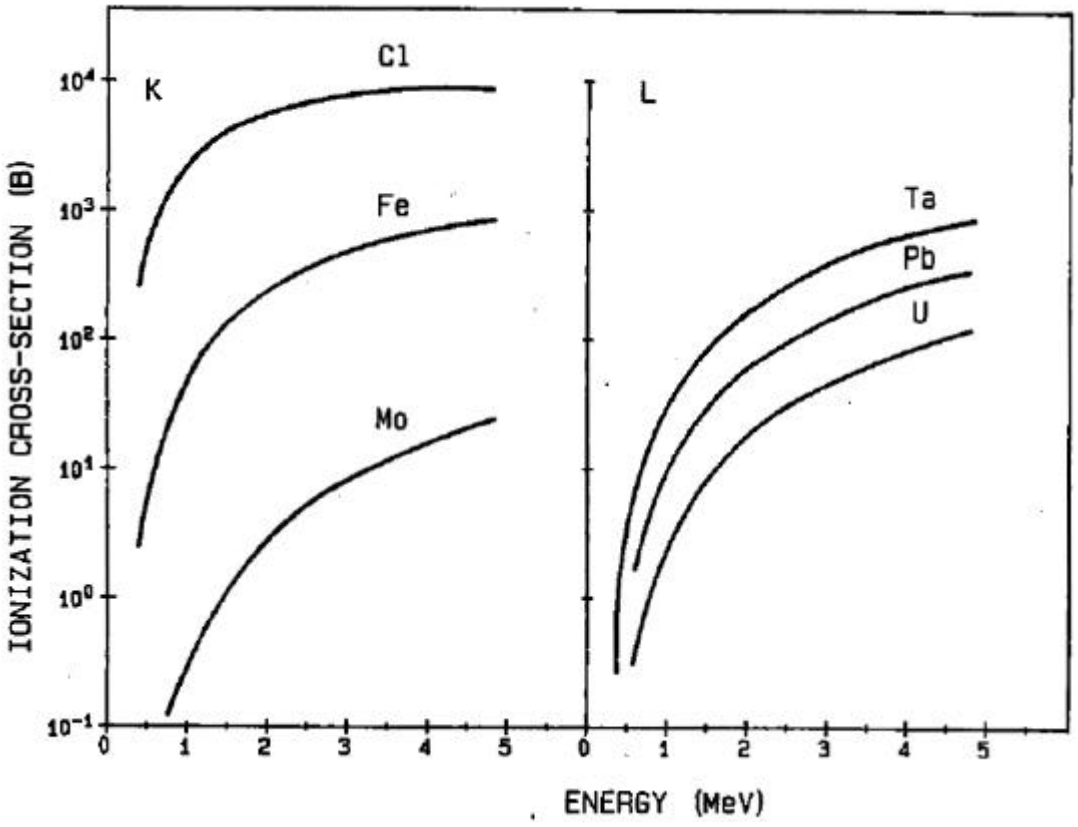

Figure 2.3: The K and L shell ionization cross-sections as a function of proton energy and target atoms. The values are the theoretical ECPSSR predictions [11].

Table 2.3: Coefficients for calculation of s_K and s_L using equation (2.8).

	K	**L**
b_0	2.0471	3.6082
b_1	-0.65906×10^{-2}	0.37123
b_2	-0.47448	-0.36971
b_3	0.9919×10^{-1}	-0.78593×10^{-4}
b_4	0.46063×10^{-1}	0.25063×10^{-2}
b_5	0.60853×10^{-2}	0.12613×10^{-2}

2.4 Numerical Values for Cross-Sections for Ionization

Enormous measured data of cross-section for protons are available in the literature. Paul et al. [15-16] have done a vast work to test theoretical or empirical predictions for K-shell case based on exiting data. They have examined and selected from the

available data, fitted deviations from the Brandt and Lapicki ECPSSR using statistical methodology. Finally, they have generated sets of so-called reference cross-sections for five specific elements. These values with their uncertainties are compared in table 2.4 with other predictions of various theoretical and empirical treatments.

Table 2.4: Cross-sections for K-shell ionization of aluminium, copper and silver by protons.

	E (keV)	Reference [16-17]	ECPSSR theory CH [12]	JJ [14]
Al	500	6050 ± 600	6120	6247
	1000	17400 ± 1700	17000	17800
	2000	29300 ± 2900	27870	30000
Cu	500	1.623 ± 0.032	1.670	1.74
	1000	15.9 ± 0.32	16.52	15.88
	2000	96.0 ± 1.9	99.07	89.7
Ag	500	$(3.77 \pm 0.30)10^{-3}$	4.18×10^{-3}	1.63×10^{-3}
	1000	0.0829 ± 0.0066	0.0827	0.0549
	2000	0.907 ± 0.073	0.894	0.689

The values coming from older JJ method are approximately close to the reference values for aluminium and copper. Whereas values are progressively worsens for heavier elements as can be seen for silver case. The results of ECPSSR theory are well agreed with the reference value. The cross-section values coming from ECPSSR theory for K-shell ionization are generally used in PIXE.

The L-shell case is relatively more complicated than the K-shell case. It is required to convert measuring x-ray production cross-section to ionization cross-sections using L-subshell fluorescence and Coster-Kronig yield. Moreover, measurements have centered upon a rather small number of elements. Figure 2.4 shows the available measured total L x-ray production cross-sections for the gold up to 1983. This figure is taken from an extensive review article [17]. The rather large error bars and the

choice of fluorescence yield schemes make it difficult to select either of the two versions of the ECPSSR model as preferable.

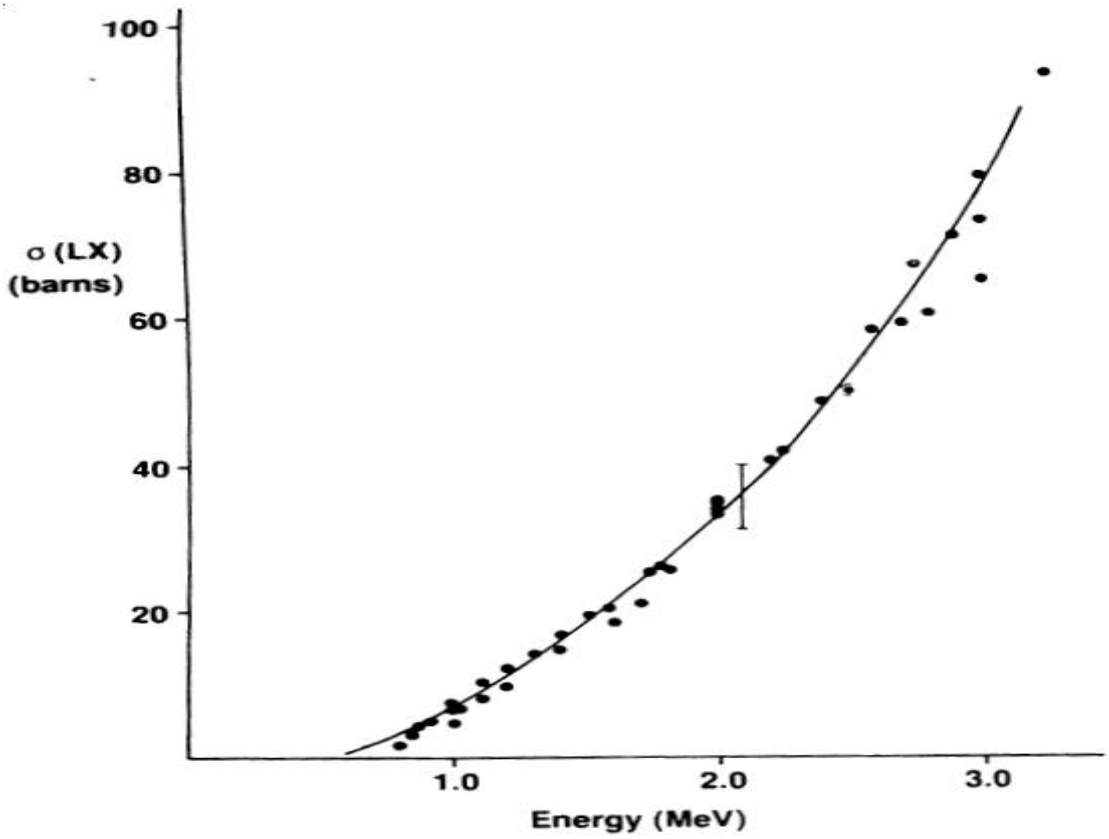

Figure 2.4: Literature values [17] for the gold L x-ray production cross-section as a function of proton energy. The curve is a quadratic fit and the error bars shown are typical quoted experimental uncertainties, i.e. at the approximately 10% level.

2.5 Background

A PIXE spectrum usually consists of two major components. One is peaks due to characteristic x-rays and second is background continuum. Figure 2.5 is a typical PIXE spectrum of a lung tissue. It can be seen from this figure that the dashed curve shows the background and solid peaks are the detected elements from the lung tissue. The background plays an important role for detecting characteristic x-rays in elemental analysis when a solid target is bombarded by heavy charge particle [18-19].

The three main backgrounds contribute in a PIXE spectrum i.e. secondary electron bremsstrahlung, primary proton bremsstrahlung and nuclear reaction gamma rays. The first one is usually most predominant. Ishii et al. [20-22] have done a large number of theoretical and experimental works of the different bremsstrahlung processes and their results indicate a good agreement between theory and measurement.

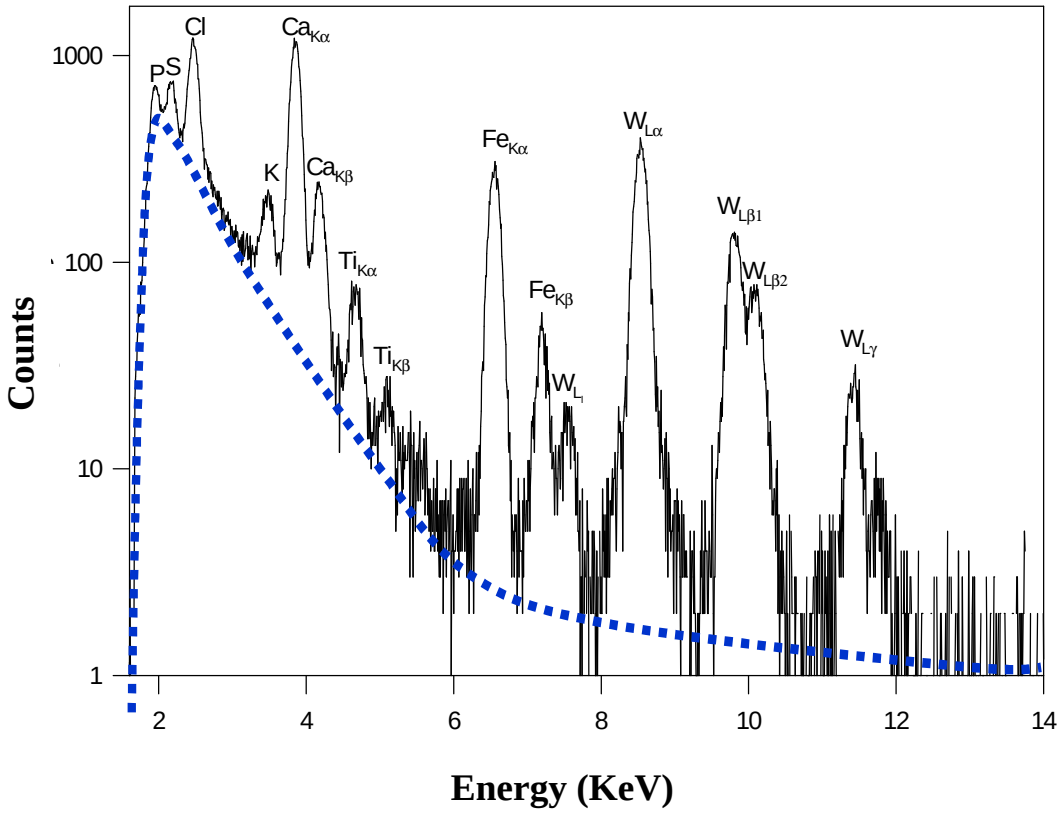

Figure 2.5: Typical PIXE spectrum of lung tissue.

2.5.1 Secondary Electron Bremsstrahlung (SEB)

Secondary electron bremsstrahlung, the major component of the continuous background comes when a target is bombarded by an incident proton which ionizes atoms along its path, ejecting electrons from the atomic shells and losing some energy in each encounter. The ejected electrons are slowing down through their interaction with the electron and the nuclei in the target, which results in the emission of so-

called secondary electron bremsstrahlung. The intensity of SEB is very strong at low energies but it decreases rapidly when the photon energy becomes larger than the maximum energy that can be transferred from a projectile to an electron. This maximum energy can be calculated by the following equation.

$$T_m = \frac{4m_e E_p}{M_p} \qquad (2.9)$$

where M_p and E_p are the mass and energy of projectile, respectively while m_e is the mass of a free electron. This bremsstrahlung is very sound below the energy of T_m but decreases speedily at higher energies.

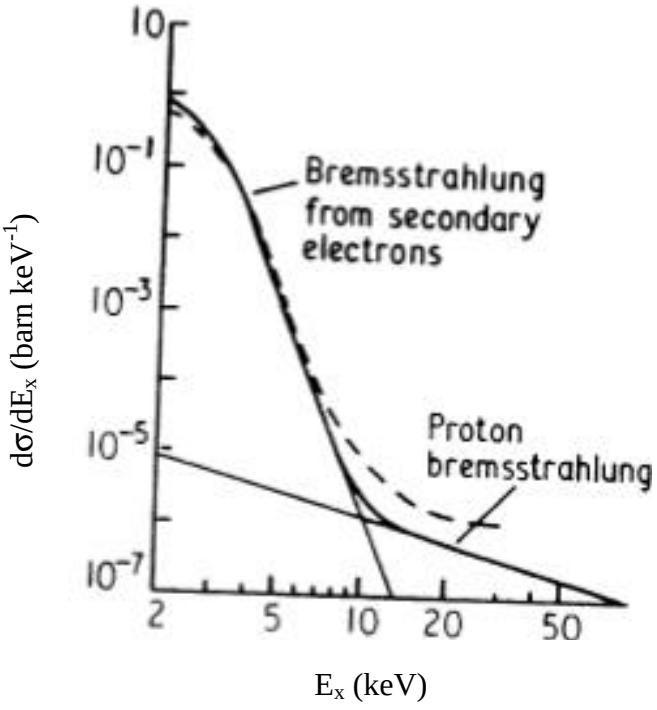

Figure 2.6: Background radiation spectra at 90^o expressed as differential cross-section dependence on photon energy E_x using 2 MeV protons on carbon. The solid curve is calculated and the dashed curve is measured [23].

2.5.2 Projectile Bremsstrahlung

When the incident protons are being slowed down in the target through the coulomb interaction with the electron and the nuclei, then they also produce bremsstrahlung called proton bremsstrahlung. In classical form, bremsstrahlung intensity emitted by a charged particle is proportional to the square of its deceleration. Although the Coulombic forces of electron and proton are the same but the masses differ by a factor of 1836. As a result, the proton bremsstrahlung should be lower in intensity by a factor of $1/(1836)^2$, negligible in contrast to electron in the case of electron microscope analysis. Proton bremsstrahlung is not strong in the energy region where SEB dominates, and also decreases with energy.

2.5.3 g-ray Background

When a projectile is engaged in a nuclear reaction with a target atom, then γ-rays emission may be possible. This background depends on the particular elements present in the specimen and on the cross-sections of the reactions induced. The γ-rays interact totally by Compton scattering in the detector. In PIXE, the nuclear reactions occur in the light elements i.e. Z<20. γ-ray emission is usually seen in biological and environmental samples due to the minor elements. Folkmann et al. [19] and others [24] have shown that this background increases rapidly with use of heavier ions. A useful set of thick target gamma ray yields have been presented by Anttila et.al. [25]. γ-ray background has been extensively studied by Johansson [26] for organic samples consisting of mainly carbon, nitrogen and oxygen.

2.6 Experimental Method

PIXE facilities in most of the laboratories are assembled by commercially available parts. A simple block diagram of PIXE setup consists of basic three parts as shown in figure 2.7, a collimator, a target chamber with sample stage and detector, and a faraday cup. However, the demand of especial analysis can make a different arrangement of the setup. Raising application of micro-PIXE has a specific arrangement where the major concerning part is beam size. Typically the beam size

for micro-PIXE is several micro meter in diameter. Producing of micron size beam has been followed by different methods in the several laboratories in the world. On the other hand, external PIXE has a great feature for analysis of liquid and large samples those are not compatible to analysis in the vacuum chamber.

The collimator usually is placed before the specimen chamber which reduces the size of the incoming beam according to its diameter. The choice of collimator material is generally graphite or tantalum compared to aluminum or steel due to low intensity of γ–rays.

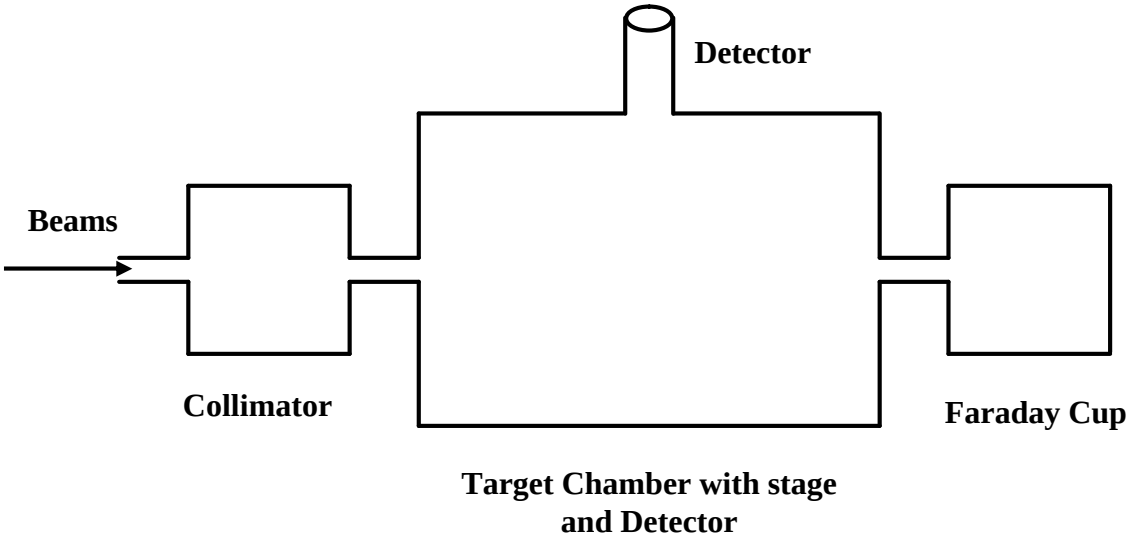

Figure 2.7: Basic block diagram of a PIXE setup.

The target chamber can be made by either steel or aluminium with a simple design. Sample holder, x-ray detector and integrated current measurement arrangement are needed in the chamber. Chamber should have the facility for multi-target treatment and usually a computer control sample stage is used which enables to move the sample holder to fix the target for irradiation. It must also have sufficient space to place an absorber in front of detector measurement. High vacuum is not essential but should keep the pressure roughly 10^{-3} torr [27] which is enough to typical PIXE

analysis. The x-ray detector generally places at either 90^o or 135^o to the beam direction. The detector geometric efficiency is prominent where the target is thin with trace elements at very low concentration. The detector is preferably placed at 135^o to the beam direction. A simple geometry of 135^o position of detector to the beam line is shown in figure 2.8.

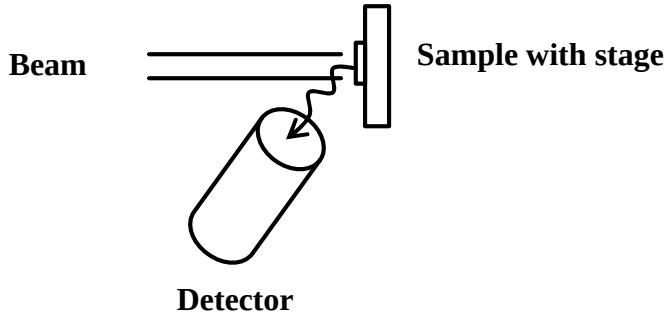

Figure 2.8: Geometry of 135^o position of detector to the beam line.

The characteristic x-rays come to the detector from the target through a window which is made by beryllium material with a thickness of several micro meters. The thinnest possible window of the detector is needed for allowing K x-rays of the light elements below atomic number 20. Whereas a windowless Si(Li) detector can be used to detect very light elements such as Fluorine and Boron etc. A large intensity of proton may be scattered from the thick target of high atomic number towards the beryllium window and when this intensity exceeds the threshold energy of nuclear reaction, an unexpected high background is generated. The general condition for designing a good target chamber is that the x-ray detector should be placed as near as possible to the target with minimizing both x-ray and γ–ray background. Typical distances between target and detector are 10-40 mm where the solid angles will be 0.0014-0.02 steradians.

The electron bremsstrahlung at low energies is occurred for huge count rate in the Si(Li) detector, therefore causes the bad resolution and increases dead-time. This bremsstrahlung problem can be reduced using a suitable absorber. Another difficulty

is often seen for detecting trace elements in the target matrix due to the high counting rate of the major elements. In this case, a choice of selective absorber can reduce the intensity of the major elements with low attenuation for the x-rays [28-29]. Generally, an absorber is placed between the detector and the target. However, it can be pointed out that the thickness of the absorber is very important and have to choose carefully otherwise it will block the expected low energy x-ray. Though it is quite difficult to choose the material of the absorber but it typically depends on the target matrix and the element of interest. Mylar film of 100-500 μm is widely used as a common absorber material for 2-3 MeV protons. A so-called "funny filter" is another approach of the absorber which has been originally introduced by Harrison and Eldred [30]. A hole at the center of the absorber is called funny filter. The area of the hole is about one-tenth of the detector active area [27]. As a result, the low energy x-rays intensity is dramatically reduced due to the reduction of the detector solid angle. However, it also allows a significant number of low energy x-rays to the detector with a reasonable count rate. The x-rays of heavier elements are unblocked by the absorber due to their relatively high energies. An elaborated description of funny filter can be found elsewhere [31].

2.7 Beam Charge Measurement

The measurement of accumulated beam charge for thin target is quite simple. This charge can be determined by integrating the incident current passing through the target. Usually, a Faraday cup of graphite is used to collect the beam current, placed behind the target. On the other hand, it becomes little bit complicate for thick target and secondary electron also may create trouble for collecting accurate charge. The conventional PIXE uses several tens of nanoamperes current whereas several picoamperes current is used in micro-PIXE. The secondary electron emission may interrupt to measure accurate current. The ratio of secondary electron to the incident proton differs noticeably among the elements [32]. The use of negatively biased secondary electron suppressor [33] can improve the measurement of current. Improper suppressor makes error in the measurement of x-ray yield per unit charge. For quantitative analysis, accurate measurement of the total charge delivered to a

target is important. In PIXE, the typical beam currents are 1-50 nA, delivered to a target of areas of few square millimeters.

The large chambers used in PIXE are often sensitive to electrical interference. Such kinds of chambers can generate spurious current integrator reading due to capacitative pick-up. These are not major problems in conventional PIXE where several tens of nanoamperes current are used, but they are very serious in microbeam work or thick target PIXE where currents of 1 nA or less are typical. It is required a good grounding of all components inside the chamber even the entire chamber to avoid these problems. Figure 2.9 shows an approach of thick target PIXE facility at the Guelph. The specimen holder is mounted on an insulating stand-off and the holder is also surrounded by a cylindrical suppressor electrode within the target chamber. Moreover, the chamber itself is grounded to a heavy copper bar connected to the main laboratory ground. Therefore, chamber acts as a Faraday cage. This system provides very accurate measurement of the typical integrated charges of a few microcoulombs enough to PIXE analysis of thick target.

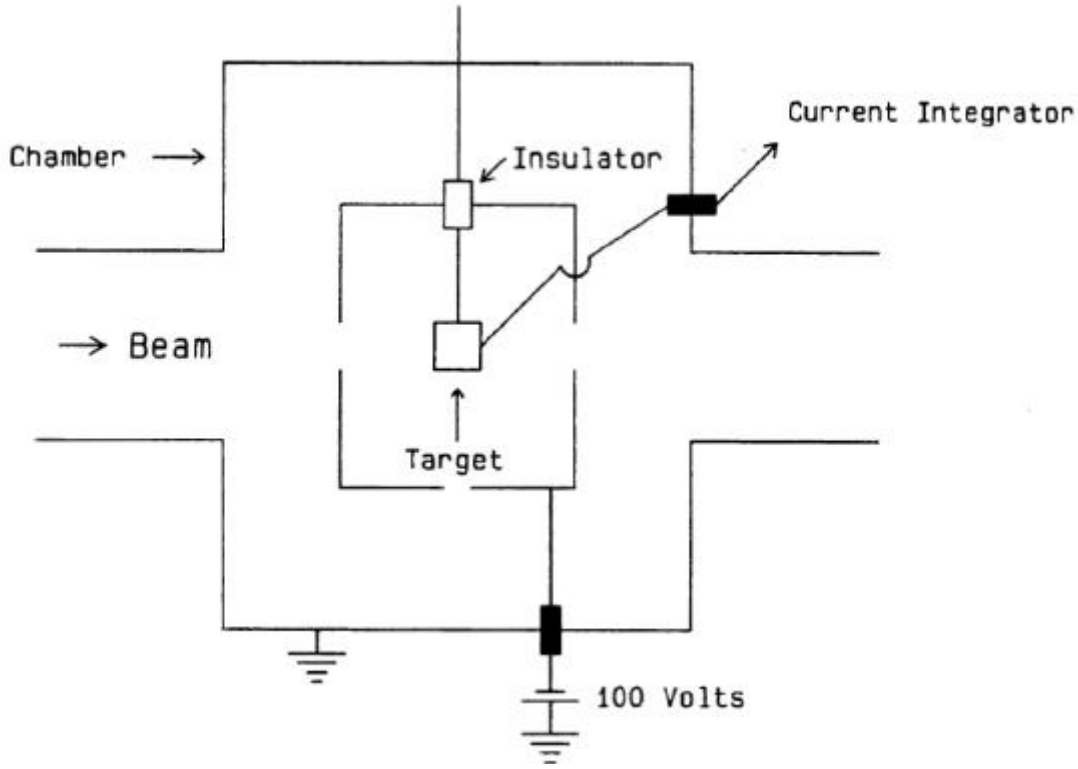

Figure 2.9: Arrangement to minimize electrical interference in charge integration on a thick target.

An insulating specimen especially a thick one makes another problem. It charges up during bombardment. The resulting periodic discharging to the nearest conductor produces bursts of bremsstrahlung. As a result, a huge background is seen in the Si(Li) spectrum. The direct measurement of the integrated charge reaching the insulator is not possible for this case.

Several approaches are available to solve this problem. The specimen coating with a conducting carbon film has been extensively used in PIXE analysis of mineralogical specimens [34]. The graphite powder can be added to a powder specimen prior to palletizing under pressure. Another approach is to use helium gas into the chamber. This approach is very effective in the context of non-vacuum PIXE. The other widely used method is to spray the specimen with an electron current sufficient to maintain neutrality. The thin metal or carbon foil is placed before the specimen to accomplish this very simply. An elegant demonstration using a 40 $\mu g/cm^2$ carbon foil placed 1 cm before a thick CaF_2 insulation target has been reported by Chaudhri and Crawford [35].

2.8 Target Preparation

The targets in PIXE analysis are generally classified in two categories such as thin and thick target. A fraction of beam energy is decreased by thin target during transition through it whereas beam stops entirely for thick target. The characteristic x-rays yield of any element in the target can be calculated by the ionization cross-section at the incident proton energy for thin target. On the other hand, an integration of over all proton energies from incident energy down to zero is desired for thick target. The surface of the thick target should be flat and smooth. The characteristic x-ray intensity is reduced in non-smooth target relative to the x-ray attenuation length in the target. The detail discussion regarding smoothness of the target has been found in literature [36]. The smooth surface of the target is assumed as a homogeneous elemental distribution within the target. Inhomogeneous target creates uncertainty in the analysis. Some targets are bulk form and also inhomogeneous, need chemical

treatment or physical reduction prior to analysis. A backing substrate is used to prepare the target. The backing foil should have some features such as high mechanical strength, good electrical and thermal conductivity, high purity, resistance to high beam intensity and non-reactivity with target material itself. Here we will concentrate our discussion about the target preparation in the light of thin target only due to use of thin target in this research.

Two cases should be considered during the target preparation that the target either larger or smaller as compared to the beam size which can be seen in figure 2.10.

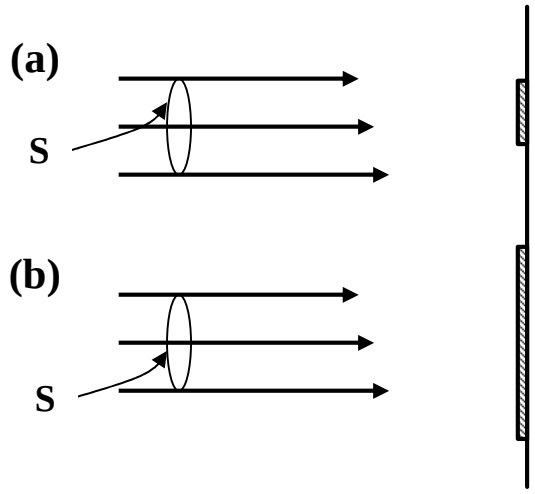

Figure 2.10: Relation between target and beam size.

If the target size is smaller compared to beam cross-section area and wholly covered by beam then the yield of characteristic x-rays can be determined by

$$Y_z = \left[\frac{s_z w_z b_z e_z N_{AV}}{A_z}\right]\frac{NM_z}{S} \qquad (2.10)$$

where s_z is the ionization cross-section, w_z and A_z are the fluorescence yield and mass of the concerned element, respectively, b_z the fraction of K or L x-rays that

appears in the K_α or L_α line, e_z the absolute detection efficiency, N_{AV} the Avogadro's number, N the number of incoming ions on the target, M_z the desired concentration of the element and S the cross-section area of the beam.

However, if beam cross-section is smaller compared to target size and covered a portion of the total target area then the yield of characteristic x-rays can be determined by the same equation only written in terms of the mass per unit area

$$M_a = M_z / S \qquad (2.11)$$

The so-called thin target sensitivity can be written as from equation 2.10

$$K_z = \left[\frac{s_z w_z b_z e_z N_{AV}}{A_z} \right] \qquad (2.12)$$

The unit of the sensitivity is $\mu g/cm^2$.

Therefore using equation 2.11 and 2.12, equation 2.10 can be written as

$$Y_z = K_z N M_a \qquad (2.13)$$

This equation is independent of whether the beam wholly covered the target or vice versa.

In PIXE analysis, target is measured followed by either external or internal standards technique. In the first case, using a pipette a droplet of standard solution is taken onto a thin backing foil and allows drying which will bear a known mass. This is then irradiated by ion beam as in figure 2.10(a) and measured the x-rays yield. However, the beam cross-sectional area also has to be measured in this case. This measurement will provide the sensitivity curve which can be denoted as the calibration of the PIXE system. The sensitivity curve should have the better accuracy, to do that a large number of measuring points should be taken. After that same procedures are followed to prepare the desired target and the measurement of the x-rays yield. Therefore, the unknown concentration of the desired target can be determined using the sensitivity curve. The droplet of the standard solution may be able to form the crystal on the backing, rather than the desired uniform deposit is the drawback of such kind

standard. The published literature [37] demonstrates that the uniformity of the target can be improved by adding a commercial liposome solution. In the second alternative approach, one element can be added to the target matrix in such a way that it can distribute uniformly within the matrix. After determining the sensitivity curve, the concentration of unknown target can be calculated using following equation

$$\frac{Y_z}{Y_s} = \frac{M_z s_z w_z b_z e_z A_s}{M_s s_s w_s b_s e_s A_z} \qquad (2.14)$$

where M_s is the mass of the present internal standard. In this equation, the masses represent the concentration.

Using equation 2.12, equation 2.14 can be simplified as

$$\frac{Y_Z}{Y_S} = \frac{M_Z K_Z}{M_S K_S} \qquad (2.15)$$

where K_Z and K_S are the sensitivity for unknown and internal standard sample, respectively.

2.9 Backing for Thin Specimens

Generally in PIXE analysis, thin targets are prepared by depositing small amount of material on a thin backing or support foil. The target material might be powder or a microtome slice or a liquid deposit. The material is dried leaving a solid residue for analysis. The thinnest possible backing foil is the best in order to minimize bremsstrahlung background. The elemental components of the backing should have the lowest possible atomic number so that it can minimize both the energy and the bremsstrahlung intensity. An additional think should be considered that it contributes no characteristic x-rays to the observed spectrum. Russell et.al. [38] has published a review article of most of the backing foil used in PIXE including their trace elements.

The vast majority PIXE analysts use commercially available polymers as a backing foil. The most widely used polymer was Mylar in the earlier days of PIXE and still remains popularity on account of its widespread availability. However, in comparison with Kimfol, Mylar shows much more elements at higher energies in the continuous spectrum as shown in figure 2.11. Therefore, Kimfol was accepted by a large number of PIXE groups.

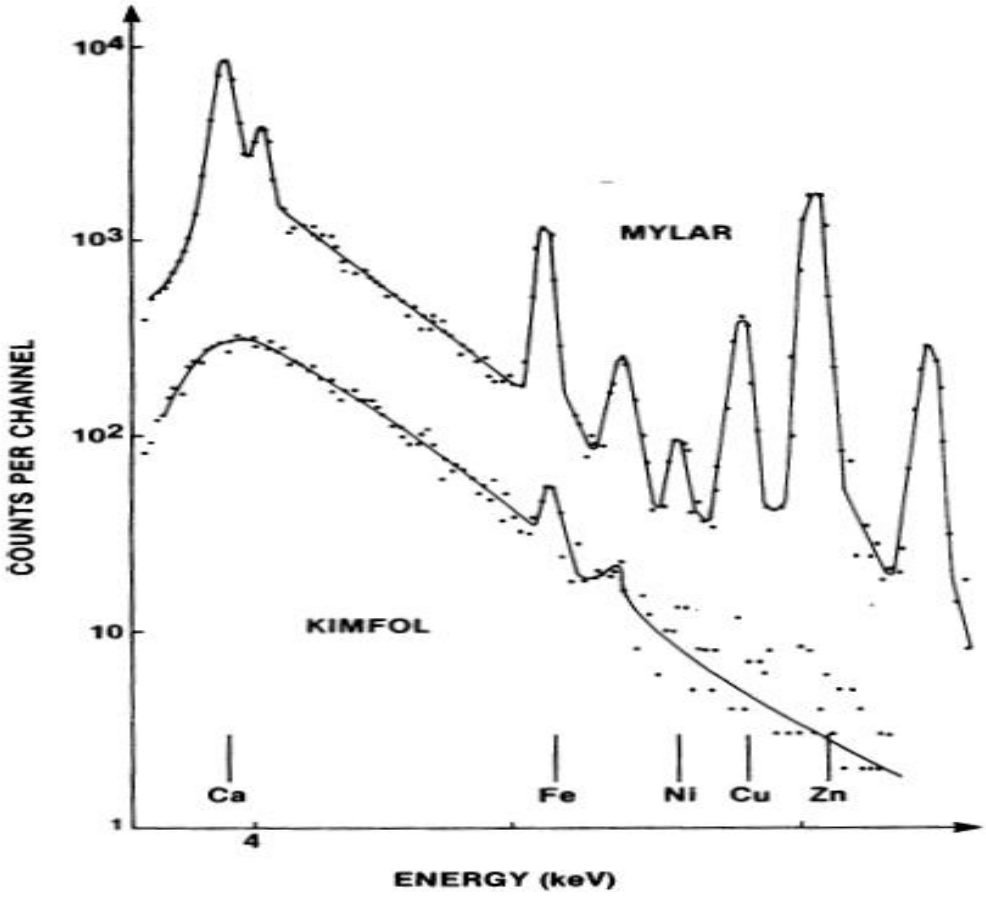

Figure 2.11: PIXE spectra [38] from backing foils of Mylar (1.06 mg/cm^2) and Kimfol (0.24 mg/cm^2).

Thin carbon foils are resistance to acid solutions and provide greater heat dissipation to the polymers. In order to improve thermal and electrical conductivity, polymers are sometimes coated with aluminium but this is not attractive because the process is time consuming and can introduce impurities.

References

[1] S. A. E. Johansson and J. L. Campbell, PIXE: A novel technique for elemental analysis (John Wiley & Sons, Chichester, 1988).

[2] W. Bambynek, B. Crasemann, R.W. Fink, H.U. Freund, H. Mark, C. D. Swift, R.E. Price and P. Venugopalo Rao, Revs. Mod. Phys., **44**, 716 (1972).

[3] M.H.Chen, B. Crasemann and H. Mark, Phys. Rev., **A21**, 436 (1980).

[4] E. Buyukkasap, Spectrochimica Acta Part B: Atomic Spectroscopy, **53**, 499-503 (1998)

[5] V. Valcovic, Trace Element Analysis, Taylor and Francis, UK (1987).

[6] J. A. Bearden, Revs. Mod. Phys., **39**, 78 (1974).

[7] J.H Scofield, Phys. Rev., **A9**, 1041 (1974).

[8] H.H. Andersen and J.F. Ziegler, The Stopping and Ranges of Ions in Matter, Vol. 2, Pergamon Press, New York, (1977).

[9] J.F. Ziegler, J.P. Biersack and U. Littmark, The Stopping and Ranges of Ions in Solid, Vol. 1, Pergamon Press, New York, (1985).

[10] C.V. Sheth, Physical Review A, **29**, 1151 (1984).

[11] D.D. Cohen and M. Harrigan, At. Data and Nucl. Data Tables, **33**, 255 (1985).

[12] H. Paul (ed), Proceedings of the Third Workshop on Inner Shell Ionization by Light Ions, Nucl. Instr. Meth., **B4** (1984).

[13] S.A.E. Johansson and T.B. Johansson, Nucl. Instr. Meth., **137**, 473 (1976).

[14] K.R. Akselsson and T.B. Johansson, Zeit. fur Phys., **266**, 245 (1974).

[15] H. Paul and J. Muhr, Physics Reports, **135**, 47 (1986).

[16] H. Paul, Zeit. fur Phys., **D4**, 249 (1986).

[17] R.S. Sokhi and D. Crumpton, At. Data and Nucl. Data Tables, **30**, 49 (1984).

[18] F. Folkmann, G. Gaarde, T. Huus, and K. Kemp, Nucl. Instr. Meth. **116**, 487 (1974).

[19] F. Folkmann, J. Borggreen, and A. Kjeldgaard, Nucl. Instr. Meth. **119**, 117 (1974).

[20] K. Ishii, S. Morita and H. Tawara, Physical Review A, **13**, 131 (1976).

[21] K. Ishii and S. Morita, Physical Review A, **30**, 2278 (1984).

[22] K. Ishii and S. Morita, Int. J. PIXE, **1**, 1 (1990).

[23] F. Folkmann, G. Gaarde, T. Huus and K. Kemp, Nucl. Instr. Meth., **116**, 487 (1974).

[24] A.W. Herman, L.A. McNelles and J.L. Campbell, Int. J. Appl. Rad. Iso., **24**, 677 (1973).

[25] A. Anttila, R. Hanninen and J. Raisanen, J. Radioanal. Chem., **62**, 293 (1981).

[26] S.A.E. Johansson, Int. J. PIXE, **2**, 33 (1992).

[27] I.M. Govil, Current Science, **80**, 1542 (2001)

[28] C.P. Swann, S.J. Fleming, Nucl. Instr. Meth., **B49**, 65 (1990).

[29] K.S. Sera and S. Futatsugawa, Int. J. PIXE, Vol. 5, No. 2&3, 181 (1995).

[30] J.F. Harrison and R.A. Eldred, Adv. X-ray Anal., **17**, 560 (1973).

[31] T.A. Cahill, Plenum Press, New York, 1975, p. 19

[32] K. Traxel and A. Mandel, Nucl. Instr. Meth., **B3**, 594 (1984).

[33] K. Malmqvist, G.I. Johansson and K.R. Akselsson, J. Radioanal. Chem., **74**, 125 (1982).

[34] L.J. Cabri, J.L. Campbell, J.H.G. Laflamme, R.G. Leigh, J.A. Maxwell and J.D. Scott, Can. Mineralogist, **23**, 133 (1985).

[35] M.A. Chaudhri and A. Crawford, Nucl. Instr. Meth., **181**, 31 (1981).

[36] J.L. Campbell, R.D. Lamb, R.G. Leigh, B.G. Nickel, and J.A. Cookson, Nucl. Instr. Meth., **B12**, 402 (1985).

[37] G. Robaye, G. Weber, J.M. Delbrouck-Habaru, M.C. Depauw and I. Roelandts, Nucl. Instr. Meth., **172**, 535 (1980).

[38] S. B. Russell, C. W. Schulte, S. Faiq and J. L. Campbell, Anal. Chem., **53**, 571 (1981).

Chapter Three

PIXE Experimental Setup at KUT

According to the discussion of chapter 1, it is strongly proved that the most prominent analytical method in the ion beam analysis is the Particle Induced X-ray Emission (PIXE) technique. The realization of multi-elements in a single analysis of a target makes this technique very much popular among others. This technique has been widely used to detect and quantify trace elements from several decades. In the light of several advantages of PIXE, our attention goes to use this technique and quantitatively analyze different elements that are dissolved in the target. However, there is no PIXE facility even though accelerator facility is available at the ion beam laboratory of Kochi University of Technology (KUT). Therefore, the aim of this thesis has been fixed to setup the PIXE facility at KUT and apply it in different fields.

3.1 Experimental Setup

The ion beam facility at Kochi University of Technology (KUT) in Japan has been extended to allow elemental concentrations analysis by PIXE, one of the principal goals in this dissertation. A target chamber has been designed to include a moving sample stage and can be used for simultaneous PIXE and RBS (Rutherford Back Scattering) analysis. Diameter of helium beam was reduced by collimator to 1 mm. Analyses were carried out in high vacuum around 10^{-6} torr.

A Nissin High Voltage accelerator (NT1700S) with a 1.7 MV (Maximum voltage) has been setup at the beginning of Ion beam laboratory at KUT. Helium ion was used as a charge particle. The inner diameter of the target chamber was 50 cm and a computer control sample holder was placed inside the chamber made by Aluminium therefore it can move 45^{o} in Y axis whereas 180^{o} in X axis. Sample holder scanning area of 25×25 mm^2, makes it a flexible chamber to analyze different types and couple number of samples. After irradiation, there is a possibility of secondary electron emission from the front face of the target and the number of this secondary electron per proton from the metal targets depend on the proton energies used in PIXE [1]. Most of the secondary electrons can be retarded using a suppressor electrode. Generally, a ring shape suppressor electrode with a sufficient negative potential is placed in front of target. Malmqvist et al. [2] and Nsouli et al. [3] have reported that the biasing negative potential of their system was 50 and 400 V, respectively. In our case this electrode was made by tantalum with a bias voltage of -250 V and was located in front of target. The applied current was measured from the sample holder using a current integrator.

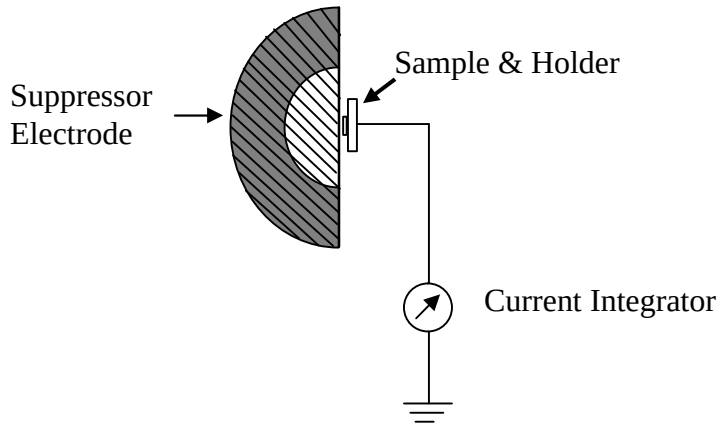

Figure 3.1: Sketch of suppressor electrode position.

Figure 3.2: Photograph of Accelerator at KUT.

Figure 3.3: Photograph of target chamber.

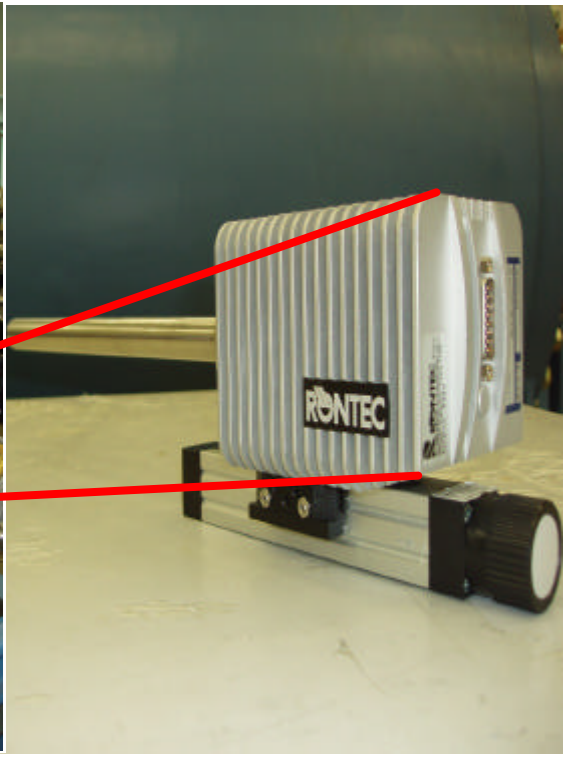

Figure 3.4: Photograph of X-ray detector used in this dissertation.

RÖNTEC XFlash 2001, a Silicon Drift Detector (SDD) type detector was fixed at the target chamber. This detector consists of a detector finger and a preamplifier. Both parts of this detector are directly connected. The active area and the silicon thickness of the detector are 10 mm^2 and 0.3 mm, respectively. The detector has dual thermoelectric cooler stage. The external cooling system is not required. A polymer coated beryllium window of 8 μm thickness is equipped with the detector. A zirconium ring with an aperture of 3.4 mm serves as a collimator.

XFlash supply unit with high resolution pulse processor is a complete detector supply unit including temperature control which was connected to the detector with a single cable. It has an internal pile-up rejector. The detector preamplifier and analog pulse processor output signals are available on rear panel LEMO-type connectors.

The ORTEC Model 572 Amplifier is a general-purpose spectroscopy amplifier that offers excellent performance which was connected to the pulse processing unit. This amplifier was used for its low noise, wide-gain range and selectable shaping networks.

The output of the ORTEC 572 amplifier was then connected to a computer via an analog to digital converter (ADC) and a multi-channel analyzer (MCA).

3.2 Data Acquisition

Prior to the experimental works in this dissertation, data acquisition and data analysis system was setup in the ion beam laboratory of Kochi University of Technology, dedicated to PIXE experiments. The data acquisition system should have the facility to improve multiple-parameter data-acquisition, on-line data visualization and monitoring which enable a wide range of ion-beam experiments. To achieve this goal, it was decided to design the system based on the existing hardware and software. In this work, the existing hardware's were configured into two ways for data acquisition system: a front-end computer with MCAWIN software system for monitor and real-time data-acquisition, and a back-end system for data collection from the detector via processing unit, pre-amplifier and multi-channel analyzer (MCA). The transportation

of data from the back-end to the front-end system is controlled by the front-end system.

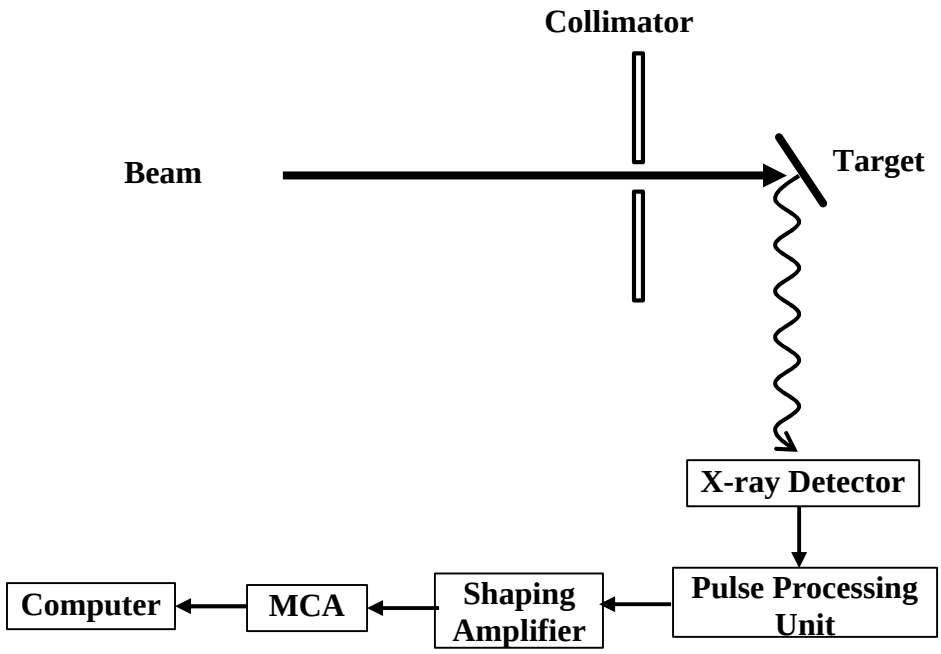

Figure 3.5: Block diagram of data acquisition system.

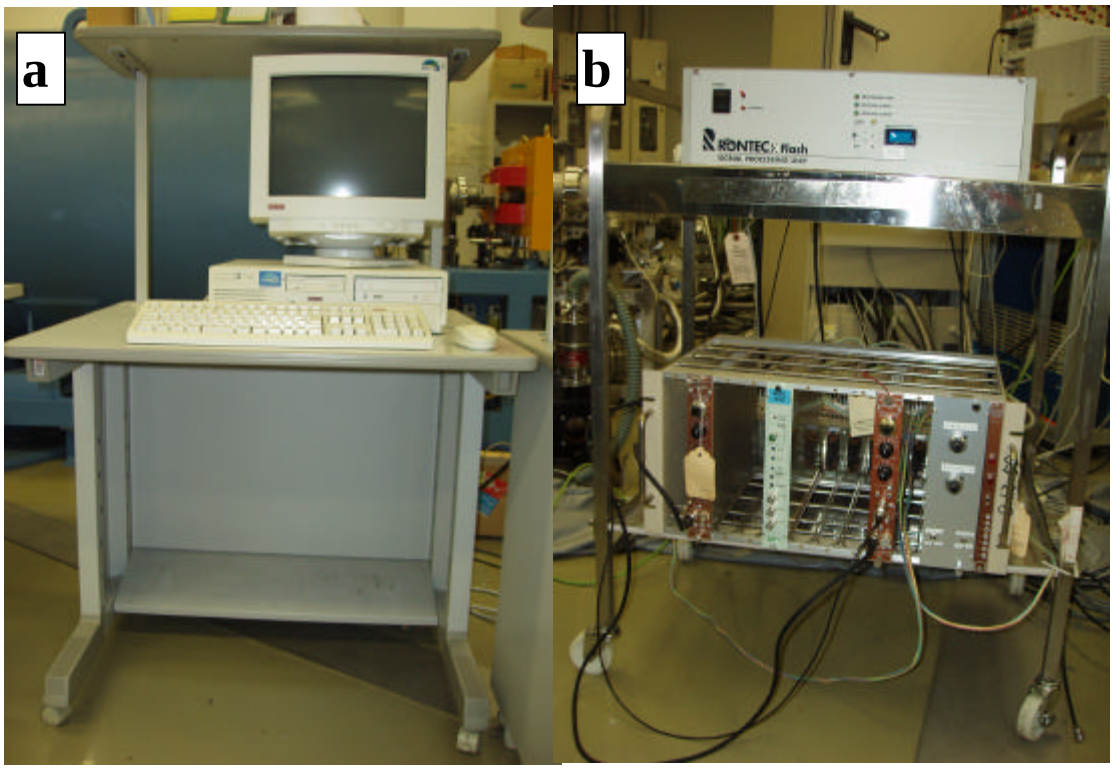

Figure 3.6: (a) Computer panel, (b) Pulse processing unit and shaping amplifier for data acquisition system.

Block diagram of data acquisition system is shown in figure 3.5. From an experimental point-of-view, energy calibration, peak shape, detector efficiency, escape peak, pile-up rejection, dead time correction and limit of detection also have to be considered in the data acquisition system, described briefly bellow.

3.2.1 Energy Calibration

An electronic detector system when it is designed, linear relationship feature is followed between the ion energy and the charge signal created in the detector. If we consider a pulse-height spectrum containing *i*th peaks for the ions of energies E_i, the centroids (Y_i) of the peak can be written by the following expression

$$Y_i = X_a + X_b E_i \qquad (3.1)$$

where X_a and X_b are constants. The centroid of a specific peak may be shifted due to high x-rays count rates, the linearity should be maintained by adjusting the value of parameters. Maenhaut and Vandenhaute [4] have reported that a third term which is exponential in photon energy is required to confirm exact calibration from about 2 to 30 keV. In the pulse processor systems, the amount of peak shifting is very small is about 1 eV at a rate of 100000 counts per second. Using the knowledge of the above equation it was done the energy calibration of the system shown in figure 3.7.

The width of any peak depends on applied energy, expressed as standard deviation of the Gaussian:

$$s_i = \left[X_c + X_d E_i\right]^{1/2} \qquad (3.2)$$

where X_c and X_d are two other constants. The values of these constants can be determined by least-squares fitting of the PIXE spectra of a small number of pure elements.

The energy resolution of any system is usually denoted as the full width at half-maximum (FWHM) of the Gaussian which is mathematically expressed by

$$\Delta E = 2.35s \qquad (3.3)$$

But it is strictly restricted for a single line at a given energy. However, it was considered in this dissertation that the energy resolution is 5.9 keV for manganese K_α line, this is a general practice for energy calibration which is easily acquired from the long-lived radionuclide ^{55}Fe. The choice of manganese K_α line due to the small separation of 11 eV between the K_α and K_β line which is negligible for the system rather than the large separation of 173 eV for choice of silver. Nevertheless, the energy resolution of a system depends not only on the detector but also on optimal shaping time and other features of ADC/MCA.

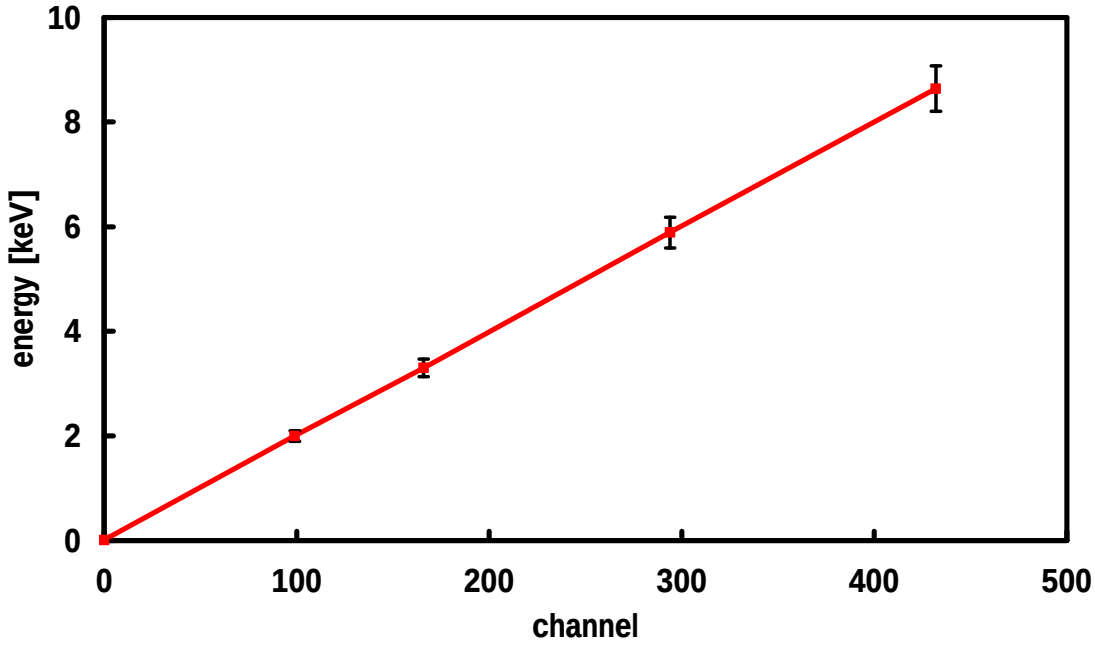

Figure 3.7: Energy calibration curve for PIXE analysis with XFlash 2001 detector.

Figure 3.7 clearly shows the linearity of energy calibration as a function of channel of the desired system with a five percent uncertainty represented by the error bar. The K x-ray line of Phosphor and Manganese are shown in figure 3.8 with indication of background level. This spectrum was used for energy calibration. It can be seen from

this figure that the system was calibrated as 20 eV per channel, i.e. Mn K_α at 295 channels.

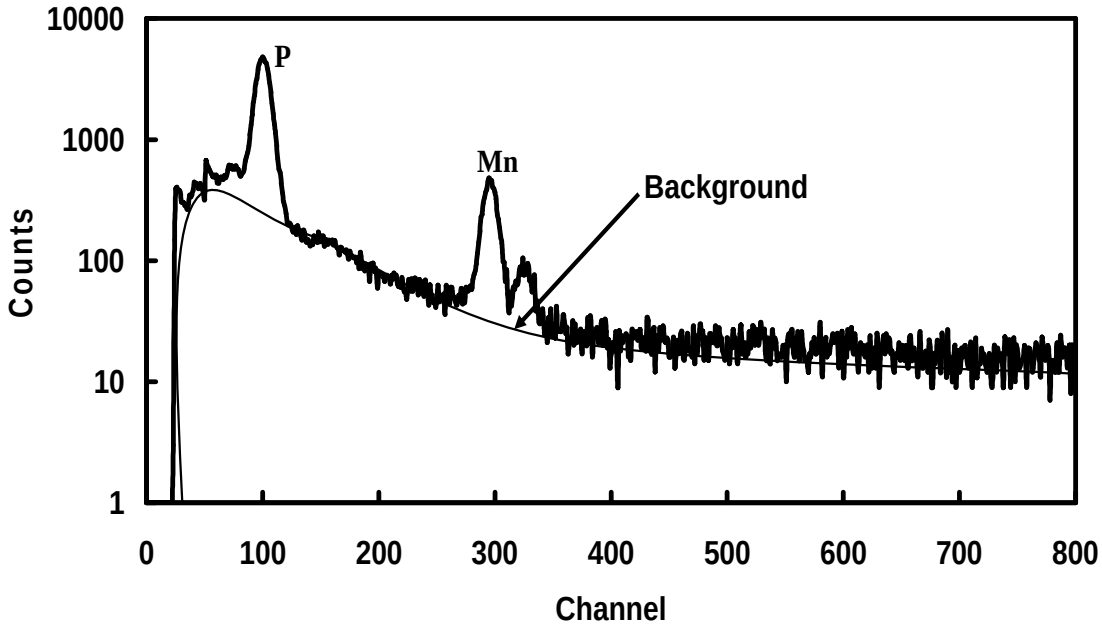

Figure 3.8: K x-ray spectra of Phosphor and Manganese for energy calibration.

3.2.2 Peak Shape

Many spectrum fitting procedures generally use a mathematical consideration for the peak shape. But the real x-ray peaks in Si(Li) spectra clearly show tailing features on the low-energy side. If these features are ignored and a Gaussian approximation is used for the lineshape, then the low-energy tails can cover-up as a set of x-ray lines of other elements. Several effects involve to this tailing feature, some internal to the detector and some external. The detector peripheral plays an important role for tailing as a source of internal artifacts. Therefore, the detector is often collimated either internally by the manufacturer or externally by the user. Surface dead layers of the detector and other imperfections influencing the charge collection process are the other reasons of tailing. The intensity of this tail relative to the overall peak area decreases very speedily with increasing photon energy. The lineshape can be predicted using Monte Carlo simulation of the charge creation and collection process

[5] in terms of basic parameters such as geometry, charge loss mechanisms in the frontal dead layer and in imperfect regions within the bulk crystal.

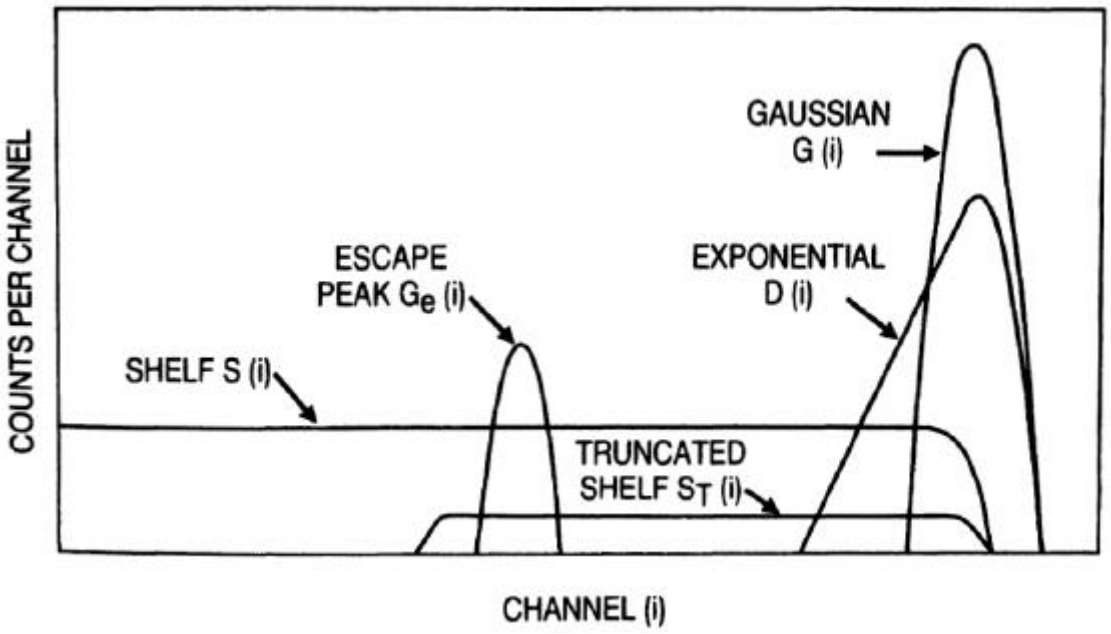

Figure 3.9: Components of lineshape of Si(Li) detector.

The contribution of these tailing features is maximum for x-ray energies just above the silicon K-edge energy i.e. 1.74 keV due to the photon interactions on the front surface of the detector. The tailing feature shows a quite different nature in at about 15 keV where it increases rapidly with increasing x-ray energy due to Compton scattering into the detector of x-rays [6]. Figure 3.9 shows the components of lineshape of Si(Li) detector. The flat and exponential features are clearly indicated by this figure. These features arise both from incomplete charge collection due to the increased defect concentration near the front surface of the detector and also from partial escape of photoelectron and Auger electron from the sensitive region of the crystal. From the above discussion, it is clear that the analysts should have sufficient knowledge regarding tailing features and should minimize these as much as possible.

3.2.3 Detector Efficiency

The detector efficiency is the product of the geometric efficiency which depends on the solid angle fraction and the intrinsic efficiency of the crystal. The intrinsic efficiency depends on the ratio of full-energy peak intensity to that of photons incident upon the crystal. The absolute efficiency of a Si(Li) detector can be calculated by following equation

$$e = \frac{\Omega}{4p}\left(\exp\left[-\sum_{i=1}^{3} m_i d_i\right]\right) f_{esc}\left[1-\exp(-m_{Si}D)\right] \qquad (3.4)$$

where Ω is the geometric solid angle as a function of $4p$, m_i is the attenuation in the various elements in front of the silicon crystal, f_{esc} is the loss of events via silicon K x-ray escape and D is the fraction of photons stopped in the bulk of the crystal. The absolute efficiency curve from about 5 to 40 keV is shown in figure 3.10. The dots are measured data and the solid curve is the least-square fitting by equation 3.4. In order to increase the efficiency of our Si(Li) detector, suitable geometry for the detector was designed considering the above parameters.

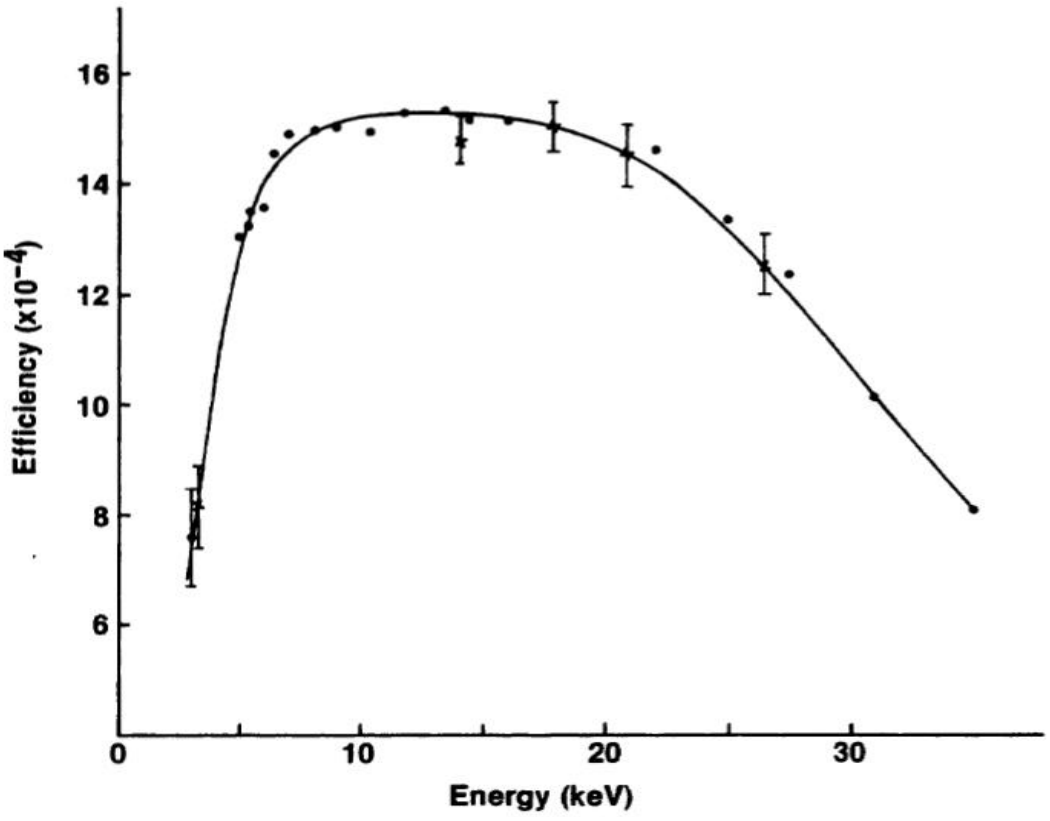

Figure 3.10: Absolute efficiency of a Si(Li) detector [7].

3.2.4 Escape Peak

In the Si(Li) detector system, each peak in a Si(Li) spectrum is accompanied by a companion peak which is displaced of 1.75 keV to the left in the spectrum. This companion peak is known as escape peak. It arises from the escape of silicon K x-rays following photo-electric interactions close to the front surface of the detector. The intensity of this escape peak is only 1% or less compared to its principal peak. The escape peak of iron K_α comes at 4.65 (6.4 – 1.75) keV which is overlapped together with titanium K_α line at 4.51 keV. As a result, it is quite important to have a better knowledge about the escape peak during the analysis of the PIXE spectrum.

Considering a hypothesis that the incident photons are perpendicular to the detector surface then the area of escape peak can be calculated using the following equation relative to the total counts in escape plus full energy peak:

$$h = \frac{1}{2} w_k (r-1)\left[1 - \frac{\left(m/r\right)_{Si}}{\left(m/r\right)_i} \ln\left(1 + \frac{\left(m/r\right)_{Si}}{\left(m/r\right)_i}\right)\right] \qquad (3.5)$$

where the silicon K fluorescence yield is ω_k, the jump ratio of K absorption edge is r, the photon mass attenuation coefficients for the incoming photon energy and the silicon K x-ray photons are $\left(m/r\right)_i$ and $\left(m/r\right)_{Si}$, respectively. Therefore, escape peak to parent peak intensities ratio is $h/(1-h)$.

Some uncertainty in the values present in equation 3.5. In practice, however, the displacement of escape peak is several electron-volts greater than 1.75 keV. Therefore, if very high accuracy is needed, it may be better to measure for a particular system and then to least-squares-fit the resulting data. Johansson [8] used a simple model employing the attenuation coefficients of the incoming x-ray and the silicon K x-ray in the silicon crystal. Her result agrees well with the prediction.

3.2.5 Pile-up

Pile-up, another considerable matter is the possibility of two photons entering the detector within an extremely short time interval and recorded as a single event. The resolving time in typical system for identifying two pulses (events) is a few hundred nanoseconds, events occur within smaller time than this value will not be identified. As a result, distorted pulses will appear. It is a difficult problem for identifying the exact peak due to the pile-up often found in PIXE spectra. It has also the probability to overlap with other peaks like escape peaks. For instant, the pile-up peak of iron K_α (2 x 6.4 keV) overlaps with the lead K_β line at 12.5 keV. This problem can be eliminated using an electronic pile-up rejector (PUR). The PUR receives the pre-amplifier pulses, sends them through a fast amplifier and generates time markers by triggering a fast leading-edge discriminator set just above the noise level. If one marker follows another within a preset time then a veto signal is generated to enable rejection of the corresponding main amplifier pulse.

XFlash pulse processor unit used in this dissertation is integrated with such kind of pile-up rejector. The TTL strobe signal is used for utilization of the internal pile-up rejector. Jaklevic et al. [9] proposed an alternative method to reduce this effect using a pair of conducting plates biased with high voltage (~2kV) placed about 1 m upstream from the target and was implemented by Thibeau et al. [10].

3.2.6 Dead Time Correction

In the data acquisition arrangement of detector-amplifier-ADC, the duration of an analysis can be realized in real time or in live time. Usually when an analog to digital converter (ADC) is digitized an event (in live time case) at that time the pulse height analyzer timing unit is blocked, the main reason of dead time. Some other reasons are involved such as amplifier processing time, longer periodic reset time and pile-up rejection circuitry. The dead time is determined by the difference between the real time and live time. The live time can be recorded directly from the intensity of the resulting peak by adding a 50 or 60 Hz pulser in the system during the measurement. Another approach, however, using pulse-height analyzers, any external dead time

may be recognized simply by feeding the “busy” signals from amplifier and pile-up rejector to the “busy” input of the analyzer. This procedure allows the system to take account of whatever external dead times are associated with an event.

In our system, it was used a Labo multi-channel analyzer (MCA) and an ADC. The dead time of the system was adjusted by changing the LLD and ULD in the ADC controlling by software. The value of the dead time was kept about 5-10% during the measurement. Several literatures [11-13] have reported that the dead time of their system was about 5-10%.

3.2.7 Limit of Detection

When the x-rays intensity become larger than that of three-standard-deviation of the underlying background then that peak can be considered for analysis, denoted as Limit of Detection (LOD) and the intensity is usually integrated over at least one full width at half maximum (FWHM) of the peak. It is important to remember that the gamma ray emission of specific trace elements such as fluorine or sodium must be excluded from the peaks but in practical, these peaks are obviously overlapped with other neighboring peaks. In early stage of PIXE development, some criterions were considered to measure the instrumental detection limit (IDL) for an isolated x-ray peak in a spectrum, discussed briefly in below.

The x-ray peak height and the background height should be equal at the same location.

the peak area and the background area should be equal within one or two FWHMs.

the peak area exceeding a defined number is not useful if the background is much greater than that number.

the x-ray peak area exceeds the statistical uncertainty of the background count in the same spectral region at a defined confidence level.

An elegant discussion of limit of detection has been presented by Keith et al. [14]. Limit of detection is obviously proportional to the solid angle. This can also be improved inversely as the square root of collected charge, which can be increased either by a longer measurement time or by an increase in the beam current. Another important discussion regarding LOD for biological sample can be found elsewhere [15]. In the light of above discussion the minimum detection level of our system has been performed and described in chapter 5.

3.3 Data Processing

A spectrum is visualized at the front-end panel of the data acquisition system after irradiation a target with sufficient ion energy. This spectrum can be stored in the computer memory for off-line analysis after completing the experimental works. PIXE spectrum usually consists of basic two parts, background and signal peak of specific elements. The signal peak is a Gaussian shape. A brief discussion of background including reasons is explained in section 2.5 in Chapter 2. The analysis of the spectrum is little bit complicated due to the presence of a large number of peaks from several elements and also some of them are overlapped to each other. Table 3.1 shows some common overlapping peaks in PIXE spectra. Some precautions are needed to reduce the overlapping, as discussed in section 3.2.4 & 3.2.5. However, background intensity from the integrated intensity in the peak region should be removed at first; the full width at half maximum (FWHM) area of the remaining peak represents the intensity of specific element. Some computer software's are now available to do analysis automatically from raw data to quantitative analysis such as GUPIX, AXIL, PIXAN and Dan32 etc. These software's are developed using least-squares fit technique for the purpose of extracting exact peak areas for all elements present in the target.

In this thesis, MCAWIN software was used in the front-end panel of the data acquisition system to acquire data and also for off-line analysis. A screen print of the software is shown in figure 3.11. A region of interest (ROI) is also shown in this figure. The bottom of the figure indicates the net count of the ROI.

Table 3.1: Common overlapping peaks in PIXE spectra.

Peak		Energy (keV)
S	K_α	2.308
Mo	L_α	2.29
Pb	M	2.346
Ba	L_α	4.463
Ti	K_α	4.509
Ti	K_α	4.509
Fe	K_α (esc)	4.647
Mn	K_β	6.49
Fe	K_α	6.399
Pb	L_α	10.54
As	K_α	10.532

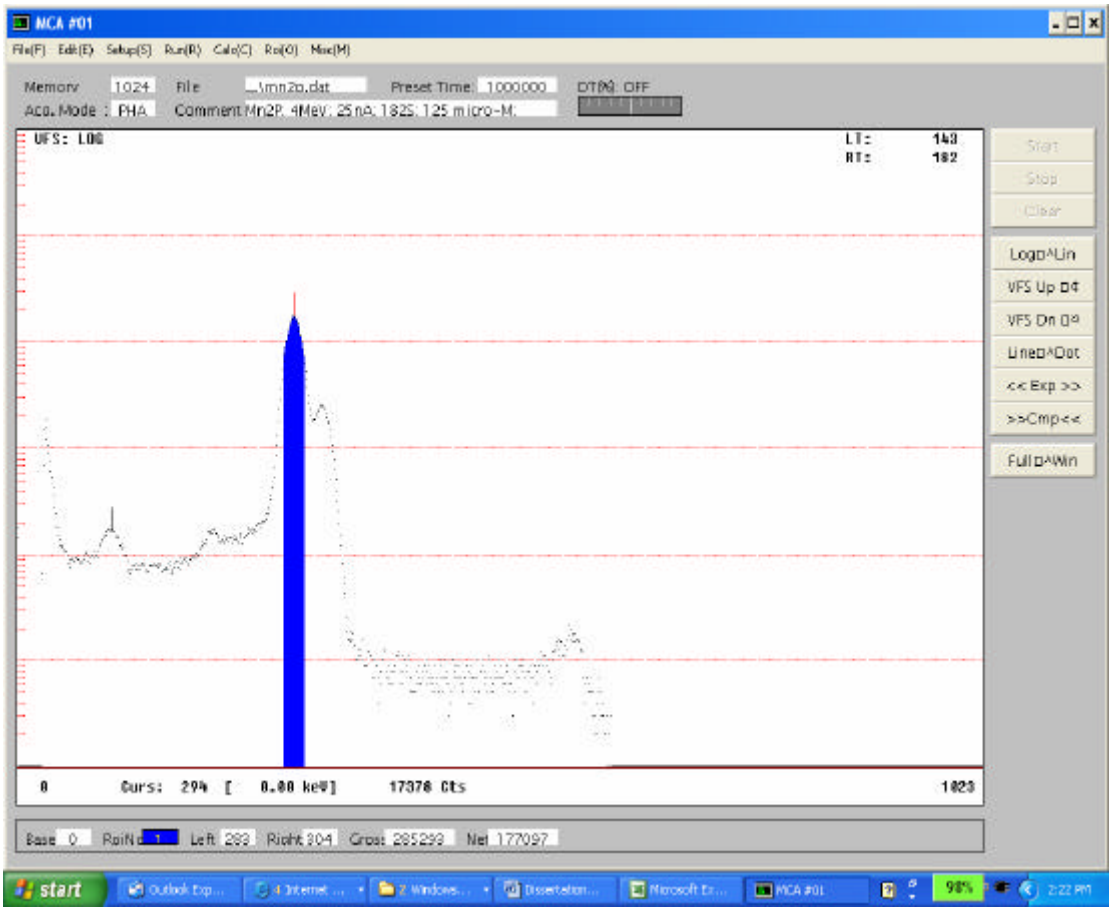

Figure 3.11: A screen print of the MCAWIN software.

References

[1] T.A. Thornton and J.N. Anno, J. Appl. Phys., **48**, 1718 (1977).

[2] K. G. Malmqvist, G. I. Johansson and K. R. Akselsson, J. Radioanal. Nucl. Chem., 74, (1-2), 125-147 (1982).

[3] B. Nsouli, T. Darwish, J. -P. Thomas, K. Zahraman and M. Roumié, Nucl. Inst.Meth., **219-220**, 181-186 (2004).

[4] W. Maenhaut and J. Vandenhaute, Bull. Soc. Chim. Belg., **95**, 407 (1986).

[5] M. Geretschlager, Nucl. Instr. Meth., **B28**, 289 (1987).

[6] J.L. Campbell, J.X. Wang and W.J. Teesdale, Nucl. Instr. Meth., **B43**, 490 (1989).

[7] J.L. Campbell and P.L. McGhee, Nucl. Instr. Meth., **A248**, 393 (1986).

[8] G.I. Johansson, X-ray spectrum., **11**, 194 (1982).

[9] J.M. Jaklevic, F.S. Goulding and D.A. Landis, IEEE Trans. Nucl. Sci., **19**, 392 (1972).

[10] H. Thibeau, J. Stadel, W. Cline and T.A. Cahill, Nucl. Instr. Meth., **111**, 615 (1973).

[11] S.O. Olabanji, O.A. Ige, C. Mazzoli, D. Ceccato, J.A. Akintunde, M. De Poli, and G. Moschini, Nucl. Inst. Meth., **B 240** (1), 350-355 (2005).

[12] S. Ouziane, A. Amokrane, I. Toumert, A. Nourreddine, and A. Pape, Nucl. Inst. Meth., **B 249** (1), 73-76 (2006).

[13] D. Zhu, H.S. Cheng, J.W. Lin and F.J. Yang, Nucl. Inst.Meth., **B 249** (1), 633-637 (2006).

[14] L.H. Keith, W. Crummett, J. Deegan Jnr., R.A. Libby, J.K. Taylor and G. Wentler, Anal. Chem., **55**, 2210 (1983).

[15] W. Maenhaut, L. De Rue, and J. Vandenhaute, Nucl. Instr. Meth., **B3**, 135 (1984).

Chapter Four

Elemental Analysis of Uranouchi Bay Seabed Sludge

Reader can get information about the quantitative elemental analysis of seabed sludge of Uranouchi Bay which is done by PIXE. Sampling points, sample preparation technique, experimental methodology, results and discussion are described in this chapter. Results indicate that the center region of the bay is mostly polluted by heavy metals in contrast to the other regions. A comparison of toxic elements found from the analyzed samples is also expressed here.

4.1 Introduction

Although Uranouchi bay in Kochi prefecture, Japan is well-known for its natural landscape and fish culturing, the sea water and the seabed of this bay are no longer clean now. It has been pointed out that increasing concentration of heavy elements is one of the causes of dirtiness of the bay. Fishermen are growing fishes in this bay and put fish foods profoundly. The concentration of certain elements in fish foods is enriched. Although some portions of the food are taken by fishes, the rest of foods are accumulated onto seabed sludge. In addition, a large number of small boats sail inside the bay and their fuel is also the reason of creating the grimy sludge. In this way, global ecological system of the bay has been changed gradually. The analysis of the seabed sludge is considered to be essential for understanding the changes of elemental concentration of heavy and toxic elements, which are expected to be liquated from the sludge and are harmful for environment. J.E. Martin et al. [1] have published an extensive work of river sediments by Thick Target PIXE (TTPIXE). They have reported that S, Cu, Zn, As and Pb concentration were high in the mining area with high levels of contamination in the sediments. They have also found Zn as the most important contamination element. In another literature [2] they have shown S, Fe, Ba, Cu, Zn, As and Pb as contaminated elements in the riverbed due to the mining activity. Pollution assessment in the river basin has been shown by T. Pinheiro et al. [3]. Though several analytical techniques have been used for this purpose, their sample preparation is generally complicated and takes a long time. The ion-beam techniques, especially PIXE [4-5] is one of the powerful techniques for material analysis, since its sample-preparation techniques are generally simple and it requires a short measuring time. This technique is also very popular because of its relatively high sensitivity and ability for multi-elemental and non-destructive analysis. The aim of this study is to find out the hazardous areas in the bay where contamination by heavy or toxic elements are serious, and also to estimate a degree of contamination.

4.2 Sampling

The Uranouchi bay is about 12km long and leads to the open Pacific Ocean through a shallow mouth (~300m wide). Samples were collected from eleven different places in

this bay as shown in figure 4.1, denoted as Sam1, Sam2, Sam3 and so on. The whole sampling area is segmented into three parts such as inlet (Sam11-Sam9), center (Sam7-Sam5) and inner (Sam4-Sam1) regions. Samples were collected randomly; Ekman dredge sampler was used to collect the seabed sludge from the top of the bottom sediment. Ekman dredges are preferred in soft mud, silt, or fine sand [6]. Then, samples were passed through a 2mm metal sieve for removing stones, woods and algae type goods. After that, samples were preserved in a refrigerator in glass bottles with small amount of Ar gas.

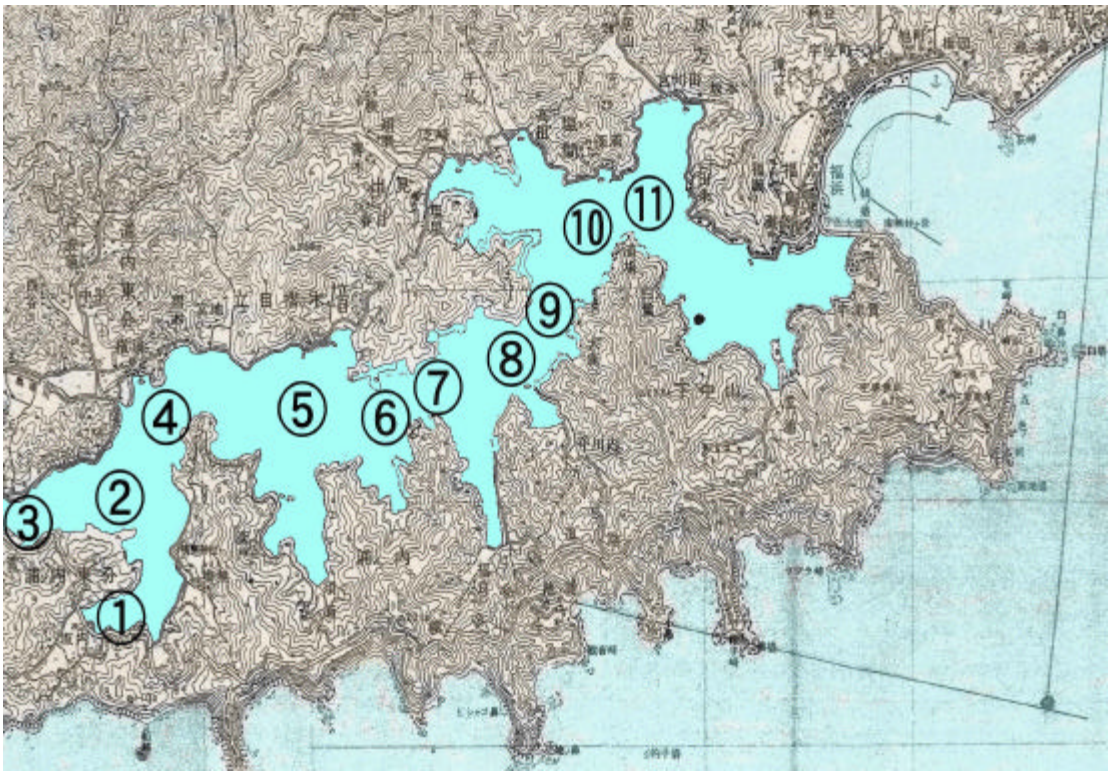

Figure 4.1: Eleven sampling points of seabed sludge in Uranouchi Bay.

4.3 Sample Preparation

Wet sludge samples were dried at room temperature. For proper ingredient mixing of all elements, samples were made into powder form. Carefully weighed 10 mg dried

sludge sample was mixed with 1 ml polyvinyl acetate (1000 ppm PVAc) and 0.5 ml Hiviswako (0.5%). After proper mixing, 15 μl liquid sample was taken for analysis which contained 100 μg sludge. Droplet of the acquired solution was then spotted onto a 4 μm thick polypropylene film which was used as substrate for samples to form a circular target spot with a size of around 4mm in diameter. At room temperature, samples were placed inside of desiccators until they were dried. The sample was then ready for PIXE measurement. From one sample solution, three targets were made and each target was measured separately.

4.4 Experimental Setup

The proton beam from the 2.5 MV Van de Graaff accelerator at Hiroshima University was used for this study. The samples were irradiated in a vacuum chamber with 6 mm in diameter ion beam which covered the entire area of target. Characteristic x-rays from targets were measured with a Si(Li) SL80175 Canberra detector (25.4 μm thick Be window). Detector was connected to a multi-channel analyzer for converting analog data to digital. Detector sensitivity area, resolution and Si thickness were 80 mm^2, 167 eV fwhm at 5.9 keV and 5 mm, respectively. Detector angle from the beam line was 150^o. Two spectra were obtained for each target: the first one was for detection of $Z \geq 20$ elements with 2.5 MeV proton energy, 5 nA beam intensity and 2 μC accumulated charge; the second one was for $Z<20$ elements with 1.25 MeV proton energy, 1.5 nA beam intensity and 1 μC accumulated charge. 250 μm thick Mylar filter without any hole and a 2.4 mm hole (funny) were placed in front of detector for the first and the second case, respectively. Funny is a filter with a hole drilled at its centre, placed in front of the detector window. This filter has been used by several groups [7-9] in order to get finite intensity. Figure 4.2 and figure 4.3 are respectively the typical PIXE spectra for 2.5 MeV and 1.25 MeV proton of Sam1(Sample number 1). It can be seen from figure 4.2 that the $Z \geq 20$ element peaks appear strongly. On the other hand, in figure 4.3, the $Z<20$ element peaks are observed prominently and the higher Z element peaks are not shown because the ionization cross-section is lower for heavy elements at low incident energy.

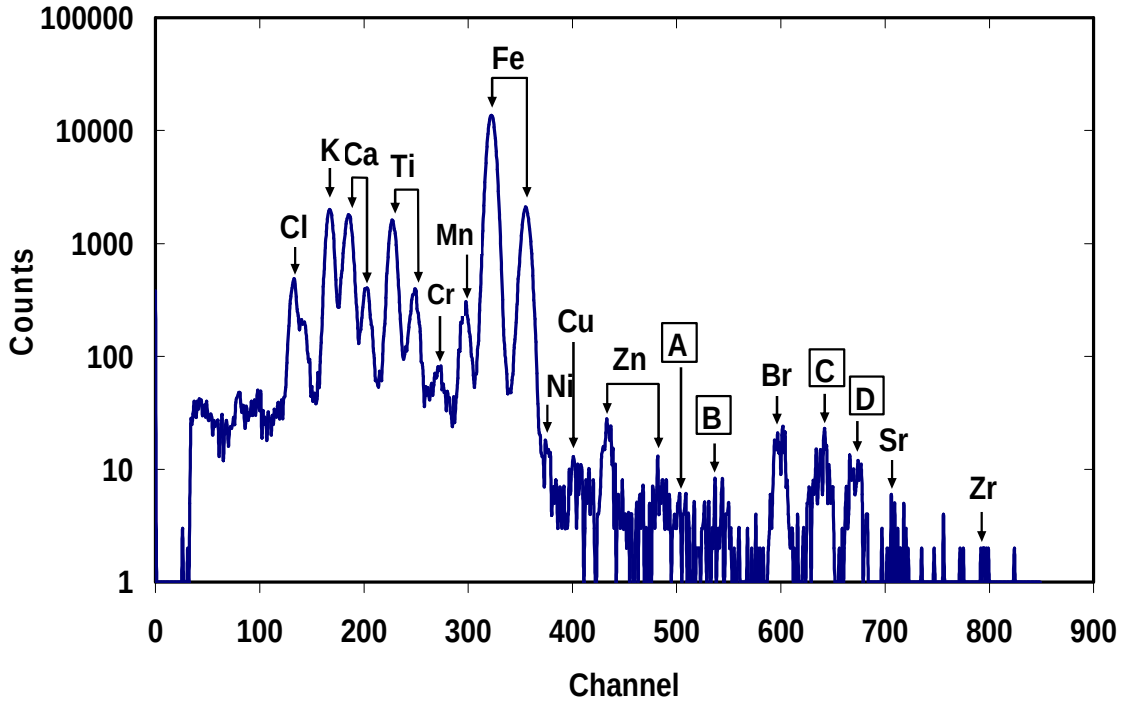

Figure 4.2: Typical PIXE spectrum of Sam1 obtained with a 2.5 MeV proton beam.

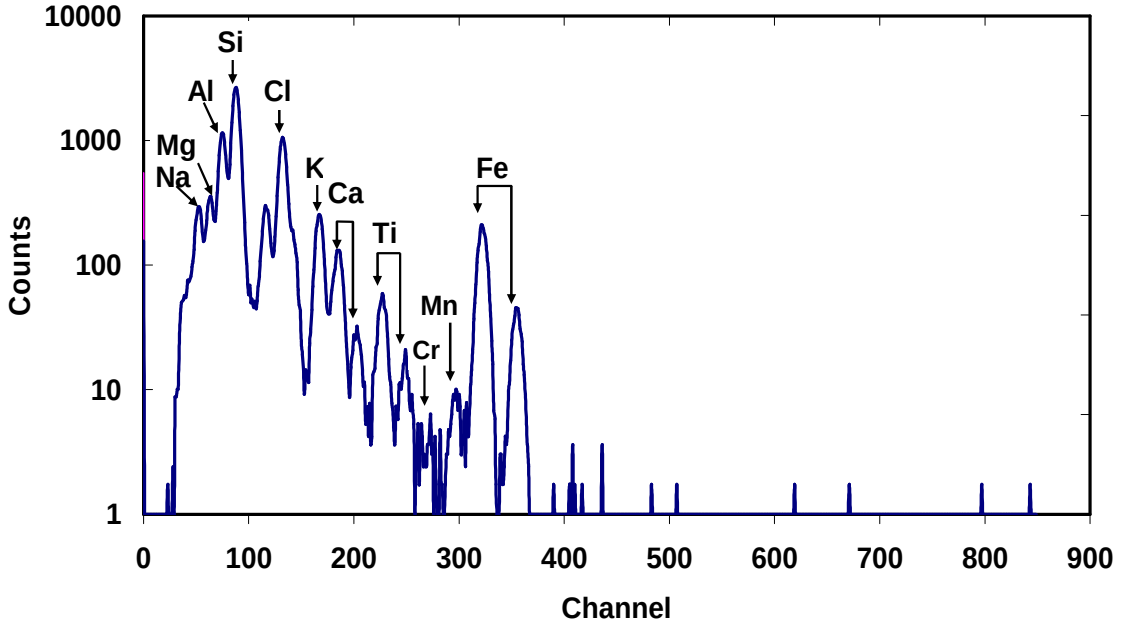

Figure 4.3: Typical PIXE spectrum of Sam1 obtained with a 1.25 MeV proton beam.

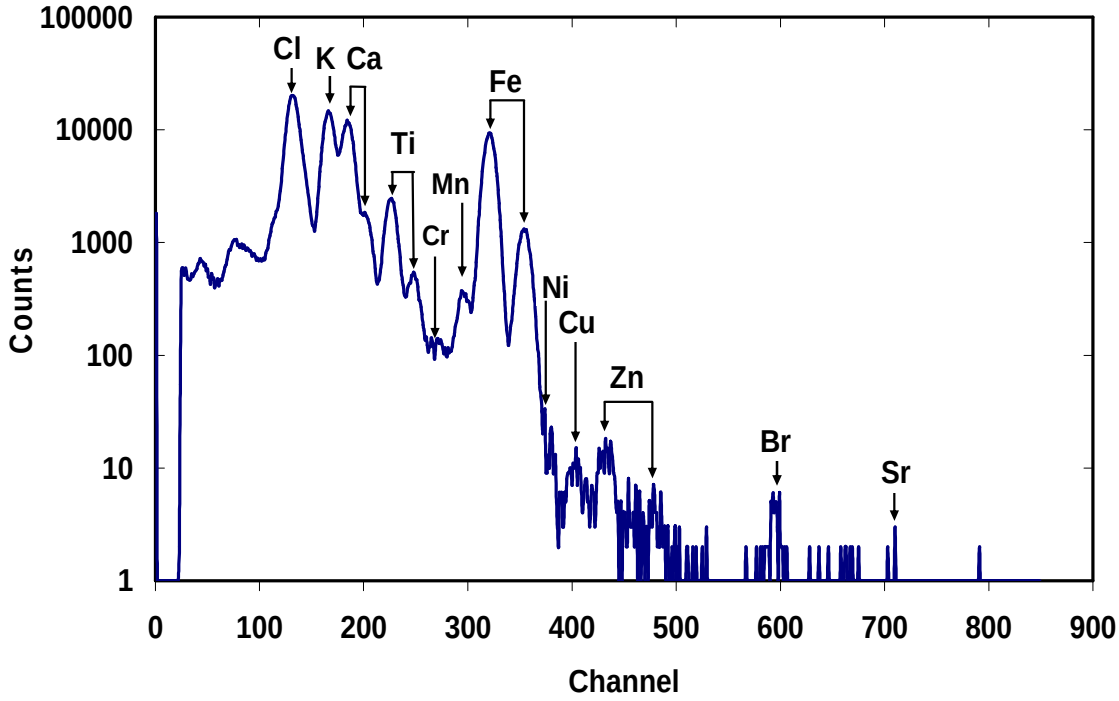

Figure 4.4: Typical PIXE spectrum of Sam7 obtained with a 4MeV Helium beam.

Figures 4.4 and 4.5 show typical PIXE spectra of the sample Sam7 obtained with 4 MeV He^{2+} and 2.5 MeV H^{+} bombardment, respectively. As these two spectra were taken under different measuring conditions, they can not be compared with each other directly. However, it is obvious on inspection that analysis with a 4 MeV He^{2+} beam has almost the equivalent relative sensitivity for low Z elements in comparison with that of a 1.25 MeV proton beams. It is known that ionization cross section is well scaled by the relative velocity of the projectile to that of the orbital electron to be ionized. As the projectile energy increases, ionization cross section also increases until the projectile velocity reaches to the mean velocity of the orbital electron. From this viewpoint, a 2.5 MeV proton beam has far higher velocity in comparison with that of a 4 MeV He^{2+} beam. The projectile velocity corresponding to the maximum cross section becomes lower as the atomic number becomes lower. On the other hand, ionization cross section is proportional to Z_1^2 (projectile charge) [4]. As a result, 4 MeV He^{2+} has the higher cross sections for low-Z elements, while 2.5 MeV proton is advantageous for detection of high-Z elements. It can be clearly seen in these figures.

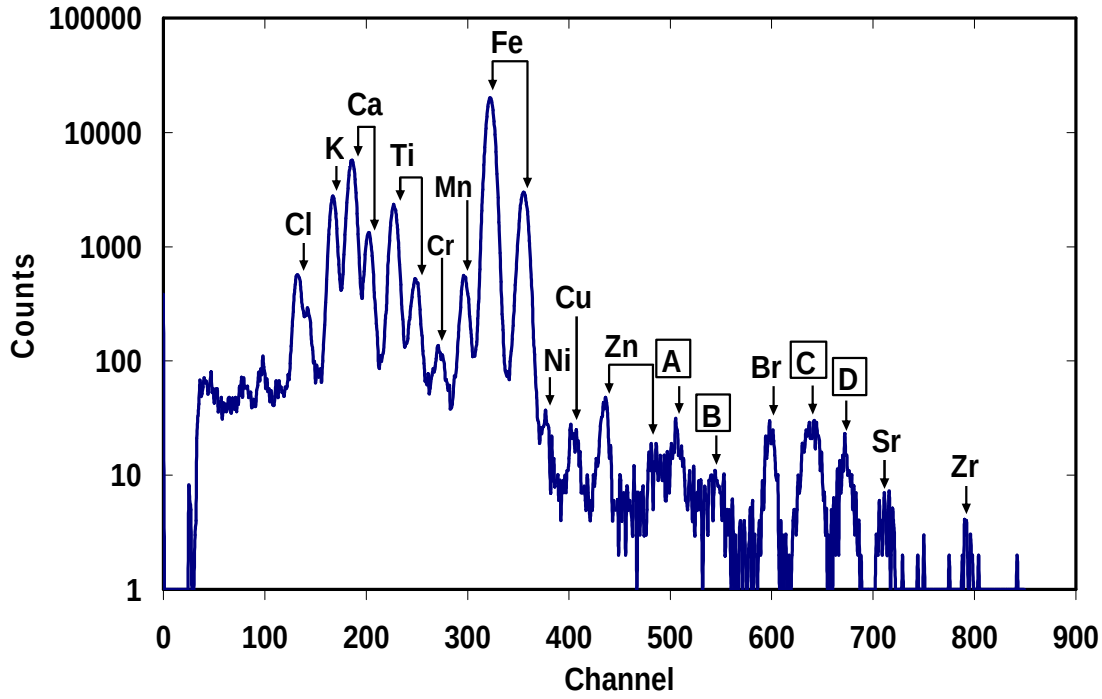

Figure 4. 5: Typical PIXE spectrum of Sam7 obtained with a 2.5 MeV proton beam.

4.5 Results and Discussion

Seventeen elements were detected in the analysis of the samples collected from eleven areas of Uranouchi bay. Typical PIXE spectra of sample number Sam7 for 2.5 MeV proton energy is shown in figure 4.5. Detected elements are designated in this figure. Though, Zr is detected in some samples in low amount, we do not consider Zr concentration in this paper. However, 4 extra peaks are clearly shown in figure 4.5 as indicated by A, B, C and D at channel 504, 540, 640 and 672, respectively. Peak (A), (B), (C) and (D) are the sum peak of Ca(K_α) + Fe(K_α), Ca(K_α) + Fe(K_β), 2*Fe(K_α) and Fe(K_α) + Fe(K_β), respectively. Sum peak is a common problem in PIXE analysis. A detail description of software program has been reported [10] which can automatically determine the sum peak in the spectrum. Experimental system has a function of pile-up rejection. Therefore, these peaks come when the system is unable to discriminate exactly simultaneous photons. Comparing figure 4.5 (Sam7) with figure 4.6 (Sam11), it is clear that the elemental concentration in Sam7 is much higher than that in Sam11.

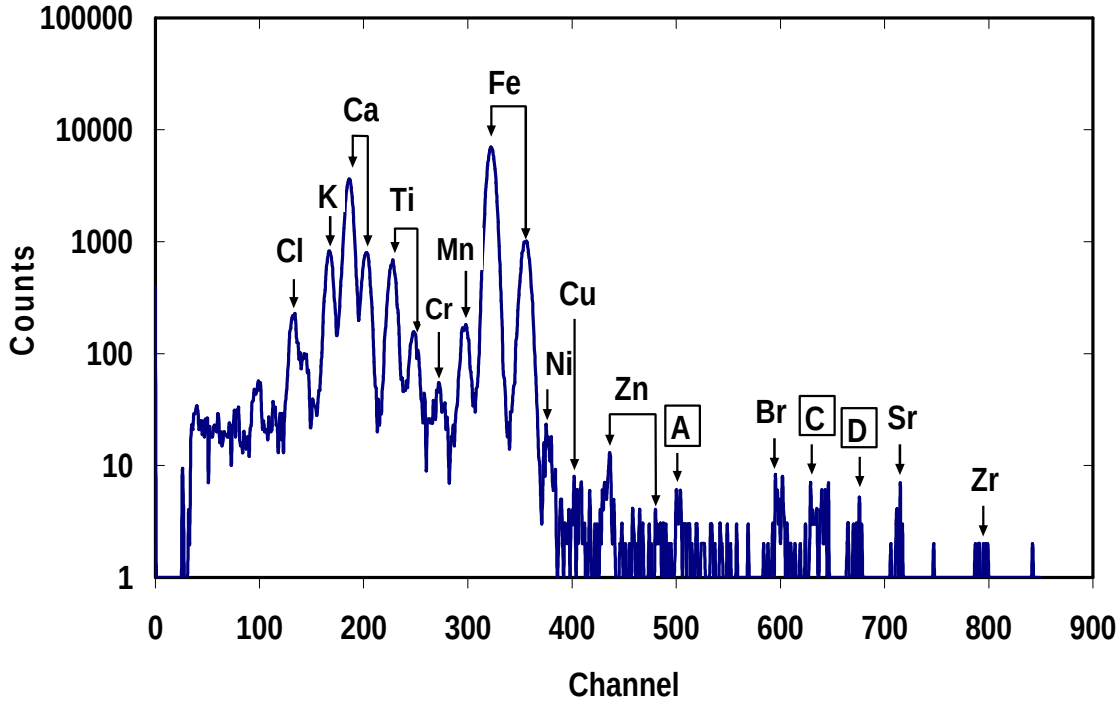

Figure 4.6: Typical PIXE spectrum of Sam11 obtained with a 2.5 MeV proton beam.

Atomic Absorption Spectrometry (AAS) standard sample were used as calibration standards for the calculation of elemental concentration. The sensitivity of each element *i* is calculated using the following equation:

$$S_i = \frac{Y_i}{Q_i} \qquad (4.1)$$

where S_i is the sensitivity for element *i*, Y_i is the peak height (counts per μg) for standard sample and Q_i is the value of charge (μC) accumulated during standard sample measurement. For calibration, sensitivity versus atomic number curves are shown in figure 4.7(a) and figure 4.7(b).

The concentration of each element in the target t is calculated using the following equation:

$$C_{it} = \frac{Y_{it} / Q_{it}}{S_{it}} \qquad (4.2)$$

where C_{it} and Y_{it} are the concentration and the average peak height of the element *i* in the target t, respectively. Q_{it} and S_{it} are the value of accumulated charge (μC) during the measurement of target and sensitivity factor for the element *i*, respectively.

Every sample was irradiated three times and then the elemental concentration of one sample was calculated from the data after averaging peak height over measurements of three targets. It is noted that about 66 spectra from 11 samples are used for calculation. The elemental concentrations of the 17 elements are shown in Table 4.1. Na, Mg, Al, Si, S, Cl, K, Ca and Fe are detected as major elements whereas Ti, Cr, Mn, Ni, Cu, Zn, Br and Sr are detected as trace elements. Some toxic elements [11-13] such as Cr, Ni, Cu and Zn are significantly increased in some sampling area with respect to other areas.

Each sample shows characteristic features in the concentration of major elements depending on the collecting areas. Especially, the center region (Sam7) has a distinguished feature in comparison with inlet region (Sam11), where sulfur concentration is considerably higher by five times than that in Sam7. On the other hand, sulfur concentration is almost equal for the samples Sam2-5. Calcium concentration increases as the sampling points become inner from the inlet (Sam11) to the center (Sam7) of the bay, and turns to decrease toward the inner side of the bay (Sam1-4), where its concentration shows similar values of around 45 ppm. Though the reason of decrease of calcium concentration is not clear, it can be said that such circumstance is not suited to fish culturing. With regard to the trace elements, chromium concentration is lower in Sam2 and Sam3 and is much higher in Sam7 in comparison with that in the other samples. Nickel concentration is higher in Sam9 and lower in Sam1 and Sam4. Iron, copper, zinc and strontium concentrations are much higher in Sam7 in contrast to that in Sam11.

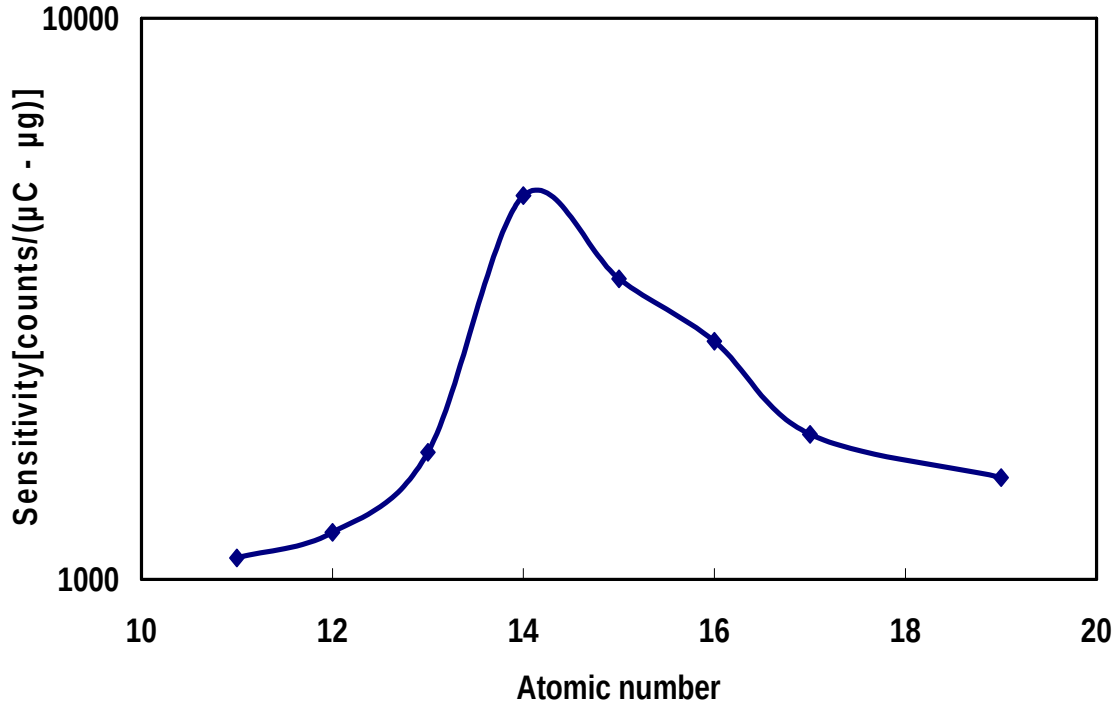

Figure 4.7(a): Sensitivity curve as a function of atomic number for the elements Z<20.

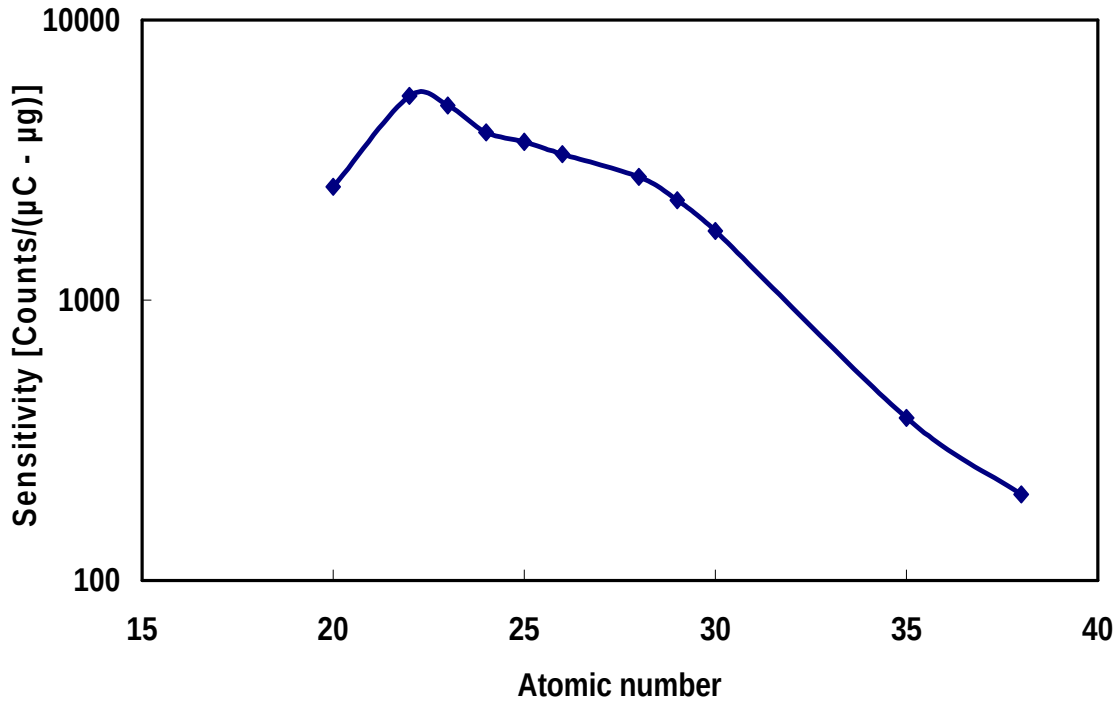

Figure 4.7(b): Sensitivity curve as a function of atomic number for the elements Z≥20.

Table 4.1. Elemental concentration in the seabed sludge samples collected at 11 regions of Uranouchi bay. Results are shown in units of 100 μg/g.

Elements	Sam1	Sam 2	Sam 3	Sam 4	Sam 5	Sam 6	Sam 7	Sam 8	Sam 9	Sam 10	Sam 11
Na	112.76	121.61	119.54	164.84	171.92	146.09	151.40	116.73	143.83	108.30	65.23
Mg	132.10	128.69	132.01	137.43	187.27	173.02	188.45	138.34	161.30	133.20	75.47
Al	421.83	385.77	455.21	352.59	456.06	309.68	569.06	339.96	409.90	332.92	179.00
Si	415.18	394.78	460.37	356.85	509.78	332.73	628.69	391.39	504.10	433.71	262.79
S	48.04	59.28	56.33	57.40	61.80	37.74	67.27	43.70	45.79	34.01	13.12
Cl	318.24	346.96	340.07	477.45	527.42	284.55	421.65	355.61	413.39	291.26	135.24
K	70.20	65.79	73.89	67.59	82.07	53.26	95.28	63.31	74.41	60.26	33.68
Ca	46.78	48.03	43.67	45.72	98.35	55.37	149.12	109.02	165.05	175.55	98.22
Ti	14.44	14.35	16.36	13.59	17.69	18.48	22.28	15.79	20.24	18.09	8.63
Cr	1.04	1.00	1.15	1.00	1.47	1.39	1.81	1.24	1.60	1.57	1.45
Mn	2.93	3.45	3.69	3.16	5.73	5.37	7.76	5.58	6.91	6.00	3.65
Fe	205.87	206.06	225.63	178.82	256.16	263.11	315.51	233.02	306.60	256.17	135.57
Ni	0.32	0.36	0.41	0.32	0.45	0.44	0.61	0.53	0.69	0.60	0.39
Cu	0.34	0.31	0.28	0.29	0.48	0.50	0.58	0.42	0.56	0.46	0.21
Zn	0.82	0.77	0.87	0.65	1.10	1.10	1.20	1.03	1.10	0.77	0.45
Br	2.85	2.46	3.20	3.86	3.90	3.64	3.68	3.51	3.64	2.11	0.96
Sr	1.48	1.48	0.90	0.99	1.23	1.40	2.05	1.15	1.89	2.05	0.90

The experimental errors were calculated in order to judge the significance of the differences in elemental concentration. The experimental errors mainly come from statistical errors of the X-ray peaks and partly from the value of X-ray transmission and detection efficiencies. In this study, we only considered the statistical errors because the other errors were negligible with respect to the statistical errors. These errors were below 4% for the elements Z<27 except Cr whereas they become higher from around 15% to 50% for the heavy elements. For Cr the error was around 10% because of less Cr count.

In summary, it is found that elemental concentration increases in the center region of the Uranouchi bay, while most elements show lowest concentrations near the inlet of the bay. The area near the inlet of the bay is not suited to fish culturing since water circulation is probably swifter in comparison with the inner regions. Fishermen have put excessive amount of foods for cultivation, and they are partly taken by fishes but the rest of them falls onto the seabed. As a result, it increases the heavy elemental concentration in the sludge. On the other hand, leakage of fuel from sea boats may be also the significant cause since a large number of sea boats are sailing in the bay. There might be some other unexpected causes which influence on the increase of concentration of the heavy or toxic elements.

Figure 4.8 shows the ratios of concentrations of toxic elements, where all values are divided by the values for Sam11. It can be seen from the figure that the concentrations of Cr, Ni, Cu and Zn pronouncedly increase in Sam5-7 and Sam9 in comparison with those in the other samples. The concentrations of Cr, Zn and Cu in Sam7 are more than 2.48, 2.6 and 2.72 times higher, respectively, while that of Ni in Sam9 is 2.58 times higher in contrast to their lowest values. Although zinc and copper is the essential trace element for marine life, they become toxic at higher concentrations [14]. In the present study, these elements show higher concentrations in the center region of the bay. Trace heavy metals as well as toxic elements have changed the ecological system of the bay and have caused deleterious effects on fishes and other aquatic organisms.

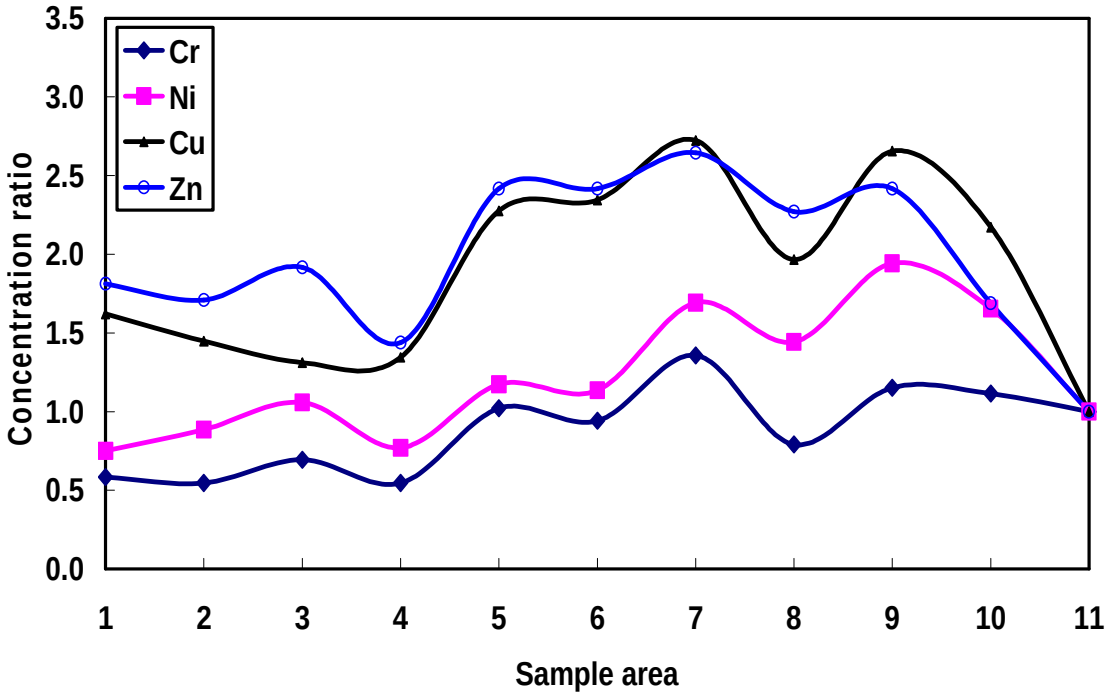

Figure 4.8: Concentration ratios of toxic elementals at each sampling area with respect to the concentrations in Sam11.

As there is no general agreement concerning the maximum acceptable limits of elemental concentration in seabed sludge, we discuss the concentration of various elements in reference to that for Sam11 collected at the inlet of the bay. As a result, it is found that all other samples collected in the inner regions in the bay are polluted. Among them, Sam7 collected in the center region in the bay is particularly contaminated.

4.6 Conclusion

Seventeen elements including toxic elements are detected from seabed sludge collected in Uranouchi bay. It is found that the center region of the bay is mostly polluted in contrast to the other regions. The highest values of copper and zinc concentration are found to be 2.72 and 2.6 times larger, respectively, in comparison with those for Sam11 collected from the inlet of the bay.

References

[1] J. E. Martín, R. García-Tenorio, M. Á. Ontalba-Salamanca, M. Á. Respaldiza and M. F. da Silva, Nucl. Instr. Meth, **161-163**, 825 (2000).

[2] J. E. Martín, R. García-Tenorio, M. Á. Respaldiza, J.P. Bolívar and M. F. da Silva, Nucl. Instr. Meth, **136-138**, 1000 (1998).

[3] T. Pinheiro, M. F. Araújo, P. M. Carreira, P. Valério, D. Nunes and L. C. Alves, Nucl. Instr. Meth, **150**, 306 (1999).

[4] S. A. E. Johansson and J. L. Campbell, PIXE: A novel technique for elemental analysis (John Wiley & Sons, Chichester, 1988).

[5] S. A. E. Johansson, J. L. Campbell K. G. malmqvist, Particle-Induced X-Ray Emission Spectrometry (PIXE), (John Wiley & Sons, New York, 1995).

[6] http://www.umanitoba.ca/faculties/science/zoology/faculty/hann/z350/#Ekman

[7] Sophie Gama, Marcel Volfinger, Claire Ramboz and Olivier Rouer, Nucl. Instr. Meth, **181**, 150 (2001).

[8] N. Menzel, B. Hietel, M. Leirer, W. Szymczak and K. Wittmaack, Nucl. Instr. Meth, **150**, 96 (1999).

[9] K. Kobayashi, Y. Koizumi, C. Nakano, S. Hatori and Y. Sunohara, Nucl. Instr. Meth, **150**, 144 (1999).

[10] E. Clayton, Nucl. Instr. Meth, **218**, 221 (1983).

[11] J. Pearson, F. Lu and K. Gandhi, Disposal of wool scouring sludge by composting, AUTEX Research Journal, **4**, (3), 147-156 (2004).

[12] R. M. Bradley, G.R. Dhanagunan, Sewage sludge management in Malaysia, Int. J. Water, **2**, (4), 267-283 (2004).

[13] V. Vijayan, R. K. Choudhury, B. Mallick, S. Sahu, S. K. Choudhury, H. P. Lenka, T. R. Rautray and P. K. Nayak, External particle-induced x-ray emission, Current science, **85**, (6), 772-777 (2003).

[14] Technical Report No. 1 July 2005, Wastewater Treatment Plants (WWTPs) into the marine environment.

Chapter Five

PIXE analysis of biological bodies

The quantitative analysis of heavy metals in shellfish have been done and presented here. The aim of this work is to examine whether the biological species are contaminated by heavy metals due to pollution of the Uranouchi bay or not, shellfish have been chosen as the representative among the biological bodies. A short introduction, sampling and sample preparation procedure, experimental methodology, results and discussion are presented here. Quantitative elemental analysis of heavy metals in shellfish of different zones has been compared with market shellfish.

5.1 Introduction

In several decades, PIXE has been widely used in the biological samples analysis [1-6] which has given valuable information to understand the mechanism of the biological bodies. In the present study we have used this technique to analyze the shellfish to gather knowledge about the heavy elemental concentration in shellfish. The shellfish were collected from different places of Uranouchi bay, a short description is mentioned in section 4.1 in chapter 4 about this bay. The environmental condition of this bay has been changed due to several anthropogenic sources. It has been clarified by analyzing seabed sludge of our previous studies that some regions of this bay are polluted by heavy metals [22]. Perhaps it affects directly the biological species those are living in this bay. Therefore, analyzing shellfish (*Ruditapes philippinarum*) as a representative of biological species, it is meaningful to know the elemental concentration in shellfish and to examine whether the biological species are contaminated by heavy metals due to pollution of the bay or not.

5.2 Sample Collection and Preparation

Three different places of Uranouchi Bay (Kochi, Japan) as shown in figure 5.1 were the sampling site for collection of shellfish, denoted as zone1, zone2, and zone3. Zone1 is very close to the inlet of the bay, whereas zone2 from inlet and zone3 from zone2 are one kilometer apart each. Shellfish were preserved in a deep freeze after washing with distilled water. There are several number of review papers which illustrate the technique of biological sample preparation in detail [7-8]. Shellfish were again washed with distilled water after removing from the shell. Samples were dried in an oven for a few minutes and then put onto the light (lamp) for several hours to completely remove the moisture. For proper ingredient mixing of all elements, samples were made into powder form using a small grinding hammer. A 10 mg powder sample was weighed carefully by electronic balance and was mixed with 1 ml polyvinyl acetate (1000 ppm PVAc) as an adhesive to the substrate. After that, carefully weighed 2 mg Mo powder was added in sample as an internal standard and was mixed uniformly. The well established internal standard method has been

followed in sample preparation. The internal standard method has been used to analyze biological samples reported in literature [9-11]. A 10 µl resulting solution was taken using a micro pipette for analysis which contained 100 µg of shellfish and 20 µg of Mo. The droplet of the obtained solution was then spotted onto a 12 µm thick carbon foil which was used as a substrate for samples to form a circular target spot with a size of around 2 mm in diameter. All samples were placed inside of desiccator at room temperature until they were dried. The sample was then ready for PIXE measurements. From one sample solution, three targets were made and each target was measured separately. Figure 5.4 shows the flow chart of the sample preparation procedure.

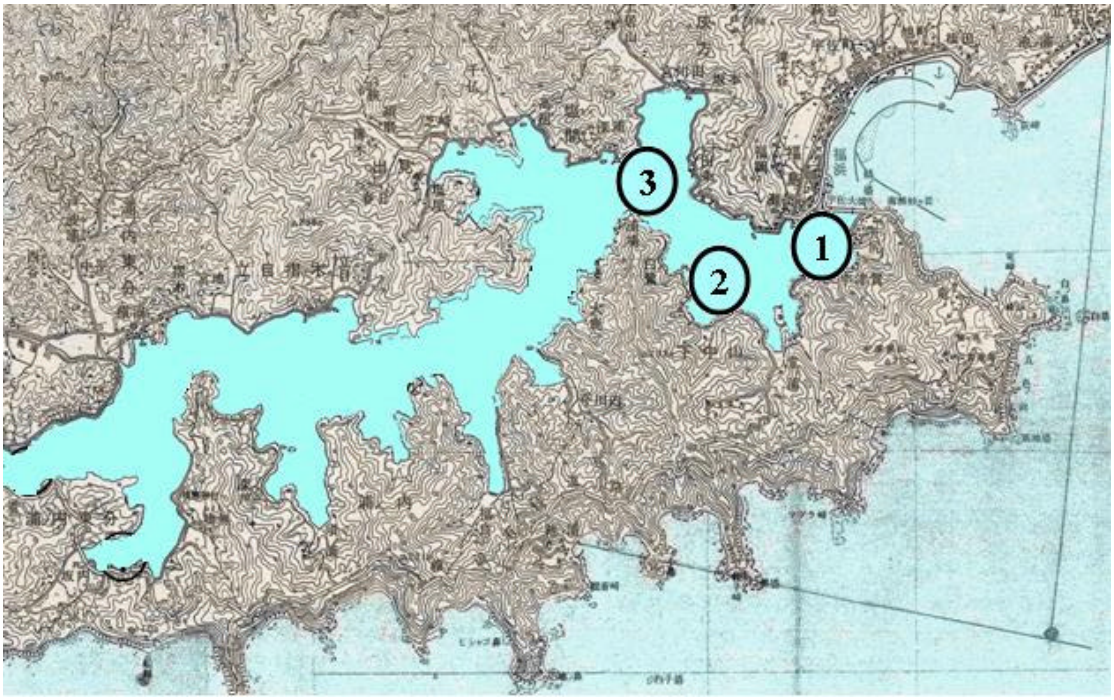

Figure 5.1: Sampling points of shellfish in Uranouchi bay.

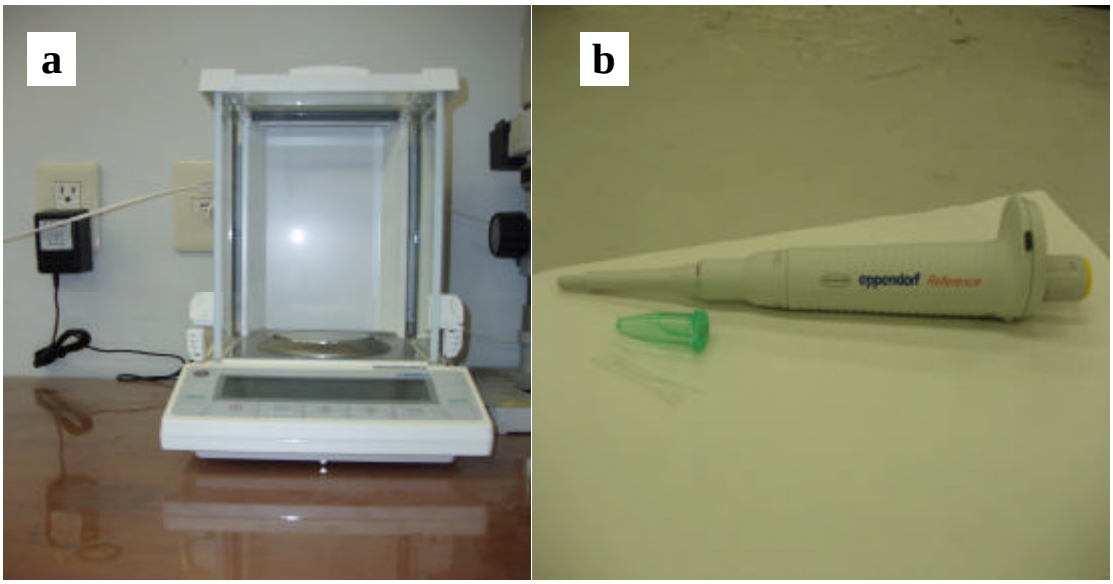

Figure 5.2: (a) Electronic Balance and (b) Pipette & Tips, used in this experiment.

Figure 5.3: Marble Mortar and Pestle used in this experiment.

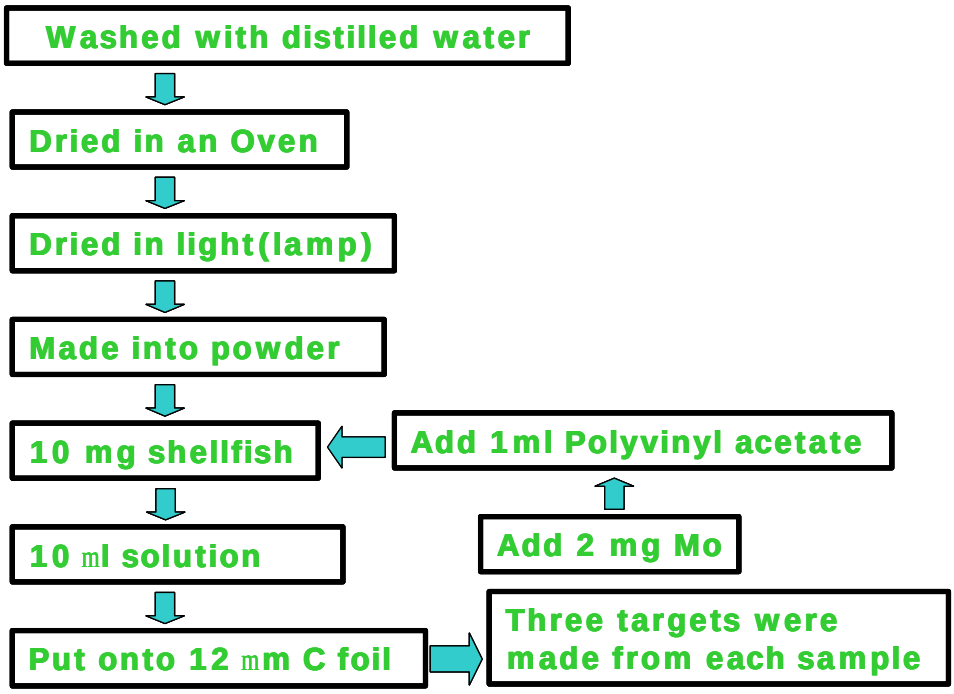

Figure 5.4: Flow chart of shellfish sample preparation technique.

5.3 Equipment and Measurements

A 4 MeV helium beam from 1.7 MeV tandem accelerator at Kochi University of Technology (KUT), Japan was used for the PIXE measurements. Beam was collimated by a graphite collimator to a size of 1 mm diameter which was used for irradiation of the samples. The beam size covered the quarter area of the samples. The shellfish samples were placed on the sample holder in a vacuum chamber straight to the beam line. Characteristic x-rays excited from targets were measured by an Si(Li) detector (8 μm thick Beryllium with polymer coating window) positioned at 135° angle to the beam line. Active area and Si thickness of detector were 10 mm^2 and 0.3 mm, respectively. A Mylar film of 125 μm thick was fixed with an aluminum holder and was placed in front of x-rays detector which was acted as a filter to attenuate lower energy x-rays and to reduce x-rays interference. The total distance from the target to Si(Li) detector was around 40 mm. The effective solid angle of the detector was 0.0063 sr. The collected charge was measured by current integration from the

sample holder which served as a Faraday cup. The charge of about 30 μC was used for each sample irradiation. A multi-channel analyzer via a preamplifier was connected to an x-ray detector for data processing. The laboratory experimental setup is shown in figure 5.5.

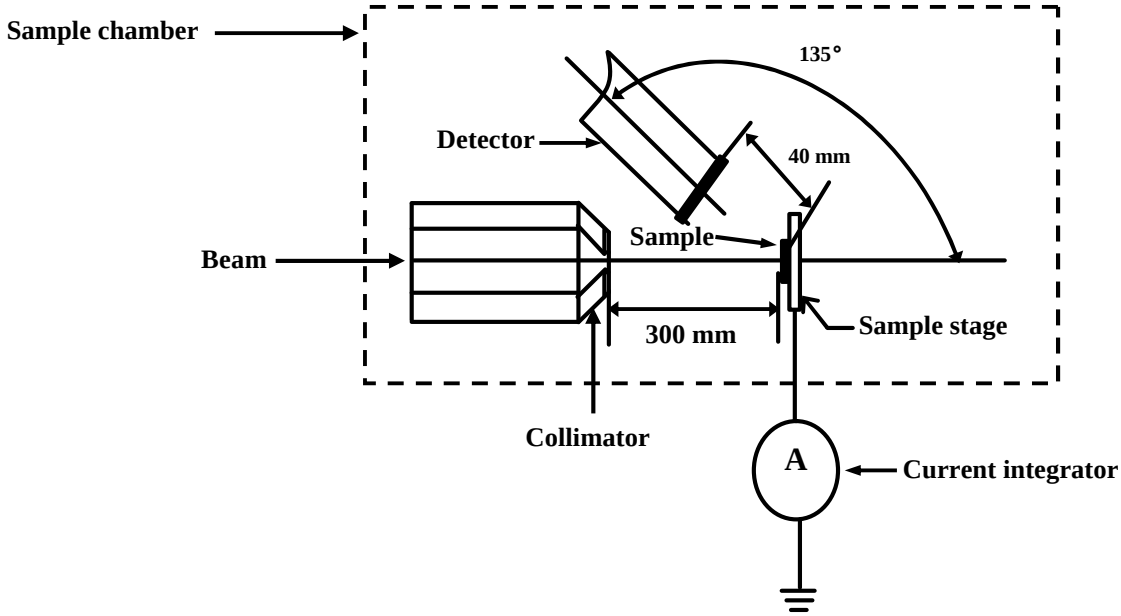

Figure 5.5: Experiment setup in the target chamber.

The typical PIXE spectrum of carbon foil obtained using 4 MeV He^{++} beam is seen in figure 5.6. A 12 μm thick carbon foil was used as a substrate for sample because this foil does not give interfering x-rays, resistant to acid solutions and also supplies better heat dissipation. However, it can be seen from this figure that some impurities are detected such as Cl, Ca, Cr and Fe with a few counts for the 30 μC irradiation. Russell et al. [12] have shown that the Ca, Fe, Cu and Zn were detected as impurities from carbon foil with the irradiation by 60 μC. We are not sure about the source of Fe and Cr x-rays. Though, Fe and Cr are main constituents of steel in PIXE chamber, so it has possibility that these x-rays come from the steel excited by stray ions. Figure

5.7 shows the typical PIXE spectrum of Uranouchi shellfish obtained with 4 MeV He^{++} beam from zone 1. The detected elements are assigned in this figure. The Mo signals come from 0.2 wt% internal Mo standard. In the present study, 4 MeV He^{++} ion beam was used which is equivalent to 1 MeV proton beam according to the scaling law of PWBA theory. Though 2-3 MeV proton beams are generally used for PIXE analysis but in this study He (Helium) ion beam was used because of some regulations in the laboratory.

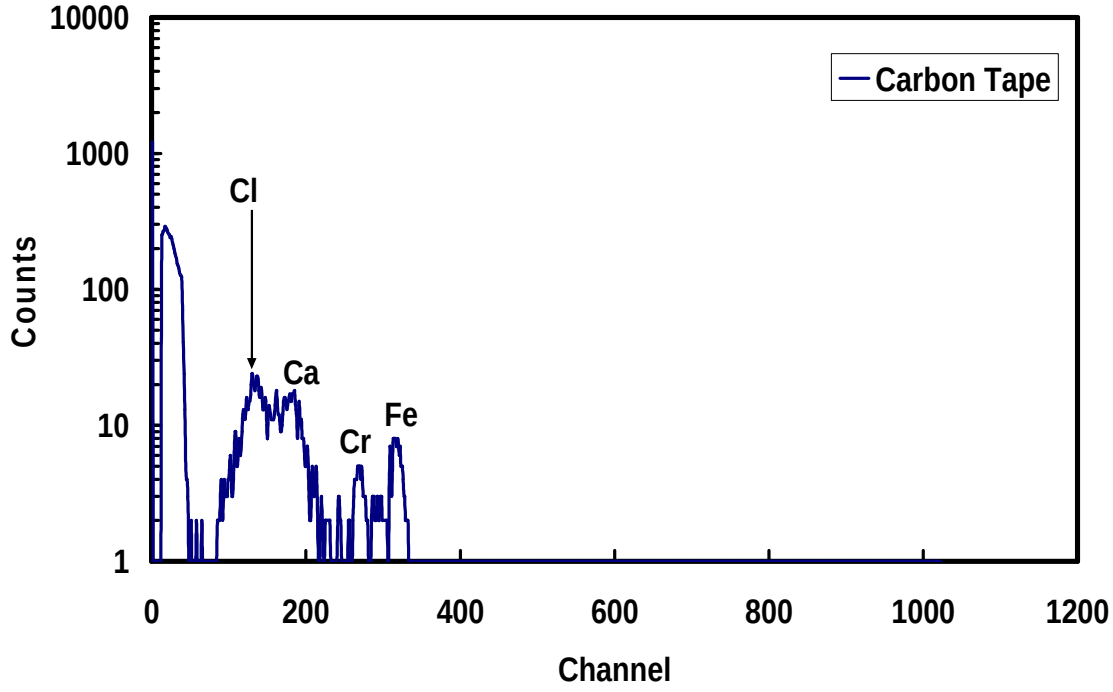

Figure 5.6: Typical PIXE spectrum of Carbon foil obtained with a 4 MeV He^{++} Beam.

Figure 5.8 shows the count rate vs concentration of internal standard (Mo) sample. The error bars show the experimental uncertainty at the approximately ±10% level. It is clearly seen from this figure that the count rate linearly increases with Mo concentration. This result indicates that the system has a good stability. The homogeneity of various elements in a sample is essential for a reliable quantitative analysis especially for applications in analytical techniques. Standard reference materials (SRMs) from various producers are generally used in trace element analysis

for quality control and methodological development purposes [13]. Though it is very difficult to maintain the homogeneity of various elements in a sample, in this work it was carefully handled by proper mixing of sample during the time of making the powder form of the sample as well as before pipetting. The homogeneity of the sample was checked by comparing three spectra taken from different places which covered the three-forth area of the sample as shown in figure 5.9. These spectra were obtained under the same beam conditions, therefore Fe/Mo ratio depending on the irradiation positions are nearly identical. It indicates that the homogeneity of both the sample itself and the internal standard within the sample is almost uniform.

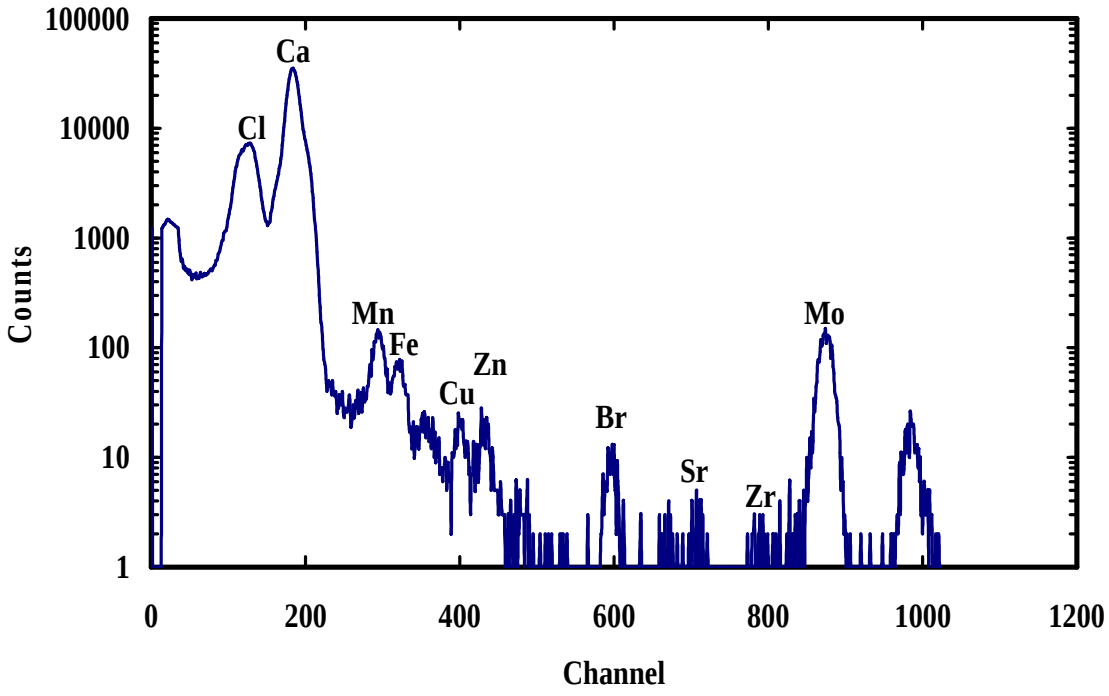

Figure 5.7: Typical PIXE spectrum of Uranouchi Shell (zone -1) obtained with a 4MeV He^{++} beam.

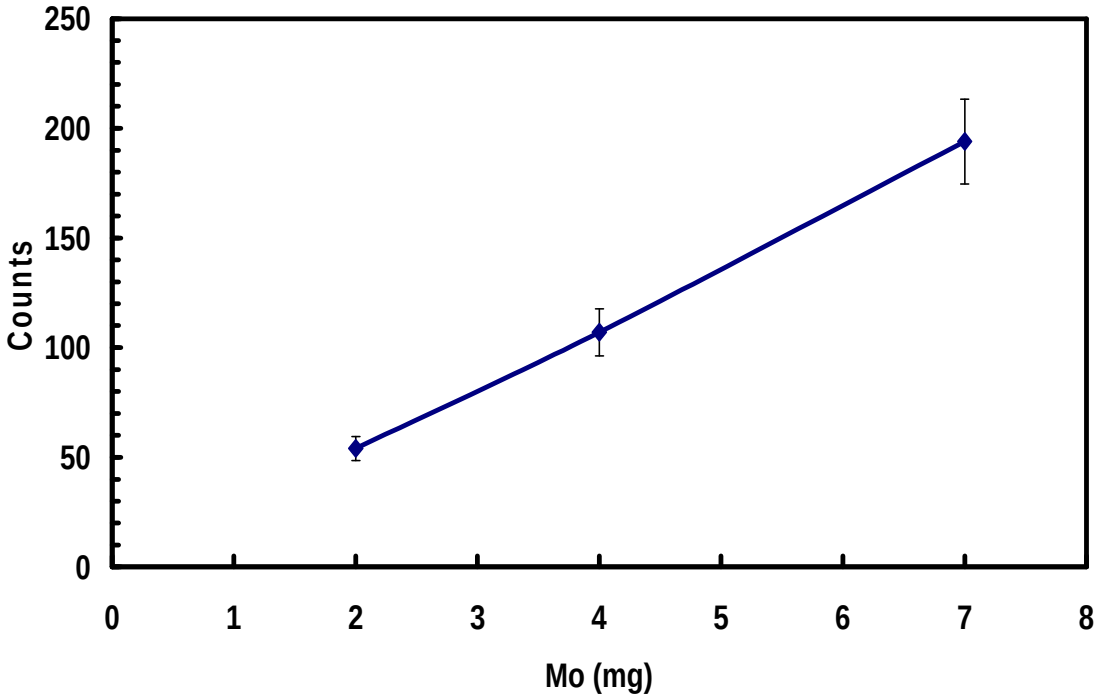

Figure 5.8: Count rate of Mo with respect to the concentration obtained with a 4 MeV He^{++} beam.

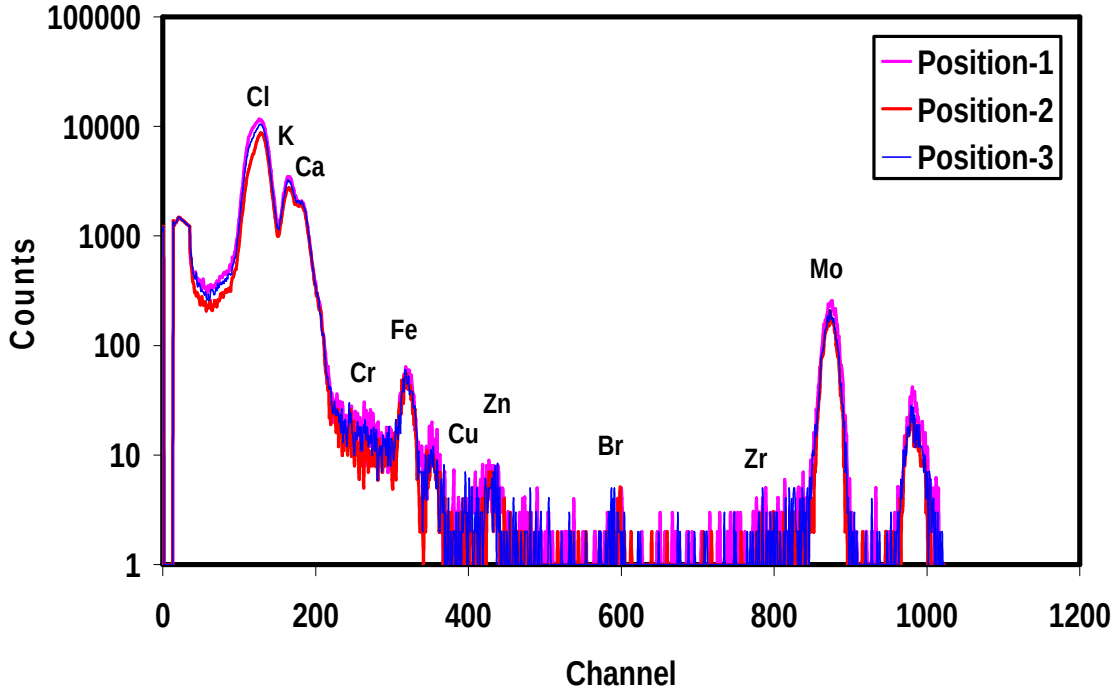

Figure 5.9: Homogeneity of the market shellfish obtained with 4MeV He^{++} beam.

5.4 Results and Discussion

Since very low amount of materials are available in the biological sample, high sensitivity of the system is required for analysis of the biological samples. The detection limit of biological sample in PIXE analysis is below 1 μg/g which indicates the ability of trace-element analysis. A suitable procedure has been developed by Kim et al. [14] for determining the elemental composition of the biological sample. The limit of detection (LOD) defines the sensitivity of a measurement system. When the fluorescence spectrum is measured, the LOD is correlated with the signal peak and the background. Different methods have been reported for calculation of the minimum limit of detection in x-ray spectroscopy [15-17]. In x-ray analysis the beam current, counting time and accelerating voltage play the key role for calculating the detection limits. The detection limits are calculated in PIXE analysis by assuming that the minimum intensity of the peak is three times the square root of the background at full width half maximum intensity as indicated by equation,

$$LOD = \frac{3\sqrt{BG}}{S} * C \qquad (5.1)$$

where, S and BG are the total number of counts in the peak and background areas, respectively. C is the known concentration of the standard element. Figure 5.10 shows that the detection limits of PIXE system used in this study which is calculated using experimentally measured data of various standard samples. It is clearly seen from this figure that the detection limit is decreased despite the higher ionization cross-section for lighter elements. This is because of decreasing fluorescence yield, increasing bremsstrahlung background for lighter elements and increasing absorption in detector window [1]. For heavier elements the detection limit does not increase sharply even though the bremsstrahlung background is smaller. Because ionization cross-section is steeply decreased for heavier elements and detector efficiency is fall-off due to the high x-ray energies enough to penetrate the detector crystal without interacting. From this figure it was found that the detection limit is 0.14 ppm for Ca. This result indicates that the system has good detection limit. If a very thin, uniformly distributed elemental sample is totally covered by an ion beam of uniform intensity distribution within its cross-sectional area and the beam hits along the normal of the

sample, then the yield of characteristic x-rays can be calculated using equation 2.10 as mentioned in chapter 2.

If we use a single added internal standard into an unknown sample and for which the spectrum is collected in the same way as for the unknown sample then the concentration of each element in the unknown sample can be calculated by using the following equation

$$C_U = \frac{Y_U X_S T_S E_S}{Y_S X_U T_U E_U} \times C_S \qquad (5.2)$$

where C_U and C_S are the unknown and known standard samples concentration, respectively. Y_U and Y_S are the characteristic x-ray yields, X_U and X_S are the differences in x-ray production cross-section, T_U and T_S are the x-ray transmission through the x-ray absorber, E_U and E_S are the detection efficiencies for unknown and standard sample, respectively.

In analysis of shellfish collected from different areas of Uranouchi bay, nine elements were detected. Each sample was irradiated three times and then the elemental concentration of one sample was calculated from the data after averaging peak areas over measurements of three targets. It can be noted that in total 27 spectra of Uranouchi shellfish were taken for analysis. The background was subtracted from each spectrum. Average concentrations of major elements are tabulated in table 5.1. Results are shown in units of 100 μg/g (ppm). It is clearly seen from this table that the Cl and Ca are detected as major elements whereas others are trace elements. The standard deviation of each element is shown within parenthesis. Some elements show higher standard deviation due to high variation in the elemental concentration.

The concentration of major elements in all samples shows the characteristic features depending on the collecting areas. The most interesting observation is Ca which shows the higher concentration among other major elements in all samples. It can be pointed out that the concentration of Ca is almost seven and three times higher in zone2 and zone1, respectively in contrast to zone3. Though shellfish is naturally rich in Ca but the higher amount of Ca content in the present study clearly indicates that

fish food has a great influence to increase the amount of Ca. Despite a pre-concentrated essential element in the biological metabolism, Cl comes due to high NaCl content in marine environment. Concerning the elemental concentration of Fe, it is increased from zone1 toward zone3 while that of Mn reflects alter nature. In comparison within zones, however, Fe shows about three times higher concentration in zone3 than that of zone1.

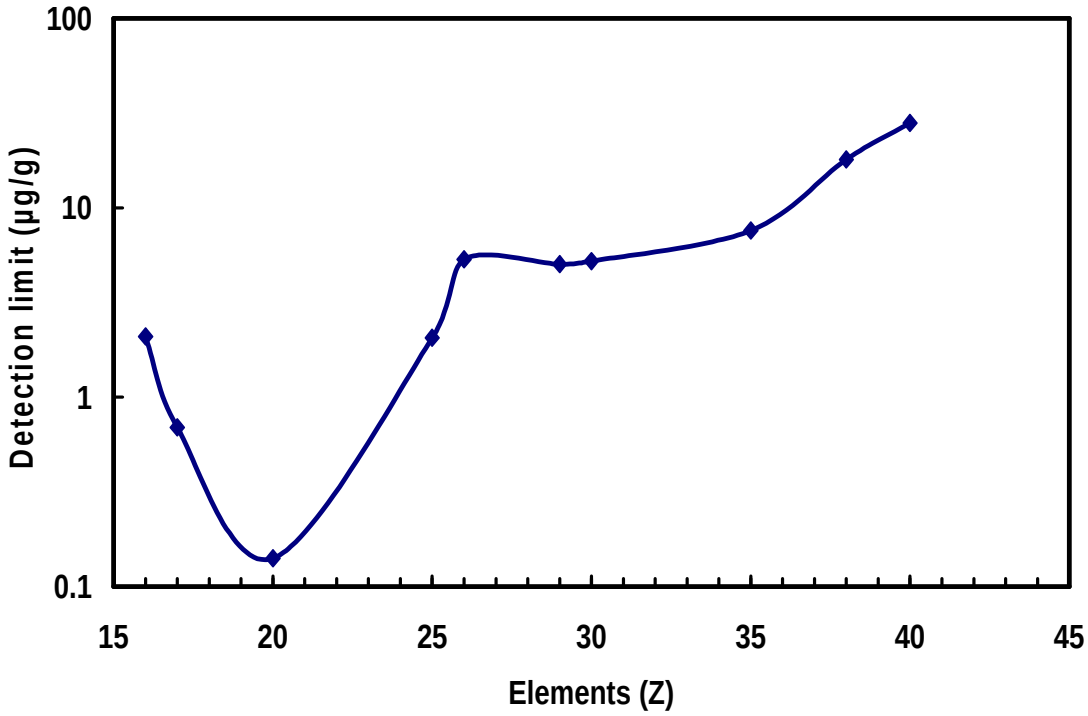

Figure 5.10: Limit of detection obtained with a 30 µC of 4 MeV He^{++} beam.

Table 5.1: The concentration of major elements in shellfish collected form Uranouchi bay. Results are shown in units of 100 μg/g (ppm).

Elements	Zone 1	Zone 2	Zone 3
Cl	**53.97 (9.67)**	**21.59 (5.40)**	**26.33 (2.83)**
Ca	**622.05 (55.42)**	**1211.58 (153.27)**	**182.09 (6.99)**
Mn	**2.85 (0.50)**	**2.41 (0.13)**	**2.33 (0.13)**
Fe	**1.03 (0.17)**	**1.88 (0.54)**	**3.41 (0.51)**

Numbers within parentheses refer to the standard deviation (±).

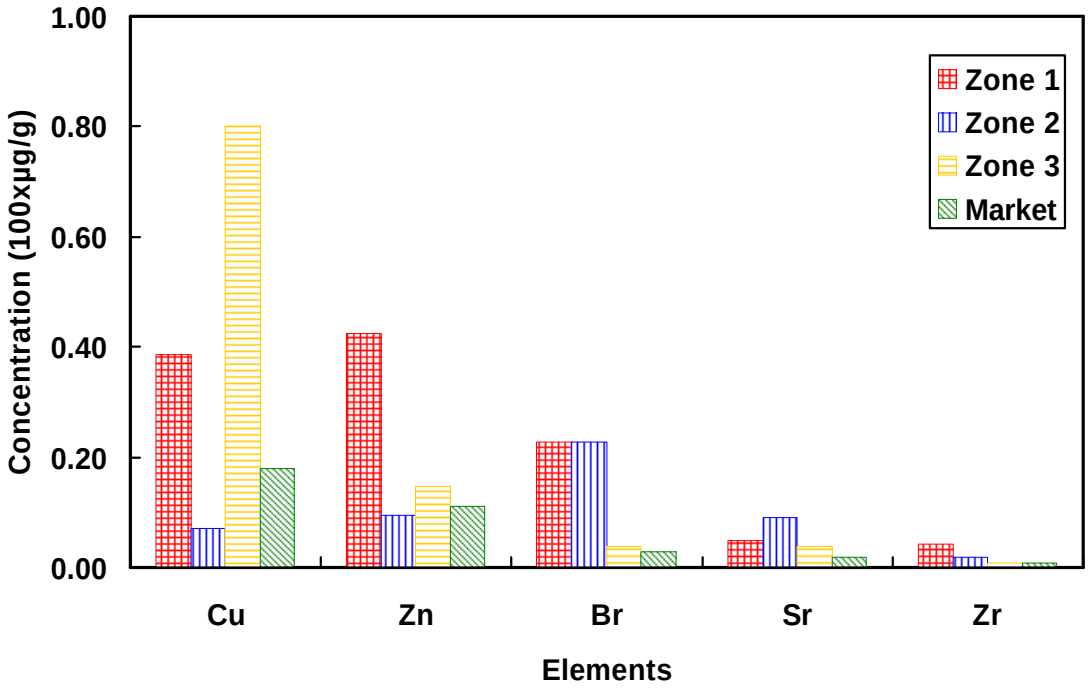

Figure 5.11: Comparison of heavy elements between Uranouchi and Market shellfish.

From the view point of heavy metals concentration, Uranouchi shellfish were compared with Market shellfish. Three samples were collected from a supermarket and each sample was irradiated three times. The same procedure was applied for sample preparation and calculating the elemental concentration as the Uranouchi cases. Figure 5.11 shows the comparison of elemental concentration of heavy metals between Uranouchi and Market shellfish. Considering the relation of elemental concentration in Uranouchi and that in Market shellfish, It is noticeably found that all heavy metals of Uranouchi shellfish show much higher concentrations than those of market one except Cu. Concentration of Cu is lower in zone2 in contrast to commercially available one but more than two and four times higher in zone1 and zone3, respectively. J.S.C. Mckee et al. have reported that Cu level is of interest in shellfish because the domoic acid toxicant is concentrated by the hepatopancreas [18]. Shellfish ingest algae, specifically the diatom species Pseudo-nitzschia which contains domoic acid naturally. Significant amounts of domoic acid can cause Amnesic Shellfish Poisoning (ASP) in humans [19]. The stress of Cu has a great influence on growth and domoic acid production in Pseudo-nitzschia species [20].

However, concentration of Zn is four times higher while that of Br is eight times higher in zone1 than that of Market. On the other hand, comparing with Market shellfish, a large amount of Sr and Zr in Uranouchi shellfish are present in zone2 and zone1, respectively.

We previously reported the results of heave metals by analyzing the seabed sludge of Uranouchi bay [22]. According to the results, Cu, Zn, Br and Sr are detected as heavy metals including some others. The higher concentration of these elements takes part in a contamination of different zones in the bay. Regarding heavy element in the present study, in addition of Zr, similar elements are detected. As a result, it can be pointed out that all these elements can be considered as either from marine origin or from directly related to the fish foods and sediment. Although Cu, Zn and Sr are pre-concentrated elements in the shellfish soft tissue of somewhat [21] but higher

concentration of these elements contrast to market one strongly indicate that the principal source of these elements in Uranouchi shellfish not only depend on shellfish themselves but also depend on the environmental conditions in where they are grown as well as their foods.

Most elements of Uranouchi bay shellfish have shown much higher concentrations as compared with Market shellfish. It may be due to the fact that the samples were collected very close to the shore, where the bay is polluted now. The reasons for the pollution of the bay can be classified as follows: 1) A large amount of fish is cultivated in this bay and fishermen have put a huge amount of foods. The concentration of several elements in fish foods is very high, and they are partly taken by fishes but rest of them falls into the seabed. As a result, the seabed sludge in several region of this bay has been polluted than that of the bay inlet as reported elsewhere [22]; 2) the house hold wastes including detergent and natural wastes come into the bay; 3) leakage of fuel from sea boat and there might be some other anthropogenic causes which increase the elemental concentration of heavy elements.

Heavy metals of Uranouchi shellfish in the present study are compared with Market one. Although we do not know the actual environmental conditions of Market shellfish in where they are grown but generally it can be assumed that these fish are grown in good environmental conditions with unpolluted water and also put a balance food for them. Therefore, they show relatively lower concentration of heavy metals in comparison with Uranouchi one. Our results regarding heavy metals are the clear evidence that the Uranouchi shellfish are affected by heavy metals.

5.5 Conclusion

Analyses of heavy metals concentration in the biological bodies of Uranouchi bay are performed using PIXE. The analysis of data obtained from several samples using this method shows that Calcium is the highest concentrated major element among others. Cu, Zn, Br, Sr and Zr are detected as heavy metals. The concentration of these heavy metals are compared with market shellfish and found that almost all heavy metals in Uranouchi shellfish show higher concentration in contrast to market one except Cu in zone 2. According to this result, it can be concluded that the biological bodies of this bay are certainly affected by the heavy metals in various ways.

References

[1] S. A. E. Johansson and J. L. Campbell, PIXE: A novel technique for elemental analysis, John Wiley & Sons, Chichester, 1988.

[2] W. Maenhaut, Nucl. Instr. and Meth. **B 35**, 388 (1988).

[3] K.G. Malmquist, Nucl. Instr. and Meth. **B 49**, 183 (1990).

[4] S. Bhuloka Reddy, M. John Charles, G. J. Naga Raju, V. Vijayan, B. Seetharami Reddy, M. Ravi Kumar and B. Sundareswar, Nucl. Instr. Meth, **207**, 345 (2003).

[5] G.J. Naga Raju, M. John Charles, S. Bhuloka Reddy, P. Sarita, B. Seetharami Reddy, P.V.B. Rama Lakshmi and V. Vijayan, Nucl. Instr. Meth, **229**, 457 (2005).

[6] E. Clayton, Nucl. Instr. Meth, **22**, 145 (1987).

[7] N.F. Mangelson, M.W. Hill, K.K. Nielson and J.F. Ryder, Nucl. Instr. Meth., **142**, 133 (1977).

[8] J.L. Campbell, Nucl. Instr. Meth., **142**, 263 (1977).

[9] W. M. Kwiatek, B. Kubica, C. Paluszkiewicz and M. Gałka, Nucl. Instr. Meth., **328**, 283 (2001).

[10] R. Ashok Kumar, V. John Kennedy, K. Sasikala, A. L. C. Jude, M. Ashok and Ph. Moretto, Nucl. Instr. Meth., **190**, 449 (2002).

[11] M.B. Chattopadhyay, S. Mukherjee, I. Kulkarni, V. Vijayan, M. Doloi, N.B. Kanjilal and M. Chatterjee, Cancer Cell International, **5**, 1 (2005).

[12] S. B. Russell, C. W. Schulte, S. Faiq and J. L. Campbell, Anal. Chem., **53**, 57 (1981).

[13] Y. Sha, P. Zhang, X. Wang, J. Liu, Y. Huang and G. Li, Nucl. Instr. and Meth. **B 189**, 107-112 (2002).

[14] K.S. Kim, J. Webb, D.J. Macey and D.D. Cohen, Nucl. Instr. Meth., **B22**, 227 (1987).

[15] V.S. Poli, M.H. Tabacniks, M.A. Rizzutto, N. Added, F.R. Espinoza-Quinones, and S.M. Palacio, Brazilian Journal of Physics, **34 3A**, 970 (2004).

[16] F.R. Espinoza-Quiñones, S.M. Palacio, R.M. Galante, F.L. Rossi, D.C. Zenatti, I.R.A. Pereira, R.A. Welter, N. Rossi, C.L. Obregon, J.M.T. de Abreu, M.A. Rizzutto, N. Added, and M.H. Tabacniks, Brazilian Journal of Physics, **35 3B**, 757 (2005).

[17] K. Baru, S. Brennan, D. Werho, L. Moro, and P. Pianetta, Recent Advances and Perspectives in Synchrotron Radiation TXRF, Nucl. Instr. and Meth. **A467-468**, 1198 (2001).

[18] J.S.C. McKee, D. Gallop, M.S. Mathur, A.A. Mirzai, Y.H. Yeo, C. Pinsky and R. Bose, Nucl. Instr. and Meth. **B49**, 225 (1990).

[19]http://www.doh.wa.gov/ehp/sf/Pubs/DomoicAcid.htm

[20] M.T. Maldonado, M.P. Hughes, E.L. Rue and M.L. Wells, Limnol. Oceanogr., **47**(2), 515, (2002).

[21] C.P. Swann, K.M. Hansen, K. Price, R. Lutz, Nucl. Instr. and Meth. **B56/57**, 683 (1991).

[22] M Hasnat Kabir, Tadashi Narusawa, Fumitaka Nishiyama and Katsuhiro Sumi, International Journal of PIXE, **16** (3-4), 221-230 (2006).

Chapter Six

Micro-PIXE Setup and Its Application

The analysis of micron size samples turn out to be significant now a day. Especially biological samples such as tissue, single cell etc. The generation of micro-PIXE is discussed in the introduction. Beam focusing system, target chamber and detector, data acquisition and processing, sensitivity and resolution, and target preparation are the fundamental part of developing a micro-PIXE system briefly discussed here. The development of microbeam at KUT, feasibility study and in-air PIXE application are also presented in this chapter. The experimental results of novel in-air PIXE technique suggest that this is a unique and simple way to obtain in-air PIXE spectra from virtually any type of samples such as solids, liquids and gases.

6.1 Introduction

The conventional high energy ion beam is a straightforward system for producing desired beam to a diameter of about 1 mm. However, special arrangements have to be performed for producing significantly smaller dimensions of beam, so-called microbeam. Many groups have taken different steps to produce microbeam from the early stage. Microbeam can be easily produced using a micron size collimator. Zirkle and Bloom [1] have introduced a microbeam of size 2.5 μm since 1950 but the intensity of the beam was not sufficient to practical use for analytical purpose. On the other hand, Mak et al. [2] and Pierce et al. [3] have demonstrated microbeams of diameter around 100 μm for the purpose of elemental analysis. After the innovation of PIXE as a powerful multi-elemental analytical technique, the attention also went to the development of micro-PIXE and collimator was used at the beginning though it suffered a lot due to some fundamental limitations. A small beam can also be produced efficiently using magnetic or electrostatic focusing. For doing so, a collimator having an aperture with diameter in the range 10-100 μm is used at first to define the beam which acts as an object in the lens system. After that the beam is focused by the lens system which produces relatively smaller beam to a diameter of about 1-10 μm. Then, this beam is used to analyze the target. The first proton microbeam with a spatial resolution of 4 μm has been developed by Cookson et al. [4]. After that they have reported proton been diameter as small as 2 μm by magnetic focusing [5]. Using electrostatic focusing system, Augustyniak [6] and Krejcik et al. [7] have demonstrated microbeams of 15 μm and 40 μm, respectively.

A typical micro-PIXE arrangement is shown in figure 6.1. The high energy ion beam coming from the accelerator passes through an analyzing magnate. This magnet stabilizes the particle energy. The object aperture is placed at a suitable place from where the lens system can focus the divergent beam properly. The lens system usually consists of magnetic quadrupoles, but electrostatic quadrupoles can also be used. A target chamber is placed at the end of the beam line. The scanning provision by moving either the target holder or the beam should be consisted in the chamber. A

zoom microscope is also required to view the target. For getting energy spectra after irradiation by microbeam, suitable detectors for x-rays and charged particles are placed in the chamber.

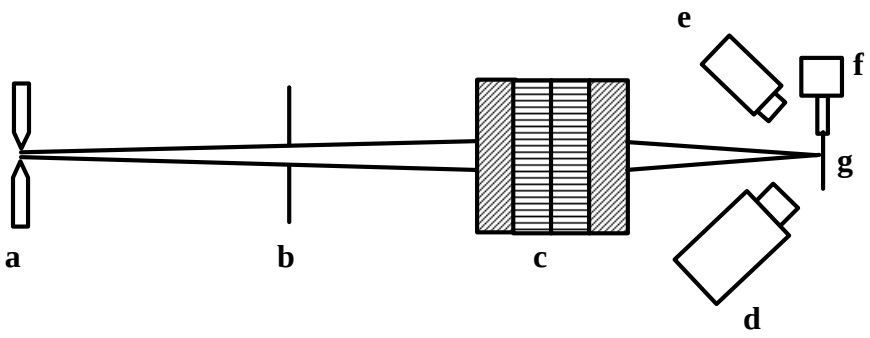

Figure 6.1: A typical schematic diagram of micro PIXE setup. (a) Object aperture, (b) aperture, (c) lens system, (d) x-ray detector, (e) microscope, (f) movable target stage, (g) target.

The use of micro-PIXE, however, provides quantitative and sensitive analysis of micron or bellow size samples. This technique comes out as a significant analytical method now a day especially for biological samples such as tissue, single cell etc. Scanning facility of this technique offers the elemental map of the target. Therefore, it can be easily identified the overall distribution of elements within the target using this map. Several merits of micro-PIXE attract us to develop this technique in our laboratory. Before developing this technique, sufficient knowledge has to be gathered about some basic parts. Beam focusing system, target chamber and detector, data acquisition and processing, sensitivity and resolution, and target preparation methodology of micro-PIXE are discussed bellow.

6.2 Beam Focusing System

The most important part of a microbeam technique is a beam focusing system. As earlier mentioned, the focusing system consist either magnetic or electrostatic

quadrupoles. In magnetic system, the diverging particles return to the original beam axis due to creating the force by magnetic field. Several arrangement of focusing systems have been reported or implemented by different groups. The number of poles in the system depends on the quality of the focusing system. At least two quadrupole lenses with alternating polarity are required to make a point focus. It has some limitation such as astigmatism. A triplet arrangement of quadrupole can give more flexibility. However, an elegant and eventually more popular system is the symmetric quadruplet in which four lenses are focused and defocused alternatively in a particular plane. Therefore, this system can give equal magnification in the x- and y-direction. On the other hand, electrostatic field may also be used in the lens system to produce microbeams. A triplet quadrupole lenses [6,8] of electrostatic focusing has been used in practice which has four rods in each lens. It can be pointed out that the electrostatic focusing is a mass-independent system. This advantage offers ions of different mass including heavy ones. The suitable combination of magnetic and electrostatic focusing is an interesting idea. This system has been developed by Martin and Goloskie [9]. They have proposed that the focal length is independent of the ion energy.

The large divergence of the beam is not acceptable to produce microbeams and it can obviously be deducted by collimators. Therefore, two things should be considered together during design the beam, one is resolution and another is beam current. In micro-PIXE analysis, the beam current is most important factor. The resulting decrease in beam current makes the beam less useful for PIXE analysis.

6.3 Target Chamber and Detector

The target is usually analyzed in a vacuum chamber which contains x-ray detector and other related equipments for the PIXE analysis. The target stage in the chamber must be fixed as perpendicular to the beam line. In PIXE microbeam, generally mapping technique is used to determine the elemental concentration in a specific region of the target. For doing so, two alternative scanning methods are applied. The first case is linear scanning where the target stage should have the movable facility so that it can be moved x- and y-direction with small steps. The movement of stage

should be kept as small as possible such as a few μm. Since target stage is moved step by step therefore x-ray spectrum can be recorded from each position. However, the alternative approach of scanning is to keep the target fixed and deflect the beam in two orthogonal directions. The second method becomes popular due to some extra advantages. The accurate positioning of the beam and the target is important in order to get better resolution of the microbeam.

It is possible to place different detector in a single target chamber to collect various results. An energy-dispersive Si(Li) detector is mandatory to collect x-rays. In order to get information about light elements using γ-ray from nuclear reactions, better performance can be found using a germanium detector. The light elements can be alternatively detected using elastic backscattering technique by means of a surface barrier detector. The detector solid angle should be considered as large as possible which can be made the choice of large crystal area of the detector and the placement of the detector as close as possible to the target. A stereomicroscope is other essential equipment for microbeam analysis. In general, better magnification of the microscope is required. Microscope is used to view the desired position of irradiation and also help to study morphology of the target. A mirror with a central hole can also be placed in front of target to the beam line for detecting the position of the beam and the size of the beam spot. The accumulated charge incident on the target should be measured carefully with highest possible accuracy for identifying the exact concentration of the elements. In thin target, it can be measured easily using a normal Faraday cup. In thick target, however, accurate charge collection is much more difficult.

6.4 Data Acquisition and Processing

In micro-PIXE, the easiest way of data acquisition is a sequential mapping, though it is little bit complicated contrast to conventional PIXE. The x-rays are collected by the x-ray detector and the pulses from the detector are recorded using a multichannel analyzer in terms of each picture element, i.e. pixel. After that the spectra are stored in a memory for off-line analysis. Since the signal comes from the detector and the x- and y-sweeps are connected to separate ADC therefore each event will give three

numbers, i.e. the x-ray energy and the x- and y-coordinates of the beam. By plotting the x-ray energy value corresponding to the x- and y-coordinate, it can easily get the elemental mapping of the element. Analyzing micro-PIXE spectra to acquire quantitative elemental concentrations is slightly different than that of conventional PIXE spectra which is directly related to the sensitivity and the accuracy of the microbeam analysis. In micro-PIXE usually the beam current is smaller therefore it is required a longer measurement time to obtain better sensitivity limits. Despite the common problem of beam/sample drifts with long measurement times, it is common practice in microbeam since the beam current is lower. The quantitative results at ppm levels are not so familiar in microbeam analysis.

6.5 Sensitivity and Resolution

The sensitivity and resolution is other most important feature in micro-PIXE analysis. In conventional PIXE, the minimum detection limit is expressed in μg/g. However, the detection limit is directly proportional to the square root of the collected charge. This is a general convention and it can be used as a condition for the sensitivity of the micro-PIXE analysis. It should be kept in mind that the current is one or two orders of magnitude smaller in microbeam and the total charge is distributed in whole scanning area. As a result, longer measuring times are required in microbeam analysis than that of conventional PIXE, perhaps by a factor of 100. The sensitivity is little bit worse in micro-PIXE contrast to conventional one but it is quite better than that of electron microprobe. On the other hand, lateral scattering is smaller in proton beam case. As a result, it has longer penetration tendency of several tens of micrometers in the target compared to electron beam. Therefore, proton microbeam shows good resolution.

6.6 Target Preparation

The target preparation is another important part of the analytical procedure. The target should be a real representative of original specimen in micro-PIXE measurement. Targets such as archaeological, artifacts, art objects microelectronic circuitry etc. can be irradiated directly. Although, some biological targets like bone,

teeth, hair and skin are irradiated as they are but many biological samples need to be cut as thin as possible. In that case, the cryofixation is the most frequently usable target preparation technique. First, raw samples are immediately preserved with liquid nitrogen. Subsequently, a thin section of the frozen sample is cut out using a cryomicrotome. This section is freeze-dried after mounting on a backing foil. Conventional target preparation techniques for instance washing, chemical fixation and staining should not be followed because of the migration, the loss of material and the changes in the elemental composition. Biological samples might have a risk of damage during the time of irradiation due to increase of temperature and radiation. A thin heat-conducting layer enveloped over the target can reduce the damage [10].

6.7 Micro-PIXE at KUT

6.7.1 Introduction

Many attempts have been taken into account to produce external PIXE setup from several years by different groups [11-15]. The most popular method is to use a very thin polymer or metal foil as the boundary of vacuum and air. In this technique, the high energy ion beam penetrate the exit foil and hit the target in the air having enough beam energy and flux intensity for analysis. However, it has a big risk to damage the accelerator when the foil is broken. Micro-PIXE analysis of various samples has been presented elsewhere [16-18]. The aspect of developing micro-PIXE system is to analyze elemental concentration of microns size sample. Microbeam usually has been produced by magnetic or electrostatic focusing in quadrupoles system as mentioned earlier. Several elegant works have been reported for producing microbeam using glass capillary optics for XRF and XRD analysis [19-24]. In those systems, x-ray beams entering the glass capillary is reduced in size as well as focused by outlet diameter. The glass capillary optics is an interesting and useful lens for ion beams also.

In the light of above discussed theoretical knowledge and other literatures report, I have jointly developed microbeam using a glass capillary optics at KUT. The focusing system in our case is completely different contrast to conventional one. This

is an external microbeam technique which introduces high energy ion beams to atmospheric environment. Here, we have taken a new attempt to utilize the glass capillary optics for in-air PIXE analysis using high energy ion beams.

Slightly tapered glass capillary optics with a few micrometers of outlet size is placed between vacuum and atmospheric environment at KUT. The capillary works as a differential pumping orifice as well as a focusing lens. This is a very simple technique to produce different size of microbeam by changing the capillary only within a few minutes. High energy ion beams (MeV) are effectively focused by the capillary. It can be pointed out the energy loss of ions during transmission is negligibly small. The capillary is originally designed as an artificial channel for ions and the mechanism of ion deflection at the wall surface is probably by the electric charge effect [25]. This technique was applied for in-air PIXE analysis. The dried and the wet samples of seabed sludge have been analyzed. We observed that the ion beam is successfully introduced to the atmospheric environment and in-air PIXE measurements can be carried out without any difficulties.

6.7.2 Experimental Setup

The inlet and the outlet diameter of the used glass capillary were 0.08 mm and 10-20 μm, respectively and the length of a few cm. The taper angle was kept approximately 0.5^{o}. The detail fabrication procedures of the glass capillary optics have been reported elsewhere [26]. The glass capillary molded into an aluminum pipe was mounted on a 4-axis goniometer. The x, y positions and the tilt angle of the capillary with respect to the ion beam line was controlled by the goniometer. A 100 l/s turbo-molecular pump was used as the differential pump. The measured typical He^{2+} ion beam current before and after the capillary was 10 nA and 200 pA, respectively. This indicates that an enhancement of the beam flux intensity is by ~2 orders. The experimental setup is shown in figure 6.5 whereas figure 6.6 is a photograph showing the actual arrangement of the glass capillary (A), the x-ray detector (B) and the sample: a seabed sludge droplet (C). The capillary was only 1 mm or less apart from the sample surface. Detector to sample distance was tried to keep as close as possible but it was limited to approximately 2 cm due to the detector housing diameter. Generally 2-3

MeV proton beam are used for PIXE analysis but in the present study He (Helium) beam was used because of some regulations in our laboratory.

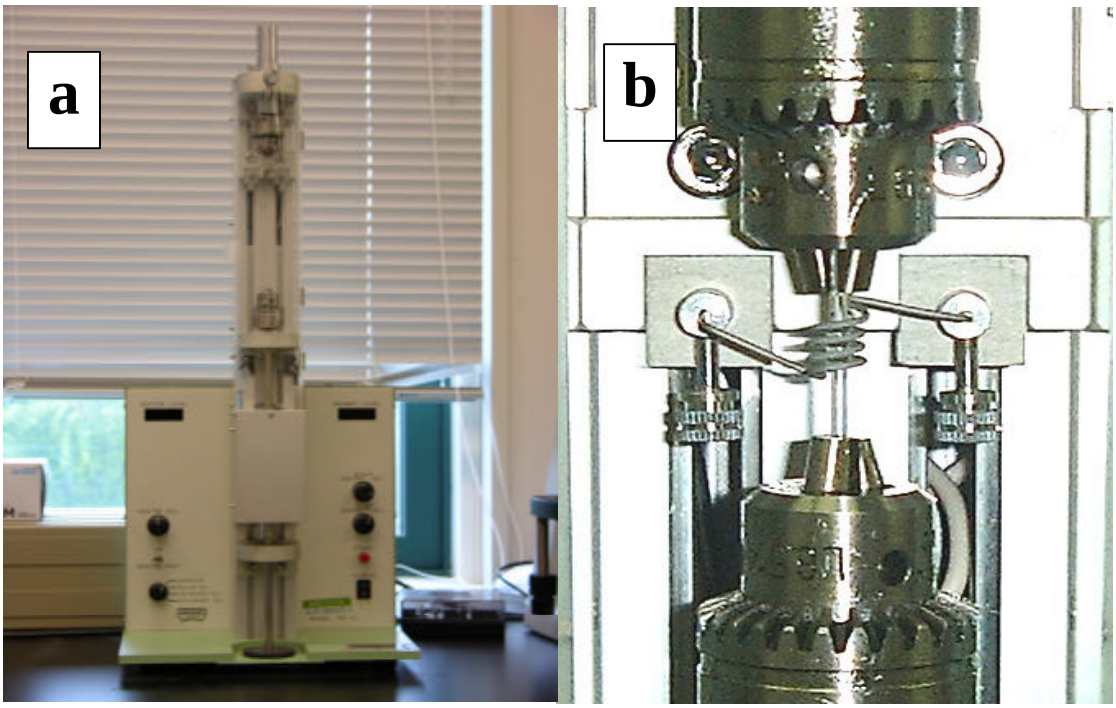

Figure 6.2: (a) Glass capillary puller used in this experiment, (b) Close-up view of puller.

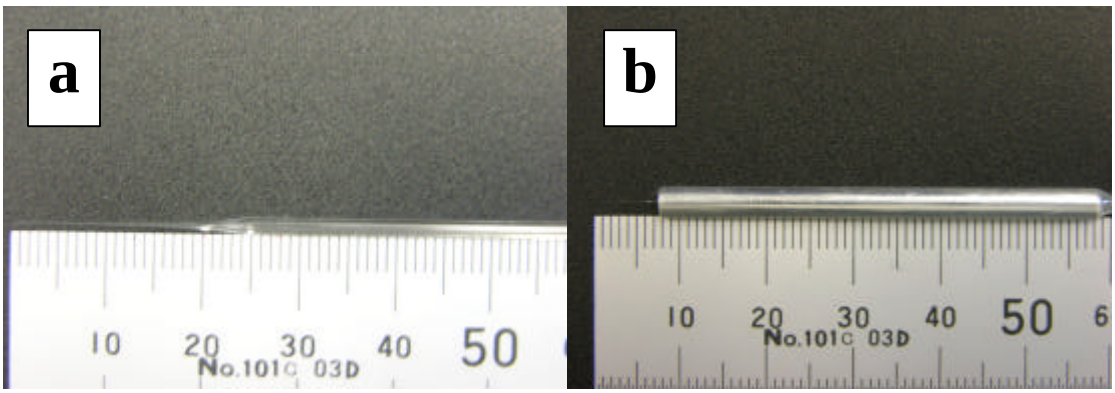

Figure 6.3: (a) Glass capillary, (b) Glass capillary molded into the Aluminum pipe.

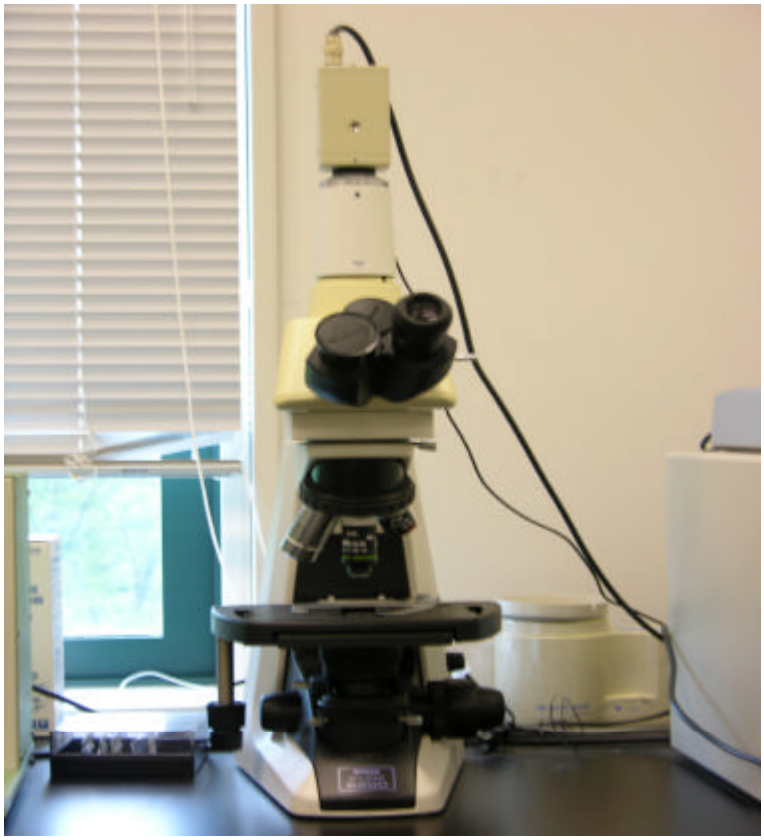

Figure 6.4: Photograph of Microscope used in this experiment for measuring glass capillary outlet diameter.

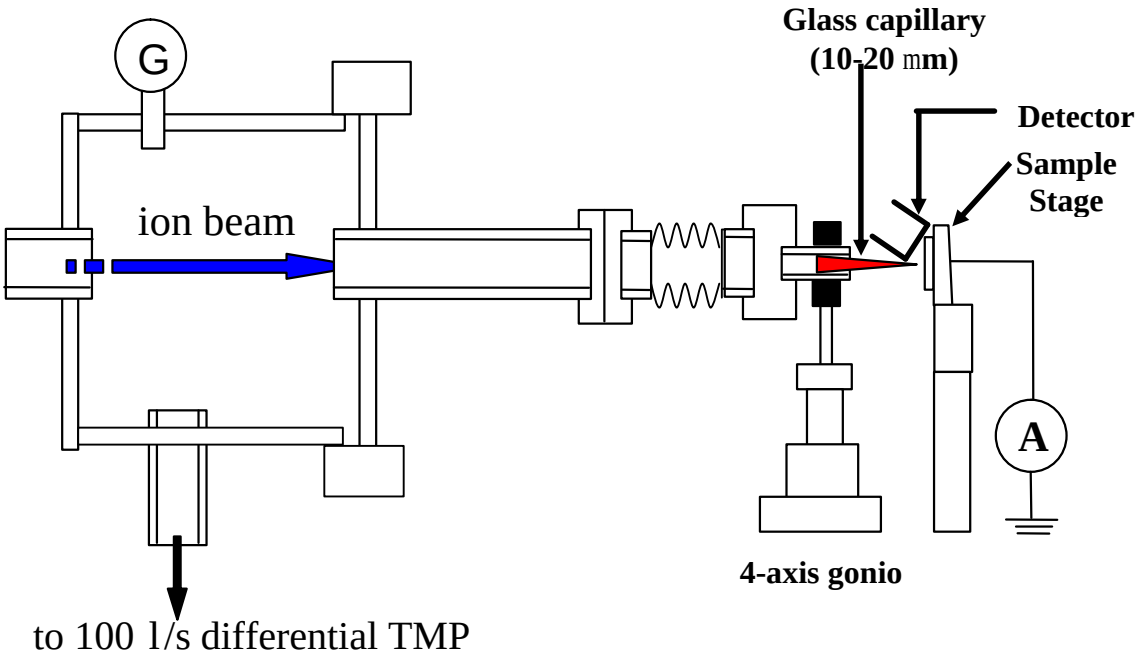

Figure 6.5: Experimental setup of microbeam at KUT.

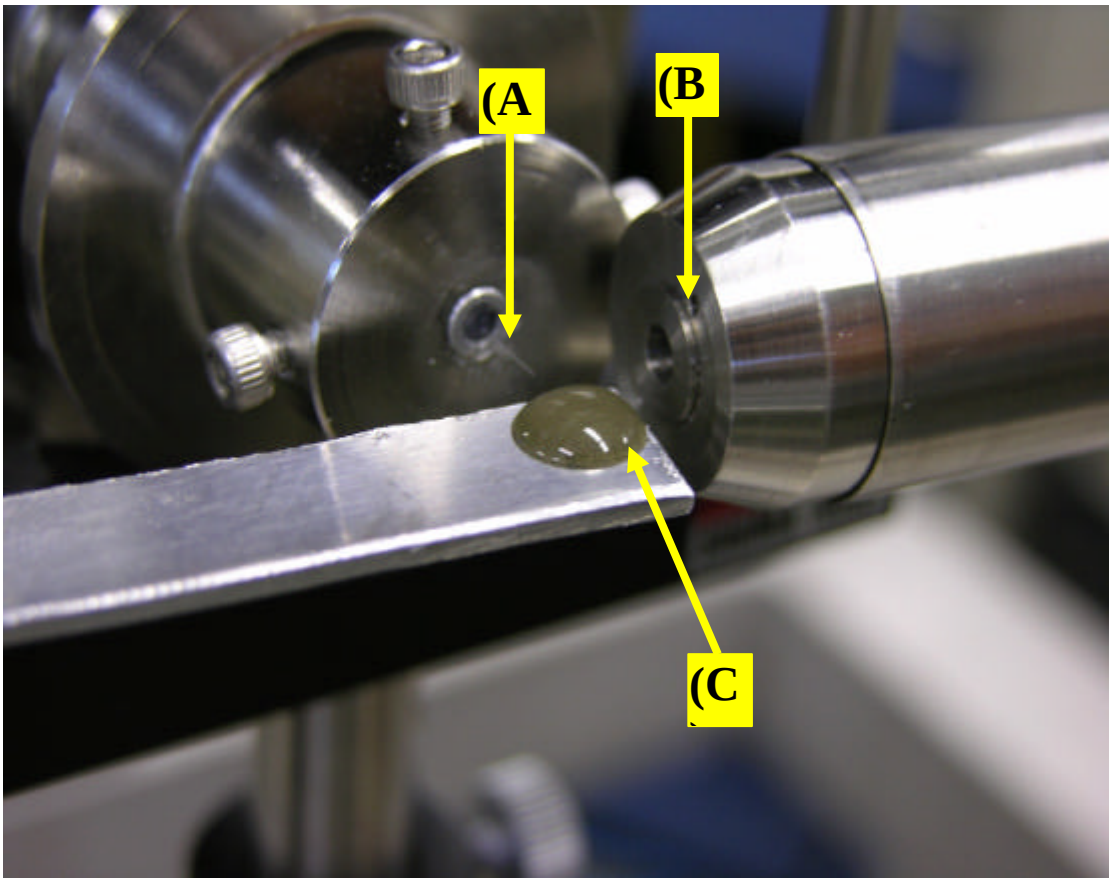

Figure 6.6: Photograph of in-air PIXE measurement arrangement; (A) the glass capillary, (B) X-ray detector and (C) the sample: a droplet of seabed sludge.

6.7.3 Results and Discussion

The feasibility of in-air PIXE analysis was first verified. For doing this $Ga_{0.7}In_{0.3}As_{0.99}$ crystal sample was mounted on a ~20 μm thick carbon foil and was irradiated by He ion beam. Figure 6.7 shows the resulting spectra for incidence energies of 2 and 4 MeV. It can be noted that the 4MeV spectrum (figure 6.7(a)) has much better sensitivity than that of 2 MeV spectrums (figure 6.7(b)) because of the ionization cross-section difference. Both spectra show designated elements of the crystal. However, giving emphasis on 4MeV spectrum, it can be seen that it has three extra peaks indicated as (A), (B) and (C) those are not related to the crystal. The x-ray energy of peak (A) clearly indicates that it comes from Si. This is probably from the glass capillary itself. Three possible reasons can be classified for this peak as shown in figure 6.8. Firstly, the outlet wall thickness of used capillary is around 10

μm. Therefore, Si x-rays emitted inside the capillary has some possibilities to penetrate the wall and come towards the detector. Secondly, x-rays generated inside the capillary come out through the outlet and reflect at the sample surface. Thirdly, scattered ions can hit the outside of the capillary and comes towards the detector. The x-ray energy of peak (B) corresponds to Ar because of Ar gas in the air. Peak (C) clearly indicates as Fe. Though the exact reason of Fe is not cleared but we suppose that this is again due to scattered ions or reflected x-rays. Despite these possible drawbacks, this technique has a great merit that external microbeams are easily obtained.

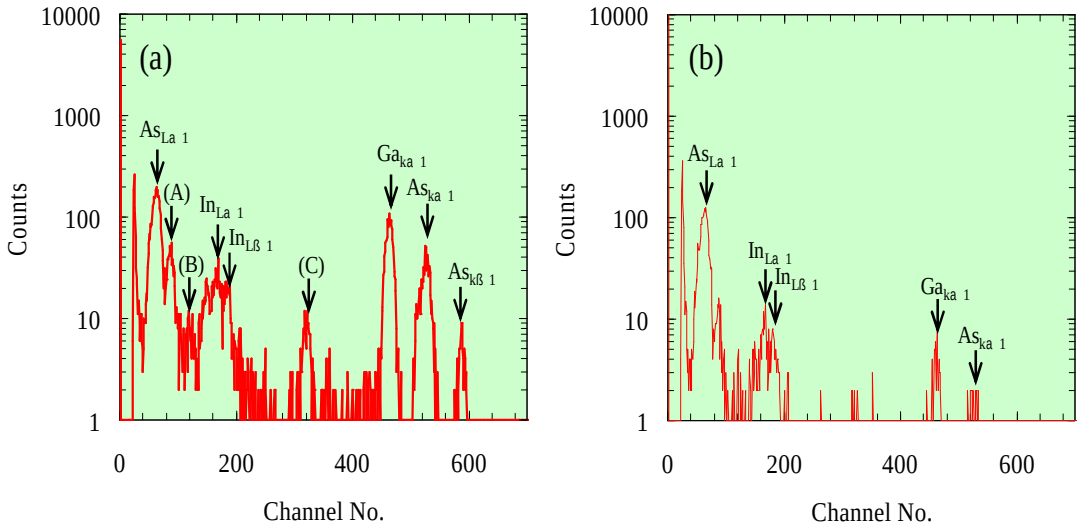

Figure 6.7: In-air PIXE spectra of the GaInNAs sample obtained with (a) 4 MeV He^{++} and (b) 2 MeV He^{+} beam. The ion beam dose is 1.4 μC.

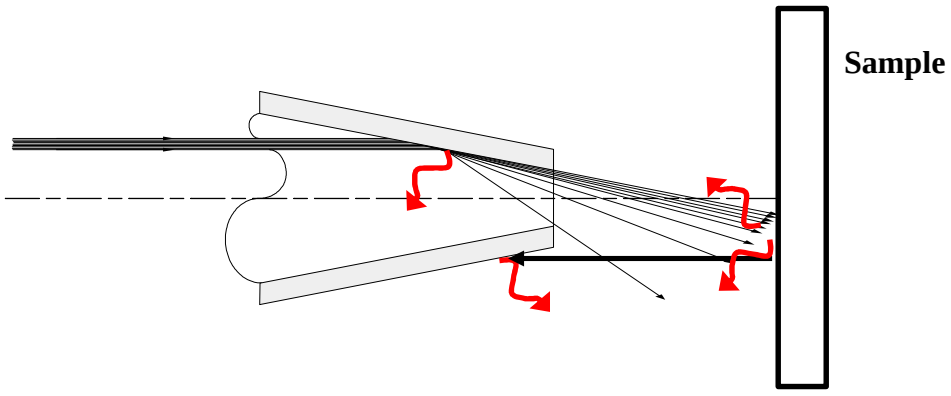

Figure 6.8: Possibility of Si x-ray generation due to glass capillary itself.

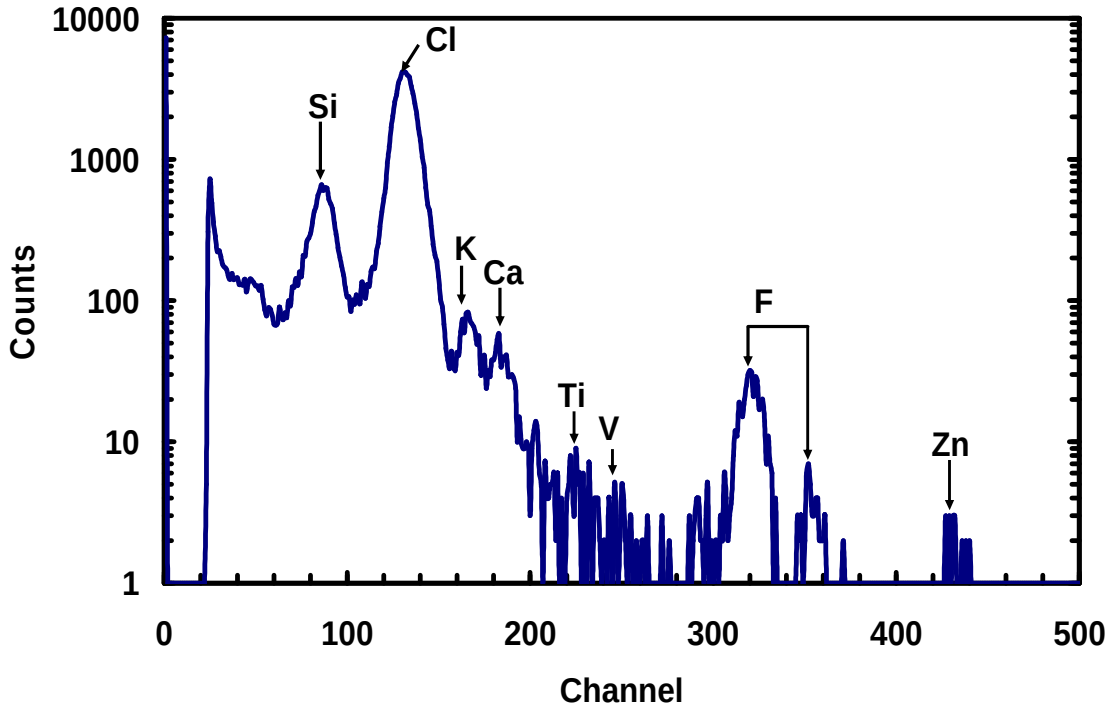

Figure 6.9: In-air PIXE spectra of dried seabed sludge obtained with a 4 MeV He^{++} beam.

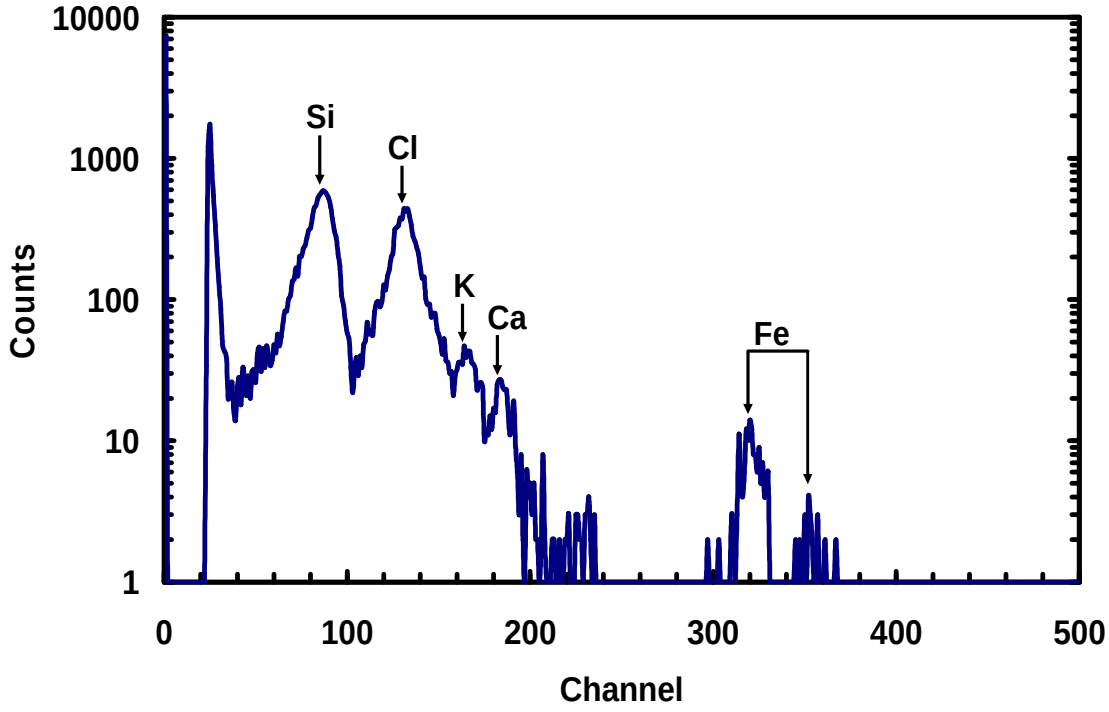

Figure 6.10: In-air PIXE spectra of liquid seabed sludge obtained with a 4 MeV He^{++} beam.

In order to in-air PIXE analysis using this technique, seabed dried and liquid sludge were irradiated by 4 MeV He^{++} beam. Samples were collected from Uranouchi bay, a brief introduction can be found in section 4.1 in chapter 4 about this bay. Typical PIXE spectra for dried and for liquid seabed sludge are shown in figure 6.9 and 6.10, respectively. Both spectra show overall agreements, but relative intensities differ considerably from each other. Particularly, the intensity of Cl-K x-ray in figure 6.9 is larger than in figure 6.10 by one order of magnitude. Though, it is not clear the origin of this difference but one possibility can be pointed out that most elements are condensed to a superficial layer in the course of drying. As a result, figure 6.9 shows relatively high counting rates. On the other hand, most elements of liquid sludge are distributed diluted in the water. Therefore, incoming ions lose their energy until they reach the target atoms, thus resulting in lower x-ray generation cross-sections in figure 6.10. It is interesting to note that the Si-K x-ray intensity is alike in both cases. This suggests that Si signal comes from some artifacts as mentioned earlier. Some experimental conditions have to be optimized for getting useful quantitative results by in-air PIXE measurements. These conditions are the ion species, the ion beam energy, the way to hold samples and the environment around the sample etc.

6.7.4 Conclusion

The proposed method is a unique and a simple way to obtain in-air PIXE spectra from virtually any type of samples such as solids, liquids and gases. The in-air analysis of this method is demonstrated by showing the results of seabed sludge measurements both in dried and in liquid condition. Results suggest that the present facility is certainly useful for PIXE analysis of various samples that are not compatible with the vacuum environment. However, some improvements are needed for practical use of the facility. The following facts can be considered for future improvements. In order to enhance the detection sensitivity and ion beam ranges in air, proton beam of 2-3 MeV can be used instead of 4 MeV He^{++} beam. The flowing of He gas around the sample able to enhance the ranges of ions and x-rays as well as can avoid dust particle from the measurement environment.

References

[1] R.E.Zirkle and W.Bloom, Science, **117**, 487 (1953).

[2] B.W. Mak, J.R. Bird and T.M. Sabine, Nature, **211**, 739 (1966).

[3] T.B. Pierce, P.F. Peck and D.R. Cuff, Nature, **211**, 66 (1966).

[4] J.A. Cookson, A.T.G. Ferguson and F.D. Pilling, J. Radioanal. Chem., **12**, 39 (1972).

[5] J.A. Cookson, Nucl. Instrum. Methods, **165**, 477 (1979).

[6] W. M. Augustyniak, D. Betteridge, and W.L. Brown, Nucl. Instrum. Methods, **149**, 669 (1978).

[7] P. Krejcik, R.L. Delglish and J.C. Kelly, J. Phys., **D12**, 161 (1979).

[8] S.H. Sie and C.G. Ryan, Nucl. Instrum. Methods, **B15**, 664 (1986).

[9] F.W. Martin and R. Goloskie, Nucl. Instrum. Methods, **197**, 111 (1982).

[10] R.D. Vis, The Proton Microprobe: Applications in the Biomedical Field, CRC Press, Boca Raton, FL, USA (1985).

[11] J.L. Ruvalcaba Sil, M. Monroy, J.G. Morales and K. López, IX International Conference on PIXE, Guelph, Canada, (2001).

[12] J. Raisanen, Nucl. Instrum. Methods, **231**, 220 (1984).

[13] V. Vijayan, R. K. Choudhury, B. Mallick, S. Sahu, S. K. Choudhury, H. P. Lenka, T. R. Rautray and P. K. Nayak, Curr. Sci., **85** (6), 772 (2003).

[14] F. Lucarelli and P.A. Mando, Nucl. Instrum. Methods, **109-110**, 644 (1996).

[15] M. Budnar, J. Vodopivec, P.A. Mando, F. Lucarelli, G. Casu and O. Signorini, Restaurator **22**, 228 (2001).

[16] M. Ahmed, M.A. Al-Ohali, M.A. Garwan, K. Al-Soufi and S. Narasimhan, Dielectrics and Electrical Insulation, IEEE, **6** (1), 95 (1999).

[17] M. Faiz, M. Ahmed, N. M. Hamdan, Kh. A. Ziq and J. Shirokoff, Supercond. Sci. Technol. **11**, 558-562 (1998).

[18] M. Massi, L. Giuntini, M. E. Fedi, C. Arilli, N. Grassi, P. A. Mandò, A. Migliori and E. Focardi, Proceedings of the Sixteenth International Conference on Ion Beam Analysis,
219-220, 722-726 (2004).

[19] Yaming Yan, JCPDS-International Center for Diffraction Data, (1997).

[20] K. Janssens, L. Vincze, B. Vekemans, F. Adams, M. Haller and A. Knochel, J. Anal. Atomic Spect., **13**, 339 (1998).

[21] D. Xunliang, He Jejun, W. Fuzhong, X. Jindong, W. Dachun, Li Yude, C. Baozhen, C. Jun and Yan Yiming, JCPDS-International Centre for Diffraction Data, (1999).

[22] L. Vincze, K. Janssens, F. Adams, A. Rindby, P. Engstrijm and C. Riekel, JCPDS-International Centre for Diffraction Data, (1999).

[23] L. Vincze and C. Riekel, X-Ray Spectrom, **32**, 208–214 (2003).

[24] W. Malzer, The Rigaku Journal, **23**, 40 (2006).

[25] N. Stolterfoht, J. H. Bremer, V. Hoffmann, R. Hellhammer, D. Fink, A. Petrov and B. Sulik, Phys. Rev. Lett., **88**, 133201-1 (2002).

[26] T. Nebiki, T. Yamamoto, T. Narusawa, M.B.H. Breese, E.J. Teo, F. Watt, J. Vac. Sci. Techno. **A 21**, 1671 (2003).

Chapter Seven

Summary and Conclusion

Particle Induced X-ray Emission (PIXE) is a highly sensitive, multi-elemental analytical technique which is already proved in all prospective areas such as thin films, water, air, archaeological and biological samples etc. This technique provides more accurate result for elemental analysis than others. From several decades PIXE is widely used in the above mentioned areas successfully. Generally this technique is used to determine the elemental concentration of different elements those are dissolved in the samples. However, there was no complete PIXE setup at Kochi University of Technology (KUT), Japan. The aim of this research is to introduce PIXE setup at KUT and its application for quantitative analysis on different fields. I have selected the Uranouchi bay (Kochi, Japan) as a sampling area. This bay is well-known for its natural landscape and fish culturing. However, the sea water and the seabed of this bay are no longer clean now. Seabed sludge and shellfish have been collected for environmental and biological application, respectively from this bay to determine the elemental concentrations.

The multielemental detection facility is a prominent feature of PIXE. The high-energy protons or alpha particles strike the target atoms and eject electrons from the innermost shell in atoms. As a result, a vacancy is created in the innermost shell. It is a common nature of an excited atom that it seeks to regain a stable energy state. Therefore, the created vacancy is filled by an electron coming from an outer shell, at that time an electromagnetic radiation in the form of characteristic x-rays is emitted which is recorded in a spectrum. Two stage procedures are followed in PIXE analysis. Firstly, elements in the target are identified from the energies of the characteristic peaks in the x-ray emission spectrum. Secondly, the quantity of a particular element in the target is determined from the intensity of its characteristic x-ray emission spectrum. This powerful technique can easily analyze various elements at the same time with atomic number as low as 12 in the ppm range.

This dissertation can be segmented into four basic parts such as general PIXE setup at KUT, analysis of seabed sludge, analysis of shellfish and micro-PIXE setup at KUT and its application. The overall summary and conclusions are presented bellow.

PIXE Setup at KUT

The ion beam facility at KUT has been extended to allow elemental concentrations analysis by PIXE. RÖNTEC XFlash 2001, a Silicon Drift Detector (SDD) type x-ray detector was used in the setup. The active area and silicon thickness of the detector are 10 mm^2 and 0.3 mm, respectively. A polymer coated beryllium window of 8 μm thickness is equipped with the detector. A zirconium ring with an aperture of 3.4 mm serves as a collimator. XFlash supply unit with high resolution pulse processor was connected to an ORTEC (Model 572) amplifier. The ORTEC 572 Amplifier is a general-purpose spectroscopy amplifier. After that, the output of this amplifier was connected to a computer via an analog to digital converter (ADC) and a multi-channel analyzer (MCA). Before doing experimental works, system was calibrated and sensitivity was checked.

Analysis of Seabed Sludge

Elemental analyses were carried out for the seabed sludge collected from Uranouchi bay. Samples were collected from eleven different places in this bay, denoted as Sam1, Sam2, Sam3 and so on. The whole sampling area is divided into three parts such as inlet (Sam11-Sam9), center (Sam7-Sam5) and inner (Sam4-Sam1) regions. Seabed-sludge contamination with heavy metals as well as toxic elements becomes one of the most serious environmental problems. The aim of the present study is to investigate the polluted areas in the bay by heavy and toxic elements. Samples were prepared using external standard method. In this method, the droplets of different standard solutions were first irradiated by ion beam and measured the x-ray yield which gives the sensitivity curve. After that, the target droplets were irradiated and using sensitivity curve the concentration of different elements was calculated. As a result of analyses of samples collected from eleven different places in the bay, seventeen elements including toxic ones were detected. It is found that the center

region of the bay is mostly polluted in contrast to the other regions. The major elements show characteristic features especially in center (Sam7) than that of inlet (Sam11), where sulfur concentration is considerably higher by five times. On the other hand, sulfur concentration is almost equal for the samples Sam2-5. Calcium concentration increases as the sampling points become inner from the inlet (Sam11) to the center (Sam7) of the bay, and turns to decrease toward the inner side of the bay (Sam1-4), where its concentration shows similar values of around 45 ppm. With regard to the trace elements, chromium concentration is lower in Sam2 and Sam3 and is much higher in Sam7 in comparison with that in the other samples. Nickel concentration is higher in Sam9 and lower in Sam1 and Sam4. Iron, copper, zinc and strontium concentrations are much higher in Sam7 in contrast to that in Sam11. The concentration ratios of toxic elements (where all values are divided by the values for Sam11) indicate that the concentrations of Cr, Ni, Cu and Zn pronouncedly increase in Sam5-7 and Sam9 in comparison with those in the other samples. The concentrations of Cr, Zn and Cu in Sam7 are more than 2.48, 2.6 and 2.72 times higher, respectively, while that of Ni in Sam9 is 2.58 times higher in contrast to their lowest values. In the present study, these elements show higher concentrations in the center region of the bay.

Analysis of Shellfish

Shellfish called Japanese littleneck clam (*Ruditapes philippinarum*) were investigated which were collected from Uranouchi Bay. The interest of this study is to examine whether the biological species are contaminated by heavy metals due to pollution of the bay or not. Shellfish have been chosen as a representative of the biological species. Three different places of Uranouchi Bay were the sampling site for collecting of shellfish, denoted as zone1, zone2, and zone3. However, zone1 is very close to the inlet of the bay, whereas zone2 from inlet and zone3 from zone2 are one kilometer apart each. The well established internal standard method has been followed to sample preparation. In this method, one or two internal standard elements are added to sample in such way that they can mix uniformly within the sample. Carefully weighed 2 mg Mo powder was added in each sample in the present study and was mixed uniformly. A 12 μm thick carbon foil was used as a substrate for samples. In analysis of shellfish, nine elements were detected. The concentration of major

elements in all samples show the characteristic features depending on the collecting areas. Especially, Ca shows the higher concentration among other major elements in all samples. It can be pointed out that the concentration of Ca is almost seven and three times higher in zone 2 and zone 1, respectively in comparison with zone 3. The concentration of Fe increases from zone 1 toward zone 3. However, Fe shows about three times higher concentration in zone 3 than that of zone 1. On the other hand, Mn is decreased from zone 1 towards zone 3. The heavy element concentrations of Uranouchi shellfish were compared with Market shellfish. It is clearly seen that all heavy elements of Uranouchi shellfish show much higher concentrations than those of market shellfish except Cu. Cu has lower concentration in zone 2 in contrast to Market but more than two and four times higher in zone 1 and zone 3, respectively. Nevertheless, Zn and Br in zone 1 are approximately four and eight times higher, respectively, while that of Sr and Zr in zone 2 and zone 1 are four times higher, respectively than that of Market. According to this result, biological bodies of this bay may be affected by heavy metals in various ways.

Micro-PIXE Setup at KUT

Generally, microbeam is produced by magnetic or electrostatic focusing lens such as quardrupoles system. At KUT, a novel microbeam was developed using a glass capillary optics. This is an external as well as microbeam technique. The system introduces high energy ion beams to atmospheric environment. Slightly tapered glass capillary optics with a few micrometers of outlet size is placed between vacuum and atmospheric environment. The capillary works not only as a differential pumping orifice but also as a focusing lens. This is a very simple technique to produce different size of microbeam than conventional one by changing the capillary only within a few minutes. High energy ion beams (MeV) are effectively focused by the capillary. This technique was applied for in-air PIXE analysis. The dried and wet samples of seabed sludge were analyzed. We observed that the ion beam is successfully introduced to the atmospheric environment and in-air PIXE measurements can be carried out without any difficulties. This result indicates that the technique is suitable to obtain in-air PIXE spectra and virtually any type of samples such as solids, liquids and gases can be measured as they are.

List of publications and presentations:

Publications:

1. **M. Hasnat Kabir**, Tadashi Narusawa, Fumitaka Nishiyama and Katsuhiro Sumi, "Elemental Analysis of Uranouchi Seabed Sludge using PIXE." International Journal of PIXE, Vol. 16, Nos. 3-4 (2006) 221-230.

2. Takuya Nebiki, **M. Hasnat Kabir** and Tadashi Narusawa, "In-air PIXE analysis by means of glass capillary optics", Nuclear Instruments and Methods in Physics Research B 249 (2006) 226-229

3. **M. Hasnat Kabir**, Tadashi Narusawa, PIXE analysis of heavy metals in shellfish of Uranouchi Bay, The 22nd International Conference on Solid Waste Technology and Management, 18-21 March 2007, Philadelphia, USA.

4. **M. Hasnat Kabir**, Tadashi Narusawa, Quantitative analysis using particle induced x-ray emission (PIXE), KUT Bulletin, 2007.

5. **M. Hasnat Kabir**, Tadashi Narusawa, PIXE analysis of biological bodies in Uranouchi bay. (Submitted)

Presentations:

1. The Japan Society of Applied Physics Conference: "New external PIXE technique using tapered glass capillary optics"
M. Hasnat Kabir, Takuya Nebiki and Tadashi Narusawa; (Oral and Poster presentation)
Tokushima University, Japan. August, 2005.

2. 22nd PIXE symposium: "Elemental Analysis of Uranouchi Seabed Sludge using PIXE"
M. Hasnat Kabir, Tadashi Narusawa, Fumitaka Nishiyama and Katsuhiro Sumi; (Oral presentation)

The Wakasa Wan Energy Research Center, Fukui, Japan. November 28-30, 2005

3. The Japan Society of Applied Physics Conference: “PIXE analysis of heavy metals in shellfish of Uranouchi Bay”
M. Hasnat Kabir, Tadashi Narusawa; (Oral presentation)
Ritsumeikan University, Shiga, Japan. August 29-31 & September 1, 2006.

4. 23rd PIXE symposium: “PIXE analysis of heavy metals in shellfish of Uranouchi Bay”
M. Hasnat Kabir, Tadashi Narusawa; (Oral presentation)
Matsushima, Sendai, Japan. November 13-15, 2006.

5. Workshop on Biomedical Applications of High Energy Ion Beams, the Abdus Salam ICTP - Trieste, Italy. 12-16 February 2007.

6. The 22nd International Conference on Solid Waste Technology and Management: “PIXE analysis of heavy metals in shellfish of Uranouchi Bay”
M. Hasnat Kabir, Tadashi Narusawa; (Oral presentation)
Philadelphia, America. March 18-21, 2007.